



If you have discovered material in AURA which is unlawful e.g. breaches copyright, (either yours or that of a third party) or any other law, including but not limited to those relating to patent, trademark, confidentiality, data protection, obscenity, defamation, libel, then please read our [Takedown Policy](#) and [contact the service](#) immediately

DEFORMATIONS OF THE
PNEUMATIC TYRE

DAVID JOHN OSBORNE

Thesis submitted for the Degree of Ph.D.

THESIS
678.065
OSB

-1 NOV 72 155845

University of Aston
in Birmingham.

August 1972.

SUMMARY

A mathematical model is developed for the general pneumatic tyre. The model will permit the investigations of tyre deformations produced by arbitrary external loading, and will enable estimates to be made of the distributions of applied and reactive forces.

The principle of Finite Elements is used to idealise the composite tyre structure, each element consisting of a triangle of double curvature with varying thickness. Large deflections of the structure are accommodated by the use of an iterative sequence of small incremental steps, each of which obeys the laws of linear mechanics.

The theoretical results are found to compare favourably with the experimental test data obtained from two different types of tyre construction. However, limitations in the discretisation process has prohibited accurate assessments to be made of stress distributions in the regions of high stress gradients.

INDEX

SUMMARY	i
INDEX	ii
ACKNOWLEDGEMENTS	iv
CHAPTER 1. INTRODUCTION	1
CHAPTER 2. REVIEW OF LITERATURE	3
2.1 Tyre mathematics	3
2.2 Mathematics of laminated structures	4
2.3 Finite element methods	6
CHAPTER 3. FORMULATION OF A MATHEMATICAL MODEL FOR THE PNEUMATIC TYRE	7
3.1 Basic assumptions	8
3.2 Elastic properties of cord-rubber composites	10
3.3 Finite element idealisation	17
3.4 Construction of local Cartesian axes	27
3.5 Stresses and strains in local co-ordinates	29
3.6 Calculation of the element stiffness matrix	30
CHAPTER 4. IMPLEMENTATION OF THE FINITE ELEMENT METHOD	40
4.1 Formation of element mesh patterns	40
4.2 Nodal co-ordinates and associated thickness vector	43
4.3 Numerical integration	46
4.4 Formation of the total stiffness matrix	48
4.5 Boundary conditions	52
4.6 Implementation of boundary conditions	54
4.7 Calculation of nodal forces	56
4.8 Stresses and strains	56
4.9 Non-linear solutions	59

CHAPTER 5.	RESULTS	61
5.1	Tyre preparation	61
5.2	Measurements	61
5.3	Solution by computer	62
5.4	Global displacements	64
5.5	Load-deflection curves	64
5.6	Contact area	67
CHAPTER 6.	CONCLUSIONS	68
FIGURES		70
TABLES		110
APPENDIX		115
BIBLIOGRAPHY		126

ACKNOWLEDGMENTS

The author wishes to express his appreciation to all who have assisted towards this thesis. In particular I would like to thank my supervisor Professor S.Rangachary, for his guidance and encouragement during the past three years. I am indebted to the Dunlop Company, Birmingham, for the use of test and computing facilities, and special thanks are extended to Dr.C.W.Barson, Mr.S.G.Whitehall and members of the Tyre Engineering Department for their invaluable advice and comments.

CHAPTER 1.

Introduction

The outward appearance of the pneumatic tyre belies the complexity of its internal construction. Because of its apparent simplicity, there is a tendency to assume that the problems of structural mechanics and deformations have long been solved. On closer examination it is seen that the modern tyre is a highly sophisticated load carrying structure, requiring detailed mathematical modelling to effect a solution.

The composite construction of cord, steel and rubber combine to form a structure which is neither homogeneous or isotropic. Each component serves a vital purpose in producing a device capable of withstanding a wide range of loading conditions.

The early stages of tyre development were concerned with improving the component materials and construction techniques. In more recent times, the emphasis on performance and service has necessitated the investigation of the finely balanced system of forces which are capable of being altered by design. The structural complexity has, for the main part, permitted only piecemeal analysis of the type to be undertaken. Furthermore, although the basic principles by which the tyre transfers load from the ground to the wheel can be propounded, no mathematical model is available for obtaining a quantitative solution of this fundamental problem.

The purpose of this thesis is to investigate the deformations of the tyre when subject to arbitrary loading, and to determine how such loads are transmitted to the wheel. To accomplish this,

the complete tyre will be represented by a mathematical model which utilises the structural characteristics and material properties of the tyre. This will be achieved by the use of finite elements.

Each element is a three dimensional sub-structure consisting of a triangle of double curvature with varying thickness. When combined, they form a realistic approximation to both the geometry and elastic properties of the tyre. The elastic properties of individual elements are derived from the laminate construction of cord ply layers. Large deflections are accommodated by the use of an iterative sequence of small incremental steps, each of which obeys the laws of linear mechanics. The displacement of the elements are formulated so as to ensure compatibility of displacements for the boundaries of adjacent elements.

The finite element method enables the overall stiffness of the tyre to be estimated. From this, the response of the structure to any arbitrary applied forces can be studied in terms of displacements and reaction forces.

An IBM 370 digital computer has been programmed to process the vast quantities of data required in the formulation, and the results compared with experimental results obtained for two different types of tyre construction.

CHAPTER 2.

Review of literature

During the last fifty years, many authors have contributed toward the theory of the mechanics of the pneumatic tyre. For the main part, mathematics pertaining to tyres can be classified into two sections. Firstly, there are the specialised theories, usually formulated by engineers and mathematicians closely involved in the tyre industry, which help in the understanding of the fundamental mechanics of tyres, and secondly general structural mathematics, of which the tyre can be considered as just one specific problem.

2.1 Tyre mathematics

Due to the commercial secrecy that surrounds any developments, the theoretical basis of tyre mathematics has tended to be slow and not well documented by way of published articles. One of the first works to become readily available was by Hofferberth [1]. In this, the tyre model was based on thin shell theory with the shell surface being comprised of a cord net which was allowed to deform such that trellising occurred at the crossing points of cord plies. The cords were assumed to experience a constant stretch along their entire length with rubber effects being ignored. The method was applied to problems of symmetric loading arising from inflation forces.

Similar equations were developed by Rivlin [2], assuming inextensible cords, and by Bukhin [3], who derived a non-linear relationship for the force-extension curve of the cords.

Lauterbach and Ames [4] incorporated a digital computer to solve these equations and obtained estimates of cord stresses. Later, Ames [5] expanded on the work of Hofferberth to include a cord extension factor which was a function of position.

This theory was further developed by Walter [6] to include the effects of centrifugal loading as induced by a spinning tyre. Zorowski [7] compared the above methods for the case of the conventional cross-ply tyre subject to inflation pressure.

All the above theories have been based upon a linear thin shell model subject to symmetric loading, with some prior knowledge of the final deformed shape. The prediction of the equilibrium shapes generated by such theories, is shown in the summary of the literature given by Frank [8]. An extension to pressurised thick shells has been attempted by Gough [9]. In the non-linear field, a paper by Usyukin [10] presents an exact solution of the large deformation of a toroidal membrane shell under inflation pressure. However, the non-linear theory is applied to a homogeneous elastic shell without cord reinforcement.

More recent work on the mathematical model of the tyre is that of Dunn [11], who uses finite elements to obtain a non-linear, thin shell solution. Again, the problem solved is that of deformations due to symmetric loading, as induced by internal pressure and centrifugal force. An attempt to obtain solutions for the arbitrary loaded case yielded poor results. The symmetric loading case was also the basis of Brewer's paper [12] who studied the non-linear behaviour of aircraft tyres under inflation loading.

2.2 Mathematics of laminated structures

The basic mathematics describing the characteristics of isotropic, homogeneous materials is well documented by Green [13] and Godfrey [14]. The pneumatic tyre, however, consists generally of cord layers in a rubber matrix, producing a composite structure which is both anisotropic and heterogeneous.

Such structures have been the centre of much research over the past decade. Reissner and Stavsky [15] considered the simplified case of a plane laminate composed of two orthotropic sheets of equal thickness such that their axes of elastic symmetry made equal and opposite angles with the axis of the composite. Clark [16,17] examined the properties of cord-rubber laminates of the type found in the pneumatic tyre. The effect of tension and compression on a composite sample was shown to produce a bi-linear form of the stress-strain curve, and the state of inter-ply stress estimated as a function of the externally applied forces.

Gough [18] documented the research carried out at the Dunlop Company by Wainwright [19] and Lawton [20], and applied the results to estimate the stiffness of the tread breaker band in radial ply tyres. A comprehensive survey of literature appertaining to the elastic characteristics of pneumatic tyres up to 1967 was given by Frank and Hofferberth [21].

With the greater use of composite materials as lightweight, high strength structures in the field of structural mechanics, authors such as Ashton [22] and Calcote [23] have published a general survey of the state of the knowledge in composite materials, of which the pneumatic tyre can be considered one application. Robecchi [24] dealt with the general mathematics of tyres, which included a detailed analysis of the laminated model.

The majority of the above research has been concerned primarily with the two-dimensional stress-strain relationship of a laminate. Solutions for a three-dimensional structure have been given by Hashin [25] and Hermans [26], and applied to tyre analysis by Brewer [12].

2.3 Finite element methods

The finite element method was first introduced by Turner and associates [31], using flat triangular and rectangular elements to analyse plane stress problems arising from the study of complex structures in aircraft design. The appearance of the method in the aeronautical industry was due partly to the need to solve involved structural problems, and also to the availability of automatic digital computing facilities, capable of handling large amounts of data. Such a machine is an essential pre-requisite of any application of the finite element method.

Over the past fifteen years, the method has been developed to a high degree of sophistication with vast quantities of literature being published at each stage. The original flat triangular element has been replaced by all manner of different elements, all of which have advantages in particular applications. A comprehensive presentation of the finite element method, its present state of development, and examples on its applications has been published by Zienkiewicz [32].

CHAPTER 3.

Formulation of a mathematical model for the pneumatic tyre

The modern pneumatic tyre is a highly complex structure, designed to function under a wide variety of loading conditions. Figure 3.1 shows a cut section from the two basic types of tyres manufactured to-day, namely the radial and cross-ply form. A third, less common type, is a combination of these two.

The tyre carcass consists of a number of rubberised layers, each possessing a high tensile strength, and consisting of either cords or steel which are fabricated to form a laminated composite structure. The cord layers are surrounded by a variable thickness rubber layer, forming an air-tight seal which simultaneously allows shearing throughout the tyre and also protects the main load carrying cord plies from damage.

The differing geometries in which the cord layers are arranged produces the two basic structures of the radial and cross-ply tyres. In the case of the radial ply tyre, it is necessary to include an extra layer of cords in between the tread rubber and the carcass plies to act as a reinforcing element, thus stiffening the tyre in a direction parallel to the rolling surface.

The cord layers are anchored to a rigid steel band which holds the tyre onto the wheel. The tread rubber provides a means of applying the external loads, which can include static radial loads, as well as tractive and cornering forces. These forces are summarised in Figure 3.2.

Thus the complete assembly results in a highly flexible structure which is neither homogeneous or isotropic. Under the action of a complex loading system, the structure will undergo large deformations even though the strains in the cords remain relatively small.

A mathematical model is required which will characterise any type of tyre, of any size and material construction, and which will simulate the tyre behaviour under any prescribed loading situation.

3.1 Basic assumptions

3.1.1 Shear effects

Previous mathematical models of the tyre have always been based upon the assumption that it's behaviour can be approximated by a thin shell of revolution. The effect of shear deformation through the shell thickness has been ignored on the basis that the cord layers, which occupy a relatively small part of the structure, are the major load bearing components of the tyre.

For the type of problems in which this particular assumption has been made, namely those of deformations due to inflation pressure and dynamic loading, the approximation is probably justifiable. However, in studying the deformation of tyres under arbitrary loading conditions, the shear effects in the structure should be included. This effectively means that account should be taken of the variation in thickness of the tyre around its profile and of the finite thickness of individual plies.

3.1.2 Tread region

The tread region of a tyre consists of a rubber slab into which a number of large grooves and slots are moulded. A consequence of these grooves is that any load applied to the tread, which is sufficient to deflect the tyre, will be accompanied by large local deformations in the tread rubber in the vicinity of the contact area. Such displacements have been investigated using finite difference techniques by Barson and Osborne [27].

In order to eliminate the undesirable effects of these compressions, the tread rubber was removed from the experimental tyres, and the mathematical model based upon this simpler construction.

3.1.3 Cord angle variation

The formation of a tyre consists of forcing a cylindrical structure into a near toroidal form, as shown in Figure 3.3. Thus a laminated body which initially consisted of cord layers of constant bias angle is transformed to one whose bias angle is a function of position. This introduces the heterogeneous material properties of the shaped structure. Mathematical analyses by Gough [28,29] of the shaping process for a cross-ply tyre have shown that:-

- (a) If the cords move subject to a pure trellising action, then the law governing the cord angle can be written as,

$$R = K \cos \phi \quad (3.1)$$

where R is the radius from the axis of symmetry (Figure 3.4)

ϕ is the new cord bias angle

K is a constant.

Further, if no cord extension takes place, then the constant, K, can be determined from the initial values of radius and bias angle of the cord plies on the build-up drum. A similar law to equation (3.1) will hold for a constant extension factor.

- (b) If ply slippage occurs, then this represents a variation in radius with no change in bias angle.

A combination of the effects of trellising, cord extension and ply slippage result generally in a non-linear form of the $R\text{-}\cos\phi$ curve, particularly as applied to cross-ply tyres, as will be shown by measurements on the test tyre. This non-linearity was incorporated into the mathematical model by fitting a second order polynomial to the measured curve of the form

$$\cos\phi = a_0 R^2 + a_1 R + a_2 \quad (3.2)$$

Changes in cord angle during shaping are accompanied by variations in the density of the cord plies. The number of cords crossing a given circumferential lines will remain constant during moulding process, so that

$$2\pi R_b n_b \cdot \sin\phi_b = 2\pi R n \cdot \sin\phi \quad (3.3)$$

$$\text{or} \quad n = n_b \cdot R_b \cdot \sin\phi_b / R \sin\phi \quad (3.4)$$

where n_b , R_b and ϕ_b refer to the ends per inch, radius, and cord bias angle respectively on the build-up drum and n , R , and ϕ refer to a position on the shaped tyre.

3.2 Elastic properties of cord-rubber composites

The basic structures of the pneumatic tyre consists of layers of orthotropic cords embedded in an isotropic rubber matrix, resulting in a composite which is both anisotropic and heterogeneous. Such a structure will possess a highly complex internal stress distribution, even for the simplest of loading configurations. Analytical simplifications can be achieved if the material is characterised

on the macroscopic scale as being orthotropic and homogeneous. The resulting stress-strain distributions for this model can then be studied on the microscopic level to reveal the state of internal stress. To enable the elastic constants associated with the simplified model to be evaluated, the properties of the individual components of the composite must first be defined.

3.2.1. Rubber properties

Much of the experimental work dealing with the elastic characteristics of rubber has been concerned with large strain applications. A typical stress-strain curve for a rubber specimen subject to uniaxial tension is given by Clark [30] and reproduced in Figure 3.5. In the case of the pneumatic tyre, the rubber is reinforced with cords which possess high elastic moduli in comparison with that of rubber. As a consequence, the structure is generally subjected to quite small strains. If the curve in Figure 3.5 is examined in the region of the origin, it is clear that, for small extensions, a linear stress-strain law will be adequate (Figure 3.6).

Further, since rubber is isotropic, only two independent elastic constants are required, namely Young's modulus, E_r , and Poisson's ratio V_r . The shear modulus, G_r , is related to these by the equation:-

$$G_r = \frac{E_r}{2(1+V_r)} \quad (3.5)$$

Rubber can be considered incompressible, and so Poisson's ratio equals 0.5. Hence equation (3.5) becomes

$$G_r = \frac{E_r}{3} \quad (3.6)$$

3.2.2 Cord properties

The cords will consist either of a steel strand or a wound fibre. In the case of steel, the cord is both homogeneous and isotropic, and the stress-strain relationship can easily be defined in terms of its material constants, E_s and V_s , where E_s is Young's modulus for steel and V_s is Poisson's ratio for steel. The shear modulus, G_s , is given by a similar expression to (3.5) as

$$G_s = E_s / 2(1 + V_s) \quad (3.7)$$

For fibre cords, the material can be approximated as being homogeneous and orthotropic, with the axis of elastic symmetry being taken in the direction of the cord axis as given in Figure 3.7. It has been shown by Brewer [12] that to define such a material, five independent elastic constants are required, namely:-

- E_{11} Young's modulus along the cord axis, x_1
- E_{22} Young's modulus perpendicular to x_1
i.e. in the $x_2 - x_3$ plane.
- G_{12} Shear modulus in the axial direction
- V_{12} Poisson's ratio in the $x_1 - x_2$ plane,
representing a contraction in the x_2
direction as a result of a stress applied
in the x_1 direction.
- V_{23} Poisson's ratio in the $x_2 - x_3$ plane.

Hooke's law for the cord can then be expressed in matrix form as:-

$$\begin{bmatrix} \epsilon_{11} \\ \epsilon_{22} \\ \epsilon_{33} \\ \epsilon_{12} \\ \epsilon_{23} \\ \epsilon_{31} \end{bmatrix} = \begin{bmatrix} 1/E_{11} & -V_{21}/E_{22} & -V_{31}/E_{33} & 0 & 0 & 0 \\ -V_{12}/E_{11} & 1/E_{22} & -V_{32}/E_{33} & 0 & 0 & 0 \\ -V_{13}/E_{11} & -V_{23}/E_{22} & 1/E_{33} & 0 & 0 & 0 \\ 0 & 0 & 0 & 1/G_{12} & 0 & 0 \\ 0 & 0 & 0 & 0 & 1/G_{23} & 0 \\ 0 & 0 & 0 & 0 & 0 & 1/G_{31} \end{bmatrix} \begin{bmatrix} \sigma_{11} \\ \sigma_{22} \\ \sigma_{33} \\ \sigma_{12} \\ \sigma_{23} \\ \sigma_{31} \end{bmatrix} \quad (3.8)$$

where the subscript 1,2 and 3 refer to the x_1, x_2 and x_3 axes of the cord.

The remaining constants in equation (3.8) can be defined in terms of the known five independent constants as:

$$\left. \begin{aligned} V_{13} &= V_{12} \\ V_{32} &= V_{23} \\ G_{31} &= G_{12} \\ E_{33} &= E_{22} \end{aligned} \right\} (3.9.a)$$

by using symmetry of the x_2, x_3 axes together with

$$G_{23} = E_{22}/2(1+V_{23}) \quad (3.9.b)$$

and from the symmetry requirement of equation (3.8) we have

$$\left. \begin{aligned} V_{21} &= E_{22} V_{12}/E_{11} \\ V_{31} &= E_{33} V_{13}/E_{11} = E_{22} V_{12}/E_{11} \end{aligned} \right\} (3.9.c)$$

3.2.3 Laminate properties

When a set of parallel fibres are embedded in a rubber matrix it forms a laminate as shown in Figure 3.8. The angle β which the cords make with the x_1 axis represents the bias angle of the ply. With reference to the x_1, x_2, x_3 axes, the laminate is assumed to behave as being homogeneous and orthotropic on the macroscopic scale. As such, Hooke's law for the three dimensional body can be written as:

$$\begin{bmatrix} \sigma_{11} \\ \sigma_{22} \\ \sigma_{12} \\ \sigma_{23} \\ \sigma_{31} \end{bmatrix} = \begin{bmatrix} D_{11} & D_{12} & D_{13} & 0 & 0 \\ & D_{22} & D_{23} & 0 & 0 \\ & & D_{33} & 0 & 0 \\ \text{symmetric} & & & D_{44} & D_{45} \\ & & & & D_{55} \end{bmatrix} \begin{bmatrix} \epsilon_{11} \\ \epsilon_{22} \\ \epsilon_{12} \\ \epsilon_{23} \\ \epsilon_{31} \end{bmatrix} \quad (3.10)$$

In the above matrix, the stresses and strains associated with the x_3 direction have been ignored. This simplification is based on the usual shell theory assumption that these components of the stress and strain vector are negligible compared with the membrane effects.

The constants D_{ij} , for $i, j = 1$ to 5 , can be evaluated according to the equations derived by Hermans [26]. These are quite cumbersome, whereas the equations for the two-dimensional case,

i.e. D_{ij} for $i, j = 1$ to 3 ,

as given by Gough [18] are easier to handle and lead to almost identical results. For a single cord layer of bias angle ϕ_k , representing the k^{th} ply of a composite lamina, the constants are:

$$(D_{11})_k = K_r + \frac{K_k}{t_k} \cos^4 \phi_k \quad (3.11)$$

$$(D_{12})_k = (D_{21})_k = K_r V_r + \frac{K_k}{t_k} \sin^2 \phi_k \cos^2 \phi_k \quad (3.12)$$

$$(D_{13})_k = (D_{31})_k = \frac{K_k}{t_k} \sin \phi_k \cos^3 \phi_k \quad (3.13)$$

$$(D_{22})_k = K_r + \frac{K_k}{t_k} \sin^4 \phi_k \quad (3.14)$$

$$(D_{23})_k = (D_{32})_k = \frac{K_k}{t_k} \sin^3 \phi_k \cos \phi_k \quad (3.15)$$

$$(D_{33})_k = G_r + \frac{K_k}{t_k} \sin^4 \phi_k \quad (3.16)$$

$$\text{where} \quad K_r = \frac{E_r}{(1-V_r)^2} \quad (3.17)$$

$$\text{and} \quad K_k = E_{c_k} \cdot A_k \cdot n_k \quad (3.18)$$

G_r = shear modulus for rubber

E_r = Young's modulus for rubber

V_r = Poisson's ratio for rubber

E_{c_k} = Young's modulus for cord in k^{th} ply.

t_k = thickness of the lamina
 A_k = cross-sectional area of the cord
 n_k = number of cords per inch measured
 perpendicular to direction of cords.

Equations (3.11) through to (3.18) can be extended to account for the composite effect of m plies, to give the constants of the composite as expressed in equation (3.10), where

$$D_{ij} = \frac{\sum_{k=1}^m t_k (D_{ij})_k}{\sum_{k=1}^m t_k} \quad (3.19)$$

so that

$$D_{11} = K_r + \frac{1}{T} \sum_{k=1}^m K_k \cos^4 \phi_k \quad (3.20)$$

$$D_{12} = D_{21} = K_r V_r + \frac{1}{T} \sum_{k=1}^m K_k \sin^2 \phi_k \cos^2 \phi_k \quad (3.21)$$

$$D_{13} = D_{31} = \frac{1}{T} \sum_{k=1}^m K_k \sin \phi_k \cos^3 \phi_k \quad (3.22)$$

$$D_{22} = K_r + \frac{1}{T} \sum_{k=1}^m K_k \sin^4 \phi_k \quad (3.23)$$

$$D_{23} = D_{32} = \frac{1}{T} \sum_{k=1}^m K_k \sin^3 \phi_k \cos \phi_k \quad (3.24)$$

$$D_{33} = G_r + \frac{1}{T} \sum_{k=1}^m K_k \sin^4 \phi_k \quad (3.25)$$

and T represents the total thickness of the lamina given by

$$T = \sum_{k=1}^m t_k \quad (3.26)$$

If the construction of the lamina is such that there are an even number of plies, consisting of pairs of plies with equal and opposite bias angle, then equations (3.22) and (3.24) reduce to

$$D_{13} = D_{31} = D_{23} = D_{32} = 0 \quad (3.27)$$

The remaining constants, D_{44} , D_{45} and D_{55} of equation (3.10) represent the shear moduli connected with the x_3 direction. It has been shown by Herman's [26] that for the shear moduli of the cord-rubber composite in the x_3 direction, the cord moduli effects are small compared with the rubber effects. The cords can be treated as rigid inclusions, and since the volume ratios of cord to rubber is usually small, the shear effects of the cords can be ignored.

The effective values of the constants are thus:

$$D_{44} = G_r \quad (3.28)$$

$$D_{45} = 0 \quad (3.29)$$

$$D_{55} = G_r \quad (3.30)$$

3.3 Finite element idealisation

The finite element method is basically a means by which a continuous structure, ideally possessing an infinite number of degrees of freedom, is approximated by dividing the continuum into an assembly of sub-structures, each having a finite number of degrees of freedom. The process can be summarised as follows:

- (a) The continuum is separated by lines or surfaces into a finite set of "finite elements".

- (b) These elements are connected at a discrete number of points, called "nodes", which are situated at the element boundaries. The displacements and rotations of these points form the unknown parameters of the problem.
- (c) The displacements within each element are defined as functions of the nodal displacements. This enables the stiffness properties of the individual structural elements to be computed, usually with reference to a local set of co-ordinate axes which are defined for each element.
- (d) The 'local' stiffness matrix is transformed from the local co-ordinate system to a form relating to the global co-ordinate system of the original complete structure.
- (e) The stiffness matrix of the complete structure, denoted by $[K]$, is assembled by adding the components of individual elemental matrices, using superposition of nodal partitions.
- (f) Equilibrium equations are thus formulated relating the vector of applied nodal forces, $[F]$, to the vector of nodal displacements, $[\delta]$, in the form

$$[F] = [K] [\delta] \quad (3.31)$$

These are a set of simultaneous equations which can be solved by standard techniques.

The actual mechanics of step (e) is dealt with in a later chapter (4.4)

The initial subdivision of the structure into elements is made after due consideration of the problem to be analysed, since the analysis is performed on the substitute structure and the results will be valid only within the degree with which the elemental model approximates to the real problem. The formulation of the element stiffness matrix is such that it obeys the following conditions:

- (a) Equilibrium. The internal forces acting at each nodal point equals the externally applied load at the nodes.
- (b) Compatibility. The element deformation pattern must be chosen so as to ensure that adjacent elements possess displacement continuity in the deformed condition.
- (c) Elastic properties. The relation between applied forces and displacements for each element must be related by the governing equations of elasticity.

The mathematical basis of the finite element method is described in the Appendix.

3.3.1. Element definition

A thick, curved, triangular element, developed by Ziekiewicz [32], was used as the basis of the mathematical model. This type of element was chosen primarily to ensure a good fit to the geometry of the tyre profile, and to permit shear deformation effects to be included. To enable the formulation to be simplified, areal co-ordinates

were used as one of the basic co-ordinate systems of the element.

3.3.1.1 Areal co-ordinates

Consider the triangle 1,2,3, of area A , lying in the $x_1 - x_2$ plane (Figure 3.9). Any point $P(x_1, x_2)$ divides the triangle into three sub-triangles. The areas of these triangles are defined as A_1, A_2, A_3 , where the subscript denotes the number of the opposite corner. Clearly,

$$A_1 + A_2 + A_3 = A \quad (3.32)$$

Then the point P can be represented uniquely by the three areal co-ordinates

$$w_i = A_i/A \quad i = 1, 2, 3 \quad (3.33)$$

where

$$\sum_{i=1}^3 w_i = 1 \quad (3.34)$$

Equation (3.34) indicates that the areal co-ordinates, w_i , are not independent. Further, the equation $w_i = \text{constant}$, represents a line parallel to the side opposite corner i . From equation (3.33) it is clear that

$$0 \leq w_i \leq 1 \quad (3.35)$$

In terms of the rectangular Cartesian co-ordinates, equation (3.33) can be re-written as:

$$w_i = \frac{1}{2} \begin{vmatrix} x_1 & x_2 & 1 \\ x_{1j} & x_{2j} & 1 \\ x_{1k} & x_{2k} & 1 \end{vmatrix}$$

$$\frac{1}{2} \begin{vmatrix} x_{1i} & x_{2i} & 1 \\ x_{1j} & x_{2j} & 1 \\ x_{1k} & x_{2k} & 1 \end{vmatrix} \quad (3.36)$$

or

$$\begin{vmatrix} x_1 & x_2 & 1 \\ x_{1j} & x_{2j} & 1 \\ x_{1k} & x_{2k} & 1 \end{vmatrix}$$

2A

(3.37)

where i, j , and k represent a cyclic permutation of the corner points 1, 2, and 3 of the triangle.

3.3.1.2 Geometry of a curvilinear triangle

Consider a curved surface in space forming a curvilinear triangle whose corner points are

$$P_i (x_1, x_2, x_3) \quad i = 1, 2, 3$$

as shown in Figure (3.10). Let the points

$$P_i (x_1, x_2, x_3) \quad i = 4, 5, 6$$

be the mid-arc points of the sides 1-2, 2-3, and 3-1, respectively.

Then, since each side is defined by three points, they can be

expressed as quadratic functions of the local areal co-ordinates

w_i , $i = 1, 2, 3$, and the global position co-ordinates of the six points

$$P_j(x_1, x_2, x_3) \quad j = 1 \text{ to } 6.$$

Thus the equation of arc 1,4,2 is given by:

$$\begin{bmatrix} x_1 \\ x_2 \\ x_3 \end{bmatrix} = \sum_{j=1,4,2} S_j \begin{bmatrix} x_{1j} \\ x_{2j} \\ x_{3j} \end{bmatrix} \quad (3.38)$$

where, as shown in the Appendix, the S_j are shape functions which have to satisfy the conditions

$$S_m(x_{1n}, x_{2n}, x_{3n}) = \begin{cases} 1 & m = n \\ 0 & m \neq n \end{cases} \quad (3.39)$$

The shape functions satisfying these criteria will thus ensure geometric compatibility across the interfaces of adjacent elements.

With reference to Figures 3.9 and 3.10, the equation of the arc 1,4,2 in the local areal co-ordinates of the curvilinear triangle is:

$$w_3 = 0 \quad (3.40)$$

The corresponding values of the co-ordinates w_1 and w_2 on the arc are

$$\left. \begin{array}{lll} w_2 = 0, & w_1 = 1 & \text{at point 1} \\ w_2 = 0.5, & w_1 = 0.5 & \text{at point 4} \\ w_2 = 1, & w_1 = 0 & \text{at point 2} \end{array} \right\} \quad (3.41)$$

Thus to satisfy conditions (3.39) subject to equations (3.40) and (3.41), the form of the 2nd degree shape function S_j in equation (3.38) is:

$$\left. \begin{array}{l} S_1 = w_1 (2 w_1 - 1) \\ S_2 = w_2 (2 w_2 - 1) \\ S_4 = 4 w_1 w_2 \end{array} \right\} \quad (3.42)$$

A similar argument can be applied to the arcs numbered 2,5,3 and 3,6,1 in Figure 3.10, to yield the remaining shape functions:

$$\left. \begin{aligned} S_2 &= w_3 (2w_3 - 1) \\ S_5 &= 4w_2 w_3 \\ S_6 &= 4w_3 w_1 \end{aligned} \right\} \quad (3.43)$$

The equations defining the three arcs, of the form of equation (3.38), can be combined to define any point on the surface. The resulting equation for any point $P(x_1, x_2, x_3)$ in the global co-ordinate system is

$$\begin{bmatrix} x_1 \\ x_2 \\ x_3 \end{bmatrix} = \sum_{j=1}^6 S_j (w_1, w_2, w_3) \begin{bmatrix} x_{1j} \\ x_{2j} \\ x_{3j} \end{bmatrix} \quad (3.44)$$

3.3.1.3 Geometry of a thick shell element

The concept of a curvilinear triangle can readily be extended to include a thickness dimension which can vary with respect to position within the element. Consider a linear co-ordinate axis, ψ_3 , which is normal to the surface of the triangle, such that the surface of the curvilinear triangle, defined by equation (3.44), represents the surface $\psi_3 = 0$. Further suppose that the surface $\psi_3 = 0$ is the mid-surface of the thick element, as shown in Figure 3.11.

If account is taken of the thickness at each node, i , by using a thickness vector \bar{t}_{3i} in the direction of ψ_3 , then the range of ψ_3 can be normalised to

$$-1 \leq \psi_3 \leq 1 \quad (3.45)$$

The equation of the mid surface $\psi_3 = 0$, in global co-ordinates of any point within the thick element, is

$$\begin{bmatrix} x_1 \\ x_2 \\ x_3 \end{bmatrix} = \sum_{j=1}^6 S_j (w_1, w_2, w_3) \left(\begin{bmatrix} x_{1j} \\ x_{2j} \\ x_{3j} \end{bmatrix} + \frac{\psi_3}{2} \left\{ \bar{t}_{3j} \right\} \right) \quad (3.46)$$

where $\{\bar{t}_{3j}\}$ is a column matrix representing the thickness vector at node j , having the three Cartesian components referred to the global axes as

$$\{\bar{t}_{3j}\} = \begin{bmatrix} t_{3x_1} \\ t_{3x_2} \\ t_{3x_3} \end{bmatrix}_j \quad (3.47)$$

3.3.1.4 Independent curvilinear co-ordinates

The geometry of the curved, thick triangular element has been defined in terms of areal co-ordinates of the mid-surface together with a linear co-ordinate axis normal to the mid-surface, (equation (3.46)). This involves four co-ordinate variables, namely w_i , $i = 1, 2, 3$, and ψ_3 , to represent a three dimensional system. The interdependency of the w_i is given by equation (3.34) as

$$w_1 + w_2 + w_3 = 1 \quad (3.48)$$

A set of three independent curvilinear coordinates ψ_1, ψ_2 , and ψ_3 which are local to the element, can be formed from the four variables above, such that

$$\left. \begin{aligned} \psi_1 &= w_1 \\ \psi_2 &= w_2 \\ 1 - \psi_1 - \psi_2 &= w_3 \end{aligned} \right\} \quad (3.49)$$

The range of the new variables is given by

$$0 \leq \psi_1, \psi_2 \leq 1 \quad (3.50)$$

which lie in the plane of the mid-surface of the element, together with ψ_3 which remains unchanged. Thus ψ_i , $i=1,2,3$, form the local curvilinear co-ordinate system for the element.

3.3.1.5 Element displacement functions

To complete the definition of the element model, it remains only to specify the manner in which the displacement vary throughout an individual element. The finite element approach requires that the displacement at any point within the element should be defined in terms of the nodal displacements. This implies a relationship of the form:-

$$\{u_i\} = [S] \{\delta\}^e \quad (3.51)$$

where $[S]$ is a matrix of shape functions which behave in the same manner as those for the position vector $\{x_i\}$ of equation (3.38), and the vector $\{\delta\}^e$ contains the unknown displacements at specified nodes. In defining the displacements at a node it should be remembered that even for comparatively thick shells, the normals to the mid-surface will remain nearly straight after deformation. This property can be used if the displacements at a node are defined in terms of three Cartesian components of displacement u_1 , u_2 , and u_3 along the global Cartesian axes, together with two rotations of the nodal thickness vector \bar{t}_3 about the local x_1^* and x_2^* axes, as shown in Figure 3.12. The local Cartesian axes, x_i^* , $i=1,2,3$ are fully explained in Section 3.4.

With the five degrees of freedom at each node specified, the displacement functions of equation (3.51) become :

$$\begin{bmatrix} u_1 \\ u_2 \\ u_3 \end{bmatrix} = \sum_{j=1}^M R_j(w_1, w_2, w_3) \begin{bmatrix} u_{1j} \\ u_{2j} \\ u_{3j} \end{bmatrix} + \frac{t_3}{2} t_{3j} \begin{bmatrix} \hat{t}_{1j} \\ -\hat{t}_{2j} \end{bmatrix} \begin{bmatrix} \theta_{2j} \\ \theta_{1j} \end{bmatrix} \quad (3.52)$$

where u_1, u_2, u_3 are the displacements in the directions of the global Cartesian axes, x_1, x_2, x_3 .

R_j are the displacement functions
 t_{3j} is the thickness of the carcass at node j .
 $\hat{t}_{1j}, \hat{t}_{2j}$ are the unit vectors in the directions of x_1^* and x_2^* at node j .
 θ_{1j}, θ_{2j} are rotations about \hat{t}_{1j} and \hat{t}_{2j} respectively, as shown in Figure 3.12, and are assumed small.
 M the number of nodes at which the unknown displacements are specified.

There are two basic possibilities for the range of the summation in equation (3.52). Firstly, the unknowns can be defined at the corner nodes so that for each element there will be fifteen degrees of freedom. The displacement shape functions $R_j, j = 1, 2$ and 3 are chosen to satisfy displacement compatibility between adjacent elements in the same manner that the shape functions S_j of equation (3.44) ensured geometric compatibility, so that

$$R_m(x_{1n}, x_{2n}, x_{3n}) = \begin{cases} 1 & m = n \\ 0 & m \neq n \end{cases} \quad (3.53)$$

Clearly the R_j for $j=1, 2, 3$ must be linear functions of w_1, w_2 and w_3 , so that a convenient form in

$$\begin{aligned} \text{for } M = 3 \quad R_1 &= w_1 \\ R_2 &= w_2 \\ R_3 &= w_3 \end{aligned} \quad \left. \vphantom{\begin{aligned} R_1 &= w_1 \\ R_2 &= w_2 \\ R_3 &= w_3 \end{aligned}} \right\} \quad (3.54)$$

An alternative formulation occurs if all six nodes of the element have unknown displacements. The value of M in equation (3.52) is then six, and the shape functions R_j will be quadratic. In fact, they will be identical with the shape functions S_j which define the element geometry, i.e.

$$\text{for } M = 6 \quad R_j = S_j, \quad j = 1 \text{ to } 6 \quad (3.55)$$

The choice between the two sets of formulae is difficult. Using $M = 3$, the number of unknowns in the problem is reduced, but since the displacement functions are linear within an element, smaller, and hence more, elements will be required to achieve good results. Using $M = 6$, the computer storage required will be greater and the formulation more difficult, although less elements will be required. These problems will be discussed in more detail in later sections.

3.4 Construction of local Cartesian axes, x_i^*

In section 3.2, the elastic properties of tyre structure were modelled as a thick homogeneous orthotropic shell. The principal directions of orthotropy were taken as the bisectors of the angles formed by the crossing of cords in alternate plies. By choosing the x_1^* , x_2^* axes to lie along the directions of orthotropy, the equations derived for material constants (3.10) can be applied directly without any further co-ordinate transformations. Thus the directions of x_1^* and x_2^* are such that they are tangential to the mid-surface of the tyre and lie in the circumferential and meridian directions respectively, as shown in Figure 3.13. The thickness vector at any node i , \bar{t}_{3i} is normal to the mid surface and in the direction of ψ_3 .

A vector in the direction of the tangent to x_1^* at node i , say \bar{t}_{1i} , is perpendicular both to \bar{t}_{3i} and to the global x_1 axis, thus

$$\left\{ \bar{t}_1 \right\}_i = \begin{bmatrix} 1 \\ 0 \\ 0 \end{bmatrix} \times \begin{bmatrix} t_{3x_1} \\ t_{3x_2} \\ t_{3x_3} \end{bmatrix}_i \quad (3.56)$$

$$\text{or} \quad \begin{bmatrix} t_{1x_1} \\ t_{1x_2} \\ t_{1x_3} \end{bmatrix}_i = \begin{bmatrix} 0 \\ -t_{3x_3} \\ t_{3x_2} \end{bmatrix}_i \quad (3.57)$$

Similarly, a vector in the direction of the tangent to x_2^* , say t_{2i} , is mutually perpendicular to \bar{t}_{1i} and \bar{t}_{3i} , so that

$$\left\{ \bar{t}_2 \right\}_i = \left\{ \bar{t}_1 \right\}_i \times \left\{ \bar{t}_3 \right\}_i \quad (3.58)$$

$$\text{or} \quad \begin{bmatrix} t_{2x_1} \\ t_{2x_2} \\ t_{2x_3} \end{bmatrix} = \begin{bmatrix} t_{1x_2} \cdot t_{3x_3} - t_{1x_3} \cdot t_{3x_2} \\ t_{1x_3} \cdot t_{3x_1} \\ -t_{1x_2} \cdot t_{3x_1} \end{bmatrix} \quad (3.59)$$

Associated with \bar{t}_1 , \bar{t}_2 and \bar{t}_3 are the unit vectors \hat{t}_1 , \hat{t}_2 and \hat{t}_3 . These form the local Cartesian axes at any point, denoted by x_1^* , x_2^* and x_3^* in Figure 3.12.

In section 3.3.1.5, the displacements, u_i , of the nodes were formulated in terms of the global co-ordinate system. If the displacements in the local co-ordinate system are required, that is, along the tangents to circumferential and meridian lines and along the normal, then these can be obtained by a simple transformation of the form

$$\begin{bmatrix} u_1^* \\ u_2^* \\ u_3^* \end{bmatrix} = [\lambda] \begin{bmatrix} u_1 \\ u_2 \\ u_3 \end{bmatrix} \quad (3.60)$$

where u_i^* , $i=1,2,3$ are the displacements along the x_i^* axes and $[\lambda]$ is the transformation matrix given by

$$[\lambda] = \begin{bmatrix} t_{1x_1} & t_{1x_2} & t_{1x_3} \\ t_{2x_1} & t_{2x_2} & t_{2x_3} \\ t_{3x_1} & t_{3x_2} & t_{3x_3} \end{bmatrix} \quad (3.61)$$

where the unit vector t_1 has components t_{1x_1} , t_{1x_2} and t_{1x_3} .

3.5 Stresses and strains in local co-ordinates

Equation (3.10) represents the Hookean stress-strain relationship for a flat test piece whose principle axes were denoted as x_1 , x_2 , and x_3 . To conform to the nomenclature of local co-ordinate system x_i^* as defined in section 3.4, equation (3.10) can be re-written as

$$\{\sigma^*\} = [D] \{\epsilon^*\} \quad (3.62)$$

where D is the fifth order matrix as defined in equation (3.10). The stress and strain components $\{\sigma^*\}$ and $\{\epsilon^*\}$ now refer to the local co-ordinate system, such that

$$\{\sigma^*\} = \begin{bmatrix} \sigma_{X_1}^* \\ \sigma_{X_2}^* \\ \sigma_{X_1 X_2}^* \\ \sigma_{X_2 X_3}^* \\ \sigma_{X_3 X_1}^* \end{bmatrix} \quad (3.63)$$

and

$$\{\epsilon^*\} = \begin{bmatrix} \epsilon_{X_1}^* \\ \epsilon_{X_2}^* \\ \epsilon_{X_1 X_2}^* \\ \epsilon_{X_2 X_3}^* \\ \epsilon_{X_3 X_1}^* \end{bmatrix} \quad (3.64)$$

For linear deflection theory, as defined by equation (7.7) of the Appendix, the components of equation (3.67) are given by

$$\epsilon_{x_i}^* x_j^* = \frac{1}{2} \left(\frac{\partial u_i^*}{\partial x_j^*} + \frac{\partial u_j^*}{\partial x_i^*} \right) \quad (3.65)$$

3.6 Calculation of the element stiffness matrix

The general definition of the element stiffness matrix is derived in the Appendix, equation (7.54), as

$$[K]^e = \int_{V_n} [C]^t [D] [C] dV \quad (3.66)$$

where V_n is the volume of the element

dV is the volume of the elementary cube of sides

dx_1, dx_2, dx_3 in global co-ordinates

$[D]$ is the fifth order matrix of material constants

$[C]$ is a matrix relating the global strains in an element

to the nodal displacements, and is defined by the

relationship

$$\{\epsilon\} = [C] \{\delta\}^e \quad (3.67)$$

The formulation of equations (3.66) and (3.67) are with respect to the global Cartesian axes, x_1, x_2 and x_3 , where the components of the column matrix $\{\epsilon\}$ are

$$\epsilon_{ij} = \frac{1}{2}(u_{i,j} + u_{j,i}) \quad (3.68)$$

and $\{\delta\}^e$ represent the global displacements of the element mid-surface

nodes at which point the displacements are unknown i.e.

$$\{\delta\}^e = \begin{Bmatrix} \delta_i \\ \delta_j \\ \cdot \\ \cdot \\ \cdot \\ \delta_M \end{Bmatrix} \quad (3.69)$$

where δ_i refers to the displacements at node i , given by

$$\{\delta_i\} = \begin{bmatrix} u_{1i} \\ u_{2i} \\ u_{3i} \\ \theta_{1i} \\ \theta_{2i} \end{bmatrix} \quad (3.70)$$

The volume V_n of equation 3.66 throughout which the integration is taken is also expressed in terms of global co-ordinates, such that an infinitesimal cube of the element has a volume:

$$dV = dx_1 \cdot dx_2 \cdot dx_3 \quad (3.71)$$

If the integrand of equation(3.66) is formulated in terms of the local curvilinear co-ordinate set, ψ_1, ψ_2, ψ_3 of the elementary triangle, and the infinitesimal volume dV of equation (3.71) is similarly transformed, then the integration limits become simple. The resulting numerical integration, as discussed in section (4.3) , becomes relatively easy to programme.

3.6.1 Transformation of strain components

The strain vector $\{\epsilon\}$ of equation (3.67) contains terms of the

form

$$\frac{\partial u_i}{\partial x_j} \quad i, j = 1, 2, 3$$

which are derivatives of displacements in the global co-ordinate system.

In the definition of the displacement functions within an element, equation (3.52), the global displacements u_1 , u_2 and u_3 are expressed as functions of the local areal co-ordinates, w_1 , w_2 and w_3 , and ψ_3 . By using a change of variable as given by equation (3.49), u_1 , u_2 and u_3 can be written as functions of ψ_1 , ψ_2 and ψ_3 .

A relationship between derivatives of u_1 , u_2 , u_3 with respect to both the curvilinear co-ordinates ψ_1 , ψ_2 , ψ_3 and global co-ordinates x_1, x_2, x_3 is expressible in the form:

$$\frac{\partial u_i}{\partial \psi_j} = \frac{\partial u_i}{\partial x_k} \frac{\partial x_k}{\partial \psi_j} \quad (3.72)$$

where the repeated suffix denotes summation. Equation (3.72) can be considered as the components of a matrix $[\Delta]$, given by

$$[\Delta] = \begin{bmatrix} \frac{\partial u_1}{\partial \psi_1} & \frac{\partial u_2}{\partial \psi_1} & \frac{\partial u_3}{\partial \psi_1} \\ \frac{\partial u_1}{\partial \psi_2} & \frac{\partial u_2}{\partial \psi_2} & \frac{\partial u_3}{\partial \psi_2} \\ \frac{\partial u_1}{\partial \psi_3} & \frac{\partial u_2}{\partial \psi_3} & \frac{\partial u_3}{\partial \psi_3} \end{bmatrix} \quad (3.73)$$

Further, equation (3.72) can be written in matrix form as

$$[\Delta] = [J] [U] \quad (3.74)$$

where

$$[J] = \begin{bmatrix} \partial x_1 / \partial \psi_1 & \partial x_2 / \partial \psi_1 & \partial x_3 / \partial \psi_1 \\ \partial x_1 / \partial \psi_2 & \partial x_2 / \partial \psi_2 & \partial x_3 / \partial \psi_2 \\ \partial x_1 / \partial \psi_3 & \partial x_2 / \partial \psi_3 & \partial x_3 / \partial \psi_3 \end{bmatrix} \quad (3.75)$$

and

$$[U] = \begin{bmatrix} \partial u_1 / \partial x_1 & \partial u_2 / \partial x_1 & \partial u_3 / \partial x_1 \\ \partial u_1 / \partial x_2 & \partial u_2 / \partial x_2 & \partial u_3 / \partial x_2 \\ \partial u_1 / \partial x_3 & \partial u_2 / \partial x_3 & \partial u_3 / \partial x_3 \end{bmatrix} \quad (3.76)$$

In equation (3.75), $[J]$ represents the Jacobian of transformation from the global x_i co-ordinate system to the local ψ_i system. The components of the strains in the global system, $\{\epsilon\}$ are contained in the matrix $[U]$ of equation (3.76). Inverting equation (3.74) gives $[U]$ explicitly as:

$$[U] = [J]^{-1} [\Delta] \quad (3.77)$$

In order to form the strain matrix $\{\epsilon\}$, the elements of the matrices $[J]$, and hence $[J]^{-1}$, and $[\Delta]$ are required.

(a) Components of matrix $[\Delta]$

The general term of $[\Delta]$, as given by equation (3.72) is

$$\partial u_i / \partial \psi_j \quad (3.78)$$

In the definition of the global displacements, u_i , of equation (3.52), the variables involved are w_1 , w_2 , w_3 and ψ_3 . To evaluate terms of the form (3.78), relationships are required

between derivatives of u_i with respect to ψ_1, ψ_2, ψ_3 , and derivatives with respect to w_1, w_2, w_3, ψ_3 . These are given by

$$\frac{\partial u_i}{\partial \psi_j} = \frac{\partial u_i}{\partial w_1} \frac{\partial w_1}{\partial \psi_j} + \frac{\partial u_i}{\partial w_2} \frac{\partial w_2}{\partial \psi_j} + \frac{\partial u_i}{\partial w_3} \frac{\partial w_3}{\partial \psi_j} + \frac{\partial u_i}{\partial \psi_3} \frac{\partial \psi_3}{\partial \psi_j} \quad (3.79)$$

for $i, j = 1, 2, 3$

These expressions can be simplified by using the conditions of equation (3.49), so that

$$\left. \begin{aligned} \frac{\partial u_i}{\partial \psi_1} &= \frac{\partial u_i}{\partial w_1} - \frac{\partial u_i}{\partial w_3} \\ \frac{\partial u_i}{\partial \psi_2} &= \frac{\partial u_i}{\partial w_2} - \frac{\partial u_i}{\partial w_3} \\ \frac{\partial u_i}{\partial \psi_3} &= \frac{\partial u_i}{\partial \psi_3} \end{aligned} \right\} \quad i = 1, 2, 3 \quad (3.80)$$

Using equation (3.52) with the relevant form of R_j , $j = 1$ to M , the expressions (3.80) can be evaluated. Consider first the case where $M = 3$. The expressions for R_j are as in equation (3.54). Then the analytical form of equation (3.80) is

$$\frac{\partial u_i}{\partial \psi_1} = u_i + \psi_3 \frac{t_3}{2} (t_{1x_i} \theta_2 - t_{2x_i} \theta_1) \Big|_{(1-3)} \quad (3.81)$$

$$\frac{\partial u_i}{\partial \psi_2} = u_i + \psi_3 \frac{t_3}{2} (t_{1x_i} \theta_2 - t_{2x_i} \theta_1) \Big|_{(2-3)} \quad (3.82)$$

$$\frac{\partial u_i}{\partial \psi_3} = u_i + \psi_3 \frac{t_3}{2} (t_{1x_i} \theta_2 - t_{2x_i} \theta_1) \Big|_{(1+2+3)} \quad (3.83)$$

where the notation

$$(m-n)$$

indicates that the expression is evaluated at node m and at node n and the results subtracted.

Equations (3.81), (3.82) and (3.83) are valid for $i=1, 2$ and 3 . They are explicit in terms of the displacements u_1, u_2, u_3 and the rotations θ_1, θ_2 of the element mid-surface corner nodes, which constitutes the unknown parameters of the tyre deflection problem. To separate the unknowns, the 3×3 matrix $[\Delta]$ can be written in terms of a 9×1 column matrix $\{\Delta'\}$, such that

$$\{\Delta'\} = [\gamma] \{\delta\}^e \quad (3.84)$$

where

$$\{\Delta'\} = \begin{bmatrix} \partial u_1 / \partial \psi_1 \\ \partial u_1 / \partial \psi_2 \\ \partial u_1 / \partial \psi_3 \\ \partial u_2 / \partial \psi_1 \\ \partial u_2 / \partial \psi_2 \\ \partial u_2 / \partial \psi_3 \\ \partial u_3 / \partial \psi_1 \\ \partial u_3 / \partial \psi_2 \\ \partial u_3 / \partial \psi_3 \end{bmatrix} \quad (3.85)$$

and $\{\delta\}^e$ is the 15×1 matrix of displacements and rotations as described by equations (3.69) and (3.70).

The matrix $[\gamma]$ will be of order 9×15 , and is tabulated explicitly in Table 3.1.

If $M=6$, the matrix $\{\delta\}^e$ now contains thirty elements, equivalent to the five degrees of freedom at each of the six nodes. A similar set of equations to (3.81), (3.82) and (3.83) can be derived, but they are cumbersome. However, they can be expressed in a form similar to equation (3.84), where now $[y]$ will be a 9×30 matrix, as shown in Table 3.2.

(b) Components of the matrix $[J]$

The general term of matrix $[J]$ is of the form

$$\frac{\partial x_i}{\partial \psi_j} \quad i, j = 1, 2, 3$$

This can be expressed in a form analogous to equation (3.79) as

$$\frac{\partial x_i}{\partial \psi_j} = \frac{\partial x_i}{\partial w_1} \frac{\partial w_1}{\partial \psi_j} + \frac{\partial x_i}{\partial w_2} \frac{\partial w_2}{\partial \psi_j} + \frac{\partial x_i}{\partial w_3} \frac{\partial w_3}{\partial \psi_j} + \frac{\partial x_i}{\partial \psi_3} \frac{\partial \psi_3}{\partial \psi_j} \quad (3.86)$$

which can be simplified to

$$\left. \begin{aligned} \frac{\partial x_i}{\partial \psi_1} &= \frac{\partial x_i}{\partial w_1} - \frac{\partial x_i}{\partial w_3} \\ \frac{\partial x_i}{\partial \psi_2} &= \frac{\partial x_i}{\partial \psi_2} - \frac{\partial x_i}{\partial \psi_3} \\ \frac{\partial x_i}{\partial \psi_3} &= \frac{\partial x_i}{\partial \psi_3} \end{aligned} \right\} \quad i = 1, 2, 3 \quad (3.87)$$

Hence using the definition of x_i , $i=1,2,3$ as given by equation (3.44) together with the shape functions S_j , $j=1$ to 6 in equations (3.42) and (3.43), equations (3.87) becomes:

$$\begin{aligned} \frac{\partial x_i}{\partial \psi_1} &= (4w_2 - 1)f_i \Big|_1 - (4w_3 - 1)f_i \Big|_3 + 4w_2 f_i \Big|_4 - 4w_2 f_i \Big|_5 \\ &\quad + 4(w_3 - w_1)f_i \Big|_6 \end{aligned} \quad (3.88)$$

where

$$f_i = x_i + \frac{\psi_3}{2} \cdot t_{3x_i} \quad (3.89)$$

together with

$$\frac{\partial x_i}{\partial \psi_2} = (4w_2-1)f_i \Big|_2 - (4w_3-1)f_i \Big|_3 + 4w_1 f_i \Big|_4 + 4(w_3-w_2)f_i \Big|_5 - 4w_1 f_i \Big|_6 \quad (3.90)$$

and

$$\begin{aligned} \frac{\partial x_i}{\partial \psi_3} = & \frac{w_1}{2} (2w_1-1) t_{3x_i} \Big|_1 + \frac{w_2}{2} (2w_2-1) t_{3x_i} \Big|_2 + \frac{w_3}{2} (2w_3-1) t_{3x_i} \Big|_3 \\ & + 2w_1 w_2 t_{3x_i} \Big|_4 + 2w_2 w_3 t_{3x_i} \Big|_5 + 2w_3 w_1 t_{3x_i} \Big|_6 \end{aligned} \quad (3.91)$$

Equations (3.88) to (3.91) are valid for $i=1,2$ and 3 .

Having evaluated the matrices $[\Delta]$ and $[J]$, the matrix $[U]$ in equation (3.77) can be evaluated, the general term being of the form

$$\frac{\partial u_i}{\partial x_j}$$

In tensorial form this can be written as

$$u_{i,j}$$

where the comma denotes differentiation with respect to the variable x_j . To enable the strain components to be evaluated in the local co-ordinate system, which involves terms of the form

$$* u_{i,j}$$

$$\text{where } u_{i,j}^* = \partial u_i^* / \partial x_j^* \quad (3.92)$$

it is necessary to subject the second order tensor $u_{i,j}$ to a transformation of axes from the global to the local system. This is defined by

$$u_{i,j}^* = \lambda_{im} \lambda_{jn} u_{m,n} \quad (3.93)$$

where λ_{im} , $i,m = 1,2,3$ are the direction cosines between the local and global Cartesian axes, as given in equation (3.61), and the repeated suffix denotes summation.

In matrix form, (3.93) can be re-written as

$$[U^*] = [\lambda] [U] [\lambda]^T \quad (3.94)$$

where

$$[U^*] = \begin{bmatrix} u_{1,1}^* & u_{2,1}^* & u_{3,1}^* \\ u_{1,2}^* & u_{2,2}^* & u_{3,2}^* \\ u_{1,3}^* & u_{2,3}^* & u_{3,3}^* \end{bmatrix} \quad (3.95)$$

Using equation (3.77), equation (3.94) becomes

$$[U^*] = [\lambda] [J]^{-1} [\Delta] [\lambda]^T \quad (3.96)$$

Since $[\Delta]$ is a function of the element node displacements $\{\delta\}^e$, as shown in equation (3.84) then so will be $[U^*]$. By appropriate choice of components of $[U^*]$, the local strain matrix, $\{\epsilon^*\}$, can be expressed in a form analogous to equation (3.67) as

$$\{\epsilon^*\} = [C^*] \{\delta\}^e \quad (3.97)$$

This enables the stiffness matrix of the element, equation (3.66) to be computed using the local axes ψ_1, ψ_2, ψ_3 as the integration variables. The modified form of the equation is thus:-

$$[K]^e = \int_{V_n} [C^*]^T [D] [C^*] |J| d\psi_1, d\psi_2, d\psi_3 \quad (3.98)$$

where $|J|$ is the determinant of the Jacobian of transformation from global to local co-ordinates.

Implementation of the finite element method4.1 Formation of element mesh pattern

In section 3, the mathematical model for the pneumatic tyre was obtained by dividing the structure into a pattern of curved, triangular, thick shell elements and then determining a stiffness matrix $[K]^e$ for each element. These matrices are to be combined to simulate the assemblage of the complete structure, resulting in a set of linear simultaneous equations of the form:

$$\{F\} = [K] \{\delta\} \quad (4.1)$$

where $\{F\}$ is the vector of all the nodal forces

$[K]$ is the stiffness matrix of the complete structure

and $\{\delta\}$ is the vector of all the nodal displacements.

The solution of equation (4.1) will be subject to the prescribed boundary condition.

Before the stiffness matrix of an element can be calculated and assembled into the total stiffness matrix of the structure, the following information is required to define the element.

- (a) The position of each of the six nodes, (three corner nodes and three mid-side nodes), which define the mid-surface of the element, with reference to the global Cartesian coordinate axes.
- (b) The three Cartesian components of the vector representing the thickness of the element at the six nodes.

- (c) An element number and its associated six node numbers, such that the element assembly is uniquely defined.

For a typical problem of the type tackled in this study, there may be about 100 elements with a total number of nodes in the region of 250. This would entail in excess of 2000 items of initial data in order to specify the problem configuration. Clearly the probability of a data error would be high, and the checking laborious, if all this information was manually determined.

To overcome this problem, programmes have been developed to automatically generate the element mesh pattern, node and element numbering schemes, node coordinates and thickness vector components, with only the minimum of data preparation. These programmes use the property that the tyre can be considered as a shell of revolution, formed by rotation about the axis of the wheel. This permits the simple calculation of Cartesian coordinates and thickness vectors at any point of the tyre surface, from an initial description of the cross-sectional profile. A variable pattern generator is used to determine the element mesh configuration and its associated node sequencing.

To obtain a good approximation to the solution, it would be advantageous to use a large number of small elements. Computer time and storage requirements, however, impose restrictions on the extent to which this is possible, and necessitates that the nodes at which displacements are to be calculated are positioned to the greatest advantage.

In the pneumatic tyre under radial load, large displacements occur within the first 30 to 40 degrees from the centre of the contact patch, and gradually reduce to almost zero at 180 degrees. Thus the nodes should preferably be concentrated within the proximity of the contact region, so as to obtain good estimates in the region of high stress gradients. This can be readily overcome by considering the mid-surface of the tyre to be initially sub-divided into curvilinear quadrilateral elements whose corners lie at the intersection of circumferential lines and meridian planes, as shown in Figure 4.1. The required "triangular" elements can then be obtained by completing a diagonal of the quadrilateral elements.

By allowing the angle between successive meridian planes to increase with respect to the angle from the centre of contact, $\theta = 0$, smaller elements will be obtained in the region of interest. This is illustrated in Figure 4.2, where the mid-surface is developed into a rectangular section.

The sequence of angle increments is taken an arithmetic progression, whose common difference is $k\theta$, where

θ is the angle between the centre line and the first meridian plane

k is a factor chosen to compress the planes towards the centre line.

Since the total number of planes, N , will have to be defined for a particular problem, the only other piece of information required in the factor k . This permits the angles of all the meridian planes to be calculated since:

$$\theta + (\theta+k\theta) + \dots + (\theta+(N-2)k\theta) = \Pi$$

$$\therefore \theta = \frac{2\Pi}{(N-1)(2+k(N-2))} \quad (4.2)$$

The effect of altering k for a fixed value of N is shown in Figure 4.3, resulting in a typical element mesh pattern as depicted in Figure 4.4(a).

Further, by allowing the number of nodes along the meridian planes to reduce as the angle from the centre of contact increases, fewer elements will be required, and the elements thus formed will tend to become more equilateral in the form (Figures 4.4(b) and 4.4(c)). Thus for a fixed available computer storage, the number of nodes in the high stress regions can be increased.

To finalise the mesh configuration, it remains only to sequence the elements and to number the nodes associated with each element. Provided the node numbering system enables the structure to be uniquely defined, then any random choice will provide the same solution. However, a specific ordering is essential to minimise the amount of computer storage required. This is discussed further when dealing with assembling the stiffness matrix $[K]$ of equation (4.1).

4.2 Nodal coordinates and associated thickness vector

The position of any node coincides with the intersection of a circumferential line with a meridian plane on the mid-surface. The global Cartesian coordinates of any point can thus be obtained from

the cross-sectional profile of the mid-surface in the x_1 - x_2 plane for the inflated tyre. Two regions require special consideration.

(a) Bead region.

The bead region is a rigid assembly of steel, cords, and rubber. The problem of defining precisely the properties of this region can be avoided if it is assumed that the effect of the bead is to fix the tyre to the wheel rim. In Figure 4.5 the point A represents the contact point of the tyre and wheel flange. The boundary node is chosen to lie at the centre of the line AA'. Then the rigidity of the bead region can be approximated to by ensuring that the position of the boundary node remains fixed for all tyre deformations.

(b) Breaker edge region.

The material constants associated with both the breaker region and sidewall region for a radial tyre can be calculated as detailed in section 3.2. In most production tyres, the position of the interface cannot be precisely determined, since not all the breaker plies will end at exactly the same circumferential line. There will be a region between the breaker and sidewall over which the material properties will change in a continuous manner. However, the simple concept of a discontinuous boundary will be adopted, and is achieved by positioning an element corner node such that it lies at the approximate breaker/sidewall interface.

Once the nodal co-ordinates in the x_1 - x_2 plane have been established, the remaining nodes which lie on the same circumferential lines can be calculated by a rotation about the x_1 axis, given by

$$\begin{bmatrix} x'_1 \\ x'_2 \\ x'_3 \end{bmatrix} = \begin{bmatrix} 1 & 0 & 0 \\ 0 & \cos \theta & -\sin \theta \\ 0 & \sin \theta & \cos \theta \end{bmatrix} \begin{bmatrix} x_1 \\ x_2 \\ x_3 \end{bmatrix} \quad (4.3)$$

where θ is the angle of rotation of the meridian plane from the initial profile, $\theta=0^\circ$.

Associated with each node on the initial profile is a thickness vector \bar{t}_3 , given by

$$\{\bar{t}_3\} = \begin{bmatrix} t_{3x_1} \\ t_{3x_2} \\ t_{3x_3} \end{bmatrix} \quad (4.4)$$

The thickness of the carcass, $|\bar{t}_3|$, is first determined for all nodes on the cross-sectional profile. The angle between the outward normal to the mid-surface and the x_1 axis, denoted by β , is also measured at each node, so enabling the components of \bar{t}_3 to be derived as

$$\{\bar{t}_3\} = |\bar{t}_3| \cdot \begin{bmatrix} \cos \beta \\ \sin \beta \\ 0 \end{bmatrix} \quad (4.5)$$

By a subsequent rotation corresponding to the required meridian plane, the components of the new vector, \bar{t}'_3 , associated with a node on the same circumferential line, can be found as

$$\{\bar{t}'_3\} = |\bar{t}_3| \cdot \begin{bmatrix} \cos \beta \\ \sin \beta \cdot \cos \theta \\ \sin \beta \cdot \sin \theta \end{bmatrix} \quad (4.6)$$

4.3 Numerical integration

Having divided the structure into elements, the stiffness matrix for the individual element, as derived in section 3.6, is given by

$$[K]^e = \int_V [S] d(\text{vol}) \quad (4.7)$$

where V is the element volume and $[S]$ is a matrix dependant upon spatial position and material properties of the element.

In terms of local curvilinear co-ordinates ψ_1, ψ_2 , and ψ_3 , equation (4.7) can be expressed as

$$[K]^e = \int_{-1}^1 \int_0^{1-\psi_1} \int_0^{1-\psi_1-\psi_2} [S] \det[J] d\psi_1 d\psi_2 d\psi_3 \quad (4.8)$$

Curvilinear co-ordinates are used to make the numerical solution of equation (4.8) straightforward. The integration technique suggested by Zienkiewicz [33] was used, which incorporates expressions developed by Hammer [34] for the $\psi_1-\psi_2$ plane of the triangle, together with a Gaussian Quadrature formula (Lanczos [35]) for integration through the thickness of the element, ψ_3 . Tables for both integration formulae are given in Tables 4.1 and 4.2.

The integration over the triangle is reduced to the form

$$\int_0^1 \int_0^{1-\psi_1} f(\psi_1, \psi_2) d\psi_1 d\psi_2 = \sum_{i=1}^m F_i \cdot f(\psi_{1i}, \psi_{2i}) \quad (4.9)$$

and for the ψ_3 direction

$$\int_{-1}^1 g(\psi_3) d\psi_3 = \sum_{j=1}^n G_j \cdot g(\psi_{3j}) \quad (4.10)$$

so that equation (4.8) becomes

$$[K]^e = \sum_{j=1}^n \sum_{i=1}^m F_i \cdot G_j \cdot h(\psi_{1i}, \psi_{2i}, \psi_{3j}) \quad (4.11)$$

where n represents the number of integration points for Gaussian quadrature

m represents the number of integration points for triangular integration

F_i are the weighting factors for triangular integration

G_j " " " " " Gaussian quadrature

and $h(\psi_{1i}, \psi_{2i}, \psi_{3j})$ is the functional of equation (4.8) evaluated at a particular point in the element.

4.3.1 Accuracy of numerical integration

The number of integrating points used in any direction is important in ensuring a good approximation to the integral. It has been shown by Zienkiewicz [32] and Irons [36] that the integration process will converge if its order is sufficient to evaluate precisely the element volume. For an element of the type used, a minimum of three points, situated at the mid-side nodes, would be sufficient to estimate the volume. This is shown by the second figure in Table 4.1. Ahmad [37], recommends that more points should be used to obtain a more exact value of the integral by taking the points shown in the fourth figure of Table 4.1, together with a two point

Gaussian integration in the ψ_3 direction.

More recent work by Zienkiewicz [38] and Pawsey [39] has shown that considerable improvement can be achieved by using the minimum integration order.

4.3.2 Explicit integration

Although it is not possible to obtain a complete explicit solution to the triple integral of equation (4.8), Zienkiewicz [38] has reduced the problem to that of a double integral over the ψ_1 - ψ_2 domain. His method assumes that the matrix of direction cosines $[\lambda]$ of the local co-ordinate axes (equation 3.61) is constant with variations of ψ_3 . It has been estimated that a saving of 50% on the calculation time for the element stiffness matrix can be achieved. However, the programming is more involved, and at the present time this method has not been adopted.

4.4 Formation of the total stiffness matrix

The stiffness matrix of each element, $[K]^e$, is derived in terms of displacements at nodal points. For all elements, the displacements are with respect to a fixed base system, namely the global Cartesian axes for the three translation components and the local mid-surface co-ordinate axes for the two rotation components.

In order to obtain the total stiffness matrix, $[K]$, of the complete structure it is necessary to superimpose sub-matrices of each $[K]^e$ so as to simulate the nodal connections between adjacent elements. To make efficient use of the computer storage space required for $[K]$, the numbering sequence of the nodes is important.

The node numbering system is dependent upon whether displacements are defined at all the nodes of a particular element or at only the corner nodes, denoted respectively by $M=6$ and $M=3$ in equation (3.52).

(a) $M=3$

Consider the mesh pattern shown in Figure 4.6a. Since the displacements of the corner nodes alone are required in equation (3.52), prime consideration is given to their sequencing. The mid-side nodes can be numbered in any unique manner. The particular equilibrium equations for the element E of Figure 4.6a is

$$\{F\}^e = [K]^e \{\delta\}^e \quad (4.12)$$

where, in terms of the node numbers 7,8, and 12 of element E, equation (4.12) can be expressed as

$$\begin{Bmatrix} F_7 \\ F_8 \\ F_{12} \end{Bmatrix} = \begin{bmatrix} k_{7,7} & k_{7,8} & k_{7,12} \\ k_{8,7} & k_{8,8} & k_{8,12} \\ k_{12,7} & k_{12,8} & k_{12,12} \end{bmatrix} \begin{Bmatrix} \delta_7 \\ \delta_8 \\ \delta_{12} \end{Bmatrix} \quad (4.13)$$

where

$$\{F_i\} = \begin{bmatrix} F_{x1} \\ F_{x2} \\ F_{x3} \\ M_{\theta_1} \\ M_{\theta_2} \end{bmatrix}_i \quad i=7,8,12 \quad (4.14)$$

and

$$\{\delta_j\} = \begin{bmatrix} u_1 \\ u_2 \\ u_3 \\ \theta_1 \\ \theta_2 \end{bmatrix}_j \quad j=7,8,12 \quad (4.15)$$

and $k_{i,j}$ is a 5×5 array, expressing the partitioned form of $[K]^e$.

The nine sub-matrices of $[K]^e$ are superimposed into the overall stiffness matrix $[K]$, having regard to the nodal numbering. The relative positions in which the partitions appear is shown in Figure 4.7a. The banded nature of $[K]$ is characteristic of finite element problems. Furthermore, since the matrix $[K]$ is symmetric, the storage requirements can be condensed to that of a rectangular array of dimensions $n \times m$, as shown in Figure 4.8, where n is the number of unknown displacements and m is the semi-bandwidth.

The value of m is obtained from the node numbering sequence by recording the maximum difference, d , between the corner nodes of an element. Then m is given by

$$m = f \cdot (d+1) \quad (4.16)$$

where f is the number of degrees of freedom at each node (five). From Figure 4.6a, $d=5$, and hence $m=30$, as illustrated in Figure 4.7a. The node numbering problem is thus reduced to ensuring that d is a minimum, so that the storage requirement for the rectangular version of $[K]$ is also minimised. This has been achieved for the mesh pattern of Figure 4.6a, although this sequence of numbering is not unique.

4.5 Boundary conditions

The set of equations (4.1) represent a singular system. To evaluate a unique solution, boundary conditions in the form of prescribed forces or displacements must be applied so as to prevent rigid body movements of the structure.

4.5.1 Initial boundary conditions

These represent the physical situation of the tyre mounted on a fixed wheel. In the case of a flat plate load, symmetry about two axes enables one quarter of the tyre, together with relevant boundary conditions, to simulate the behaviour of the complete structure. For the developed section shown in Figure 4.1, each side possesses different types of boundary conditions. Only the nodes on the boundaries are affected by the initial conditions.

(a) Boundary 1

This represents a circumferential line near to the bead of the tyre. It will be assumed that points on this line are fixed, so that the u_1, u_2 and u_3 components of displacement are all zero. Furthermore, the rotations θ_1 and θ_2 about the local x_1^* and x_2^* axes will be small and can be ignored.

(b) Boundary 2

This is the line of symmetry of the circumferential line passing through the crown points of the tyre. Thus along this edge u_1 and θ_1 will be zero.

(c) Boundary 3 and 4

These boundaries lie on the axis of symmetry of the contact area centre line. For points on these edges, both u_3 and θ_2 are zero.

A summary of these results is given in Table 4.3

4.5.2 Deflected boundary conditions

The effect of subjecting the tyre to different loading conditions, such as static load, braking, or cornering, can be simulated by a set of boundary conditions. These can be applied in two distinct ways.

(a) Forces specified.

Research work by Gough [40] and Clark [41] has shown that the pressure distribution inside the contact area is extremely complex. Using the finite element method, the continuous force distribution is approximated by a set of discrete forces acting at the node points located inside the contact region. Attempts by Dunn [11] to analyse a loaded tyre by using a Fourier series solution were inconclusive

(b) Displacements specified.

If the contact pressure distribution is considered as being the result of applied deflections rather than the cause, the boundary conditions can be defined in terms of initial displacements. Using this method, the result of a load applied by contact with a flat plate can easily be simulated. It is only necessary to scan through the global (x_1, x_2, x_3) co-ordinates of the node points to detect which lie below the boundary plane, as shown in Figure 4.9. Then the displacement in the x_2 direction for such a node is given by

$$(u_2)_i = (x_2)_{\max} + \delta - (x_2)_i \quad (4.18)$$

where $(x_2)_i$ is the x_2 co-ordinate of node i

$(x_2)_{\max}$ is the maximum x_2 co-ordinate of the tyre

δ is the applied deflection (positive)

This will ensure that all points inside the region cut off by the plane of contact remain upon it. However, points which are close to the edge of the contact area will tend to move away from the plane. The special treatment necessary for these points is dealt with later.

Having fixed a value for u_2 , then the displacements in the other directions can either be fixed at zero to simulate a high friction surface, or permitted to move freely as in the case of a lubricated surface.

4.6 Implementation of boundary conditions

To solve equations (4.1) subject to the boundary conditions determined above, consider the i^{th} equation given by

$$k_{i1}d_1 + k_{i2}d_2 + \dots + k_{ii}d_i + \dots + k_{in}d_n = f_i \quad (4.19)$$

where k_{ij} are the components of matrix $[K]$ which is of order n .

d_j are the n unknown degrees of freedom, representing displacements and rotations.

f_i are the components of the force vector.

Suppose the displacements d_i is prescribed by a boundary condition, say

$$d_i = D \quad (4.20)$$

Then the set of equations (4.1) can be modified in the following manner :

- (a) Multiply the diagonal term, k_{ii} , of $[K]$ by a large number, say 10^{10} .
- (b) Replace the force component f_i by the new diagonal term multiplied by the displacement, D .

Then equation (4.19) becomes

$$k_{i1}d_1 + k_{i2}d_2 + \dots + 10^{10} k_{ii}d_i + \dots + k_{in}d_n = 10^{10} k_{ii}D \quad (4.21)$$

The solution of such an equation is, to a close order of approximation, $d_i = D$, as required by equation (4.20). This process can be repeated with all the prescribed boundary conditions to yield a non-singular set of equations.

The solution of simultaneous linear equations fall into two categories :

(a) Iterative methods, as described by Varga [42], and Hestenes [43], which have been applied to finite element problems by Fried [44] and Fox [45]. All these techniques use a successive approximation based upon on initial assumed solution.

(b) Direct methods. These use the special properties of $[K]$ to maximum advantage, since they operate directly on the modified rectangular form of $[K]$, as described in section 4.4.

To solve equation (4.1), the direct Gaussian elimination is chosen (Kunz [46]). Algorithms based upon this method are well known and published in CACM [47]. These required only minor modifications to solve the condensed form of equation (4.1).

4.7 Calculation of nodal forces

The contact area forces and reaction forces in the bead region can be obtained by back substitution of the calculated displacements into the original equations (4.1). The component of force F_2 , associated with the displacement u_2 , measures the applied loads for nodes in the contact area. The distribution of these point loads, together with the air pressure effect, will produce an estimate of the contact pressure distribution.

The direction of the force F_2 should be the same as that of the applied load. If the sign at any node is in the reverse sense, it indicates that this particular node is being incorrectly held onto the boundary plane. The true situation is obtained by removing the boundary conditions for this node and re-solving the equations. This situation will arise for points near to the edge of the contact area which will tend to move away from the contact plane during deflection.

4.8 Stresses and strains

The local strain vector $\{\epsilon^*\}$ is defined in terms of strain components whose general form is a second order tensor, $u_{i,j}^*$, $i, j=1, 2, 3$. Such a term obeys laws of transformation

$$u_{i,j}^* = \lambda_{im} \lambda_{jn} u_{m,n} \quad m, n = 1, 2, 3 \quad (4.22)$$

The formulation of $u_{m,n}$ can be written in the form of a column matrix, as in equation (3.85), which is given in tensorial form as

$$u_{m,n} = \gamma_{mnk} \delta_k \quad (4.23)$$

$$\begin{aligned} \text{where } k &= 1 \text{ to } 15 \text{ for } M=3 \\ k &= 1 \text{ to } 30 \text{ for } M=6 \end{aligned} \quad (4.24)$$

If δ_k , the displacement tensor, is partitioned into its translation and rotation components, given by δ_t and δ_r respectively, then equation (4.23) becomes

$$u_{m,n} = \gamma_{mnt} \delta_t + \gamma_{mnr} \delta_r \quad (4.25)$$

$$\begin{aligned} \text{where } t &= 1, 2, 3, \quad 6, 7, 8, \quad \dots \\ r &= \quad 4, 5, \quad 9, 10, \dots \end{aligned} \quad (4.26)$$

From Table 3.1 and 3.2 it will be seen that

(a) γ_{mnt} is a function of the areal co-ordinates w_1 and w_2 only, and consequently a function of the local co-ordinates ψ_1 and ψ_2 so that

$$\gamma_{mnt} = \gamma_{mnt}(\psi_1, \psi_2) \quad (4.27)$$

(b) For $n=1$ and 2

$$\gamma_{mnr} = \psi_3 \cdot \gamma'_{mnr}(\psi_1, \psi_2) \quad (4.28)$$

where γ'_{mnr} is a function of ψ_1 and ψ_2 only.

(c) For $n=3$, γ_{mnr} is a function of ψ_1 and ψ_2 so that

$$\gamma_{m3r} = \gamma_{m3r}(\psi_1, \psi_2) \quad (4.29)$$

Equation (4.20) can now be written as

$$\begin{aligned}
 u_{i,j}^* = & (\lambda_{im} \lambda_{jn} \gamma_{mnt} \delta_t)_{n=1,2,3} \\
 & + (\lambda_{im} \lambda_{jn} \gamma'_{mnr} \delta_r \psi_3)_{n=1,2} \\
 & + (\lambda_{im} \lambda_{jn} \gamma_{mnr} \delta_r)_{n=3}
 \end{aligned} \tag{4.30}$$

In terms of the variables ψ_1, ψ_2 and ψ_3 this can be expressed as the functional relationship

$$u_{i,j}^* = u_{i,j}^*(\psi_1, \psi_2) + \psi_3 \cdot V(\psi_1, \psi_2) \tag{4.31}$$

where $u_{i,j}^*(\psi_1, \psi_2)$ refers to a position on the mid-surface $\psi_3=0$.

The numerical integration process described in section 4.3 requires the evaluation of equation (4.31) at six points in the element, comprising pairs of points whose ψ_3 co-ordinate is equal in magnitude but opposite in sign for a fixed ψ_1 and ψ_2 . The ψ_1, ψ_2 co-ordinates correspond to the mid-side nodes. Thus for a particular node, s , equation (4.31) gives

$$\begin{aligned}
 (u_{i,j}^*)_{s+} &= u_{i,j}^*(\psi_1, \psi_2)_s + \psi_3 \cdot V(\psi_1, \psi_2)_s \\
 (u_{i,j}^*)_{s-} &= u_{i,j}^*(\psi_1, \psi_2)_s - \psi_3 \cdot V(\psi_1, \psi_2)_s
 \end{aligned} \tag{4.32}$$

corresponding to positive and negative values of ψ_3 . Hence the value of the mid-surface strain components at node s , together with the variation across the element, V , can be calculated as

$$u_{i,j}^*(\psi_1, \psi_2)_s = [(u_{i,j}^*)_{s+} + (u_{i,j}^*)_{s-}] / 2 \tag{4.33}$$

$$V(\psi_1, \psi_2)_s = [(u_{i,j}^*)_{s+} - (u_{i,j}^*)_{s-}] / 2 \quad (4.34)$$

Equations (4.33) and (4.34) enable the strain components at any point to be calculated as defined by equation (4.31), and hence the strain vector $\{\epsilon^*\}$ of equation (3.97).

4.9 Non-linear solutions

In many problems of solid mechanics the governing equations are formulated adequately by assuming a linear system. This implies that both the stress-strain and strain-displacement relationships are linear. For a pneumatic tyre subjected to an arbitrary load, it is necessary to ascertain the validity of these underlying principles. In the general deflected state, large deformations can occur even though the internal strains experienced by the structure are relatively small. With this in mind, the linearity of the stress-strain law is quite plausible. However, the linearity of the strain-displacement law was based upon small deflection theory, and clearly this does not hold in the case of the tyre.

To overcome this difficulty two methods are available.

(a) A more complex, non-linear, relationship between strains and displacements can be derived. This would be an extension of the linear form to include second order (or higher) terms. Using such a system, the resulting set of simultaneous equations (4.1) will now be non-linear and will require some iterative scheme to effect a solution. Such a method was adopted in the research work of Oden [51], Brebbia [52], and Martin [53].

(b) The non-linear, large deflection system can be approximated by

a step-by-step method of small increments. These steps are chosen so that a linear model can be used for each. In the limit, as the increment size decreases, the solution obtained will converge to the non-linear form. The incremental model is applied in the following manner :

The initial geometry of the structure is defined piecewise by the global co-ordinates $(x_i)_j$ $i=1,2,3$ at the nodal point j , together with the directions of the local co-ordinate axes $(x_i^*)_j$. The latter are functions of the nodal thickness vector. At each increment of deflection, the set of equations (4.1) are solved to produce the vector of displacements $\{\delta\}$ for the entire structure. $\{\delta\}$ will consist of $(u_i)_j$ for $i=1,2,3$ and $(\theta_k)_j$ for $k=1,2$ at each node j . Using this information, the geometry of the system can be modified to obtain a new set of nodal co-ordinates and local Cartesian axes. This enables a different stiffness matrix to be calculated for the updated structure. This process is repeated at each increment of deflection.

CHAPTER 5.

Results

5.1 Tyre preparation

Two standard production tyres were selected to verify the accuracy of the mathematical model. These were a four ply, rayon, 6.40/50 - 13 D75 cross-ply tyre, and a 165 SR70 - 13 radial tyre with a four ply nylon breaker. Each was chosen from a batch on the basis of good uniformity. The tread rubber was removed from both tyres. On the cross-ply tyre, a section of sidewall rubber was removed to expose the outer cord layer. This enabled measurements of the cord bias angle to be made. The results are given in Figure 5.1 .

5.2 Measurements

5.2.1 Load-deflection curves

A series of load-deflection curves were obtained at varying inflation pressures (Figures 5.2 and 5.3), under the application of a flat plate load. Using techniques described by Cooper and Gough [54], the curves were extrapolated to obtain the structural stiffness of the tyres at zero inflation pressure.

5.2.2 Sidewall deflections

An initial measurement of the cross-sectional inflated profiles were taken (Figures 5.4 and 5.5) which enabled the position of the mid-surface profile to be calculated. An air pressure of 25 psi was maintained during these tests.

Deflections of 0.5 and 1.0 inches were applied to the tyres.

At each deflection, measurements were taken of displacements along the global Cartesian axes at points marked on the tyre surface.

Figures 5.6 to 5.11 give the cross-ply deformations, and Figures 5.12 to 5.17 apply to the radial tyre.

5.3 Solution by computer

5.3.1 Application of mathematical model

An IBM - 370 digital computer has been programmed with the finite element model of the pneumatic tyre. The differences in manufacturing techniques between the main types of tyre constructions require only minor changes to the basic programmes, as it is only necessary to define the geometry and material properties of the tyre components in mathematical form.

The programmes are capable of solving the equations of equilibrium which relate applied forces to displacement at discrete points in the tyre structure, for any arbitrary loading condition. However, the limits of direct access storage space has permitted only the solution of symmetric flat plate load problems. This analysis enables symmetry to reduce the model to represent one quarter of the tyre.

The simplest form that the loading can take is that due to internal air pressure. The solution of this problem has not been pursued here, since far simpler (symmetric) methods are available as reviewed in section 2.1. Moreover, the mathematical model is more suited to boundary conditions which are applied in terms of displacements rather than forces, since the 'geometric' boundary conditions can be precisely determined in terms of nodal displacements

for a given deflected tyre situation, whereas any applied force distribution must first be approximated by a set of discrete nodal forces.

It will therefore be assumed that the initial state of the structure is that of an inflated tyre, subject to stresses and strains due to the moulding and inflating processes, and that methods are available for obtaining quantitative values for the internal forces. The programs will solve for applied deformations of the inflated tyre and the results will be in the form of variations in the geometry and internal forces. By superposition, the conditions relating to the inflated, deflected tyre will be obtained.

5.3.2 Choice of theory

In section 3.3, two forms of the mathematical model were described. These were denoted by values of 3 and 6 for the index M in equation (3.52), where M defined the number of element nodes at which the displacements were to be calculated.

Comparison of solutions have shown that similar results can be obtained using the two methods. However, the more exact theory ($M=6$) has advantages over the $M=3$ method, namely

- (a) To produce the load-deflection curve of Figure 5.18, larger incremental steps can be used.
- (b) Fewer elements are required for the same number of evaluation points, as shown in the mesh patterns of Figure 5.19.
- (c) The effect of the above is to reduce the overall computation time.

5.4 Global displacements

The solution of the equilibrium equations (4.1) produce directly the displacements u_i $i=1,2,3$ of the node points along the global Cartesian axes. Using deflection increments of 0.25 inches, and superimposing the solutions, the displacements associated with deflections of 0.5 and 1.0 inches were obtained. The agreement with test results are good, as shown in Figures 5.6 to 5.17 .

The fundamental difference in displacement patterns between the cross-ply and radial tyres is clearly visible. The positions of maximum displacement tend to lie along the cord path of the carcass plies. This produces two peaks for the cross ply tyre, situated at angles of $\pm 25^\circ$ from the centre of contact, and a single peak for the radial tyre situated at 0° . The stiffening effect of the breaker in the radial tyre is demonstrated by the small changes in displacement across the breaker region, as shown in Figures 5.12 to 5.17.

5.5 Load-deflection curves

The load carrying mechanism of the pneumatic tyre has been fully described by Gough [55]. The transmission of forces from the contact area to the wheel rim is a combination of the tyre behaving as a structure and as an inflated membrane. In the former case the inflation pressure is not involved, and in the latter the loading is a function of both pressure and geometric deformations.

5.5.1 Structural effect

The mathematical model describes the structure of the tyre in the form of the stiffness matrix [K] of equation (4.1). Having

obtained the displacements of all the nodes, the associated nodal forces along the Cartesian axes can be calculated by solving equation (4.1) as described in section 4.7. These nodal forces represent the externally applied forces necessary to displace the contact region while maintaining the bead region fixed. The result is a series of point loads which approximate to the distribution of forces in the contact region, together with an equal and opposite reaction at the bead. All forces at nodes removed from the boundary will be zero. The summation of either the contact area forces, or the bead region forces in the x_2 direction, will produce the load-deflection curve of the structure at zero inflation pressure, as shown in Figures 5.2 and 5.3.

The results for the radial ply tyre are about 50% greater than those estimated from the test curves, whereas the cross-ply values are acceptable. This can be attributed in part to the assumed discontinuity of the elastic properties at the edge of the breaker. The true situation of a gradual change in material properties from the breaker to the sidewall over some finite range can only be accounted for by increasing the number of elements. At the present time, computer storage limitations make this difficult.

5.5.2 Air pressure effect

The effect of inflating the tyre is to introduce membrane tensions which are equated by reactions at the bead. The relationship between forces, pressure, and the geometry of the tyre cross-section have been derived by Gough [56]. With reference to Figure 5.20a, the radial force on a unit length of bead, due to air pressure, can be expressed as

$$F_p = \frac{p \cdot (R_b^2 - R_s^2)}{2 \cdot R_b \cdot \tan \beta_b} \quad (5.1)$$

where p = inflation pressure

R_b = radius of bead from axis of rotation

R_s = radius of maximum tyre width from axis of rotation

β_b = angle between normal to mid-surface at the bead
and the x_1 axis.

From equation (5.1) the total force in the x_2 direction applied to both beads is given by

$$F = \int_0^\pi F_p \cdot \cos \theta \, d\theta \quad (5.2)$$

where θ is the angle about the axis of revolution measured from the positive x_2 axis.

Since F_p is independent of θ , then the expression for F in equation (5.2) is identically zero. This describes the condition of symmetric inflation loading with no external applied forces in the x_2 direction.

If the inflated structure is now deformed by contact with a plane, the angle β_b and the radius R_s will alter, as shown in Figure 5.20 b. Furthermore, the new values of these variables will be functions of θ , so that the force integral of equation (5.2) will now possess a non-zero value. This represents the force in the x_2 direction necessary to overcome the internal inflation pressure for the prescribed deflection. This force, by virtue of equation (5.1), is proportional to the air pressure, and thus enables the membrane load-deflection curve at any pressure to be constructed. The structural and membrane effects can then be added to produce the

total load-deflection curve, as given in Figures 5.2 and 5.3

The applied load is equated by a reaction at the boundary nodes in the bead region. The radial component of reaction is shown in Figures 5.21 and 5.22. The amount by which the bead and cord tensions change cannot be precisely determined, since the point of application of the reaction load is on a circumferential node line some distance away from the centre of the bead.

5.6 Contact area

The total force, F , of equation (5.2) is balanced by the transmission of contact pressure through the contact region of area A , such that

$$F = p.A \quad (5.3)$$

Equation (5.3) enables the magnitude of the contact area to be evaluated. The linear dimensions of the contact boundary can be estimated by noting that certain nodal points are situated inside the region of contact. These points arise from the analysis of section 5.5.1. The positions of these points, the area magnitude, together with the approximate elliptic shape of the contact boundary, enables the the contact boundary to be sketched, as shown in Figure 5.23.

CHAPTER 6.Conclusions

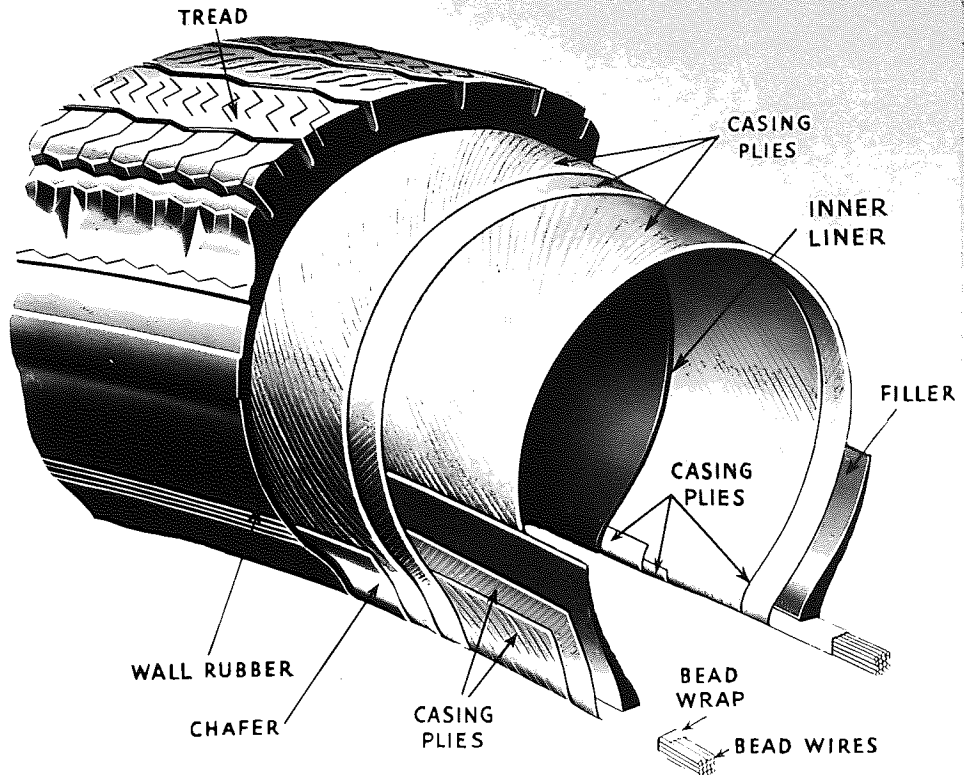
A mathematical model for the pneumatic tyre has been developed using thick shell finite elements of double curvature. The model incorporates the anisotropy of the cord-rubber assembly and is applicable to all types of tyre construction. The formulation is capable of evaluating the geometric deformations and associated reactive boundary forces associated with an arbitrary loading configuration. Large deflection problems are solved by means of linearised incremental procedures which update the geometry of the deformed structure after each load increment.

To confirm the accuracy of solution, the model has been applied to both the cross-ply and radial-ply tyre constructions. Good correlation with test results has been achieved for both the geometric deformations and the load-deflection curves. The greatest error was in the estimate of the structural stiffness of the radial tyre. This is probably due to the difficulty in modelling the breaker edge region, where the elastic continuity of the structure from the breaker region to the sidewall has not been accounted for. In principle this can be overcome by dividing the structure into more elements, but at the present time the availability of direct access computer storage space limits the maximum number of elements that can be used.

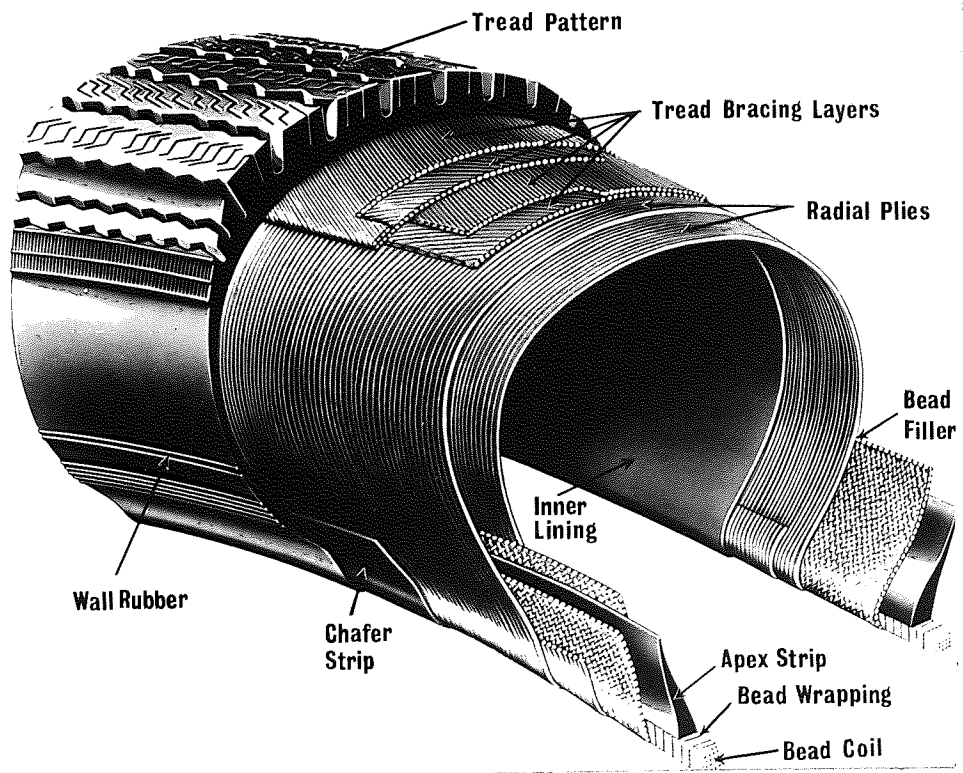
More storage space could be obtained by introducing sophisticated programming techniques. Irons [57], has developed methods which eliminate the construction of the large stiffness matrix of the structure. However, any substantial increase in the

number of elements will be accompanied by a greater increase in computation time. This is already at a high level due to the iterative solution techniques involved in the incremental method.

The theory of finite elements enables the stresses and strains within the elements to be estimated, and consequently the load distributions of the cords can be calculated. Although the mathematical model ensures displacement compatibility between adjacent elements, the strains are discontinuous across the boundaries. Estimates of the internal stresses can be obtained by averaging the discontinuities, but to obtain accurate values of the peak stresses, such as those associated with fatigue failures, it will be necessary to reduce considerably the size of each element. Such detailed analyses are outside the present limits of practicability, but with the advent of larger and faster computers it should be possible to extend this work to include more complex loading situations, even though accurate predictions of important stresses cannot be obtained.



(a) Cross ply tyre.



(b) Radial ply tyre.

Figure 3.1 Basic types of tyre construction.

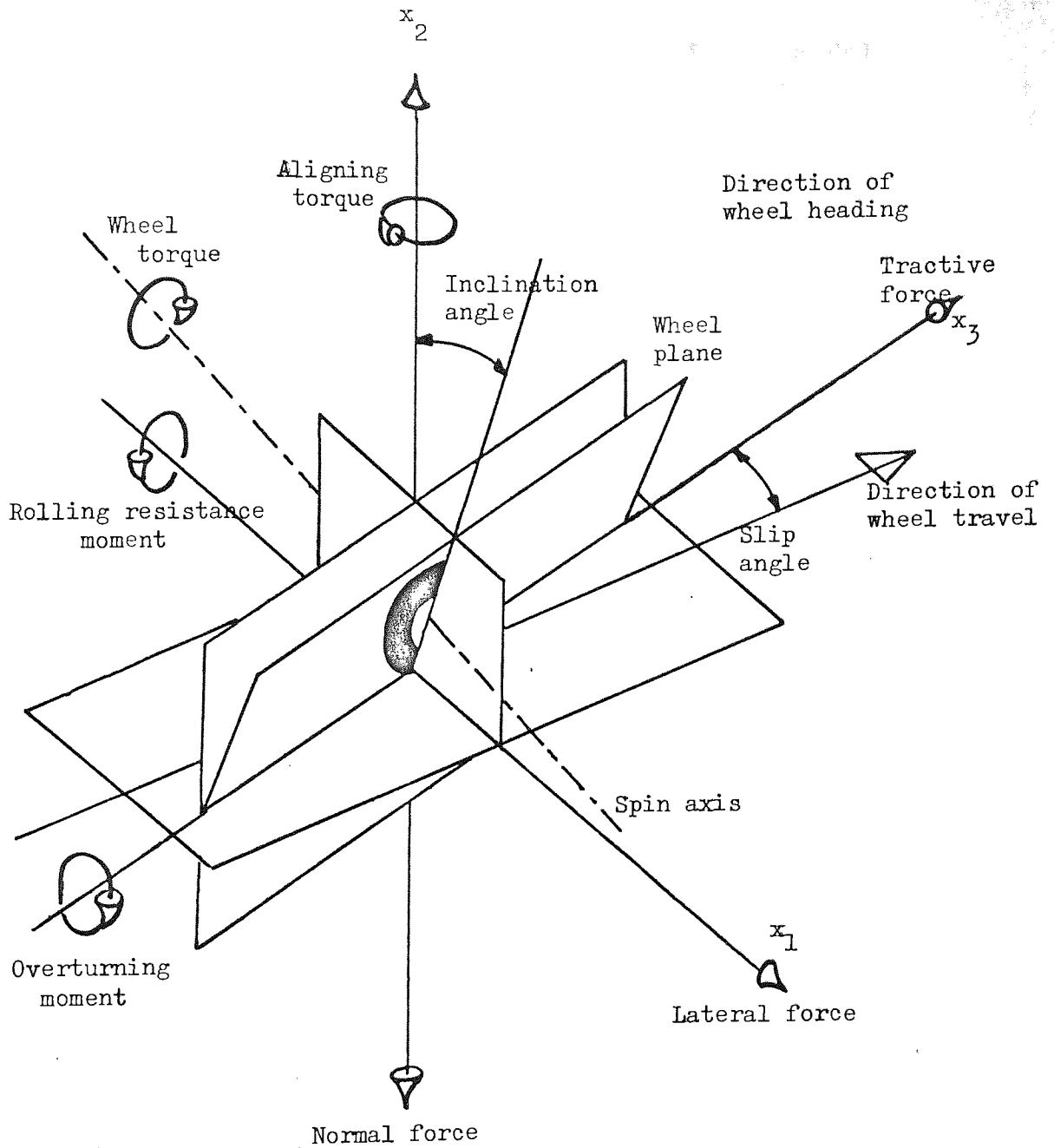


Figure 3.2 Tyre force system.

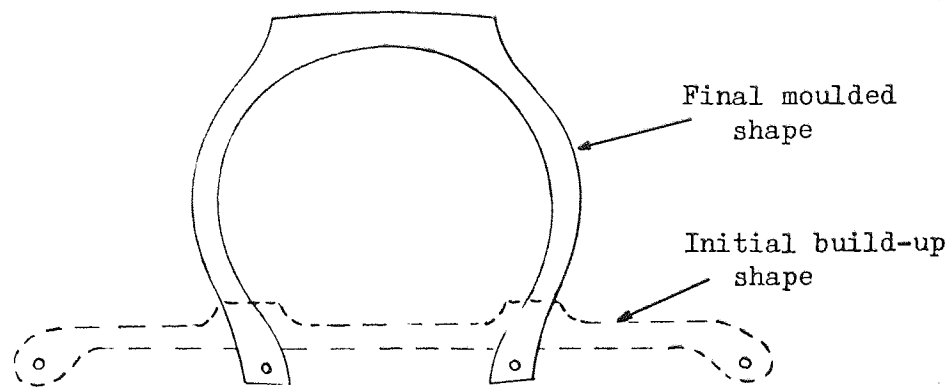


Figure 3.3 Sectional shape change during moulding.

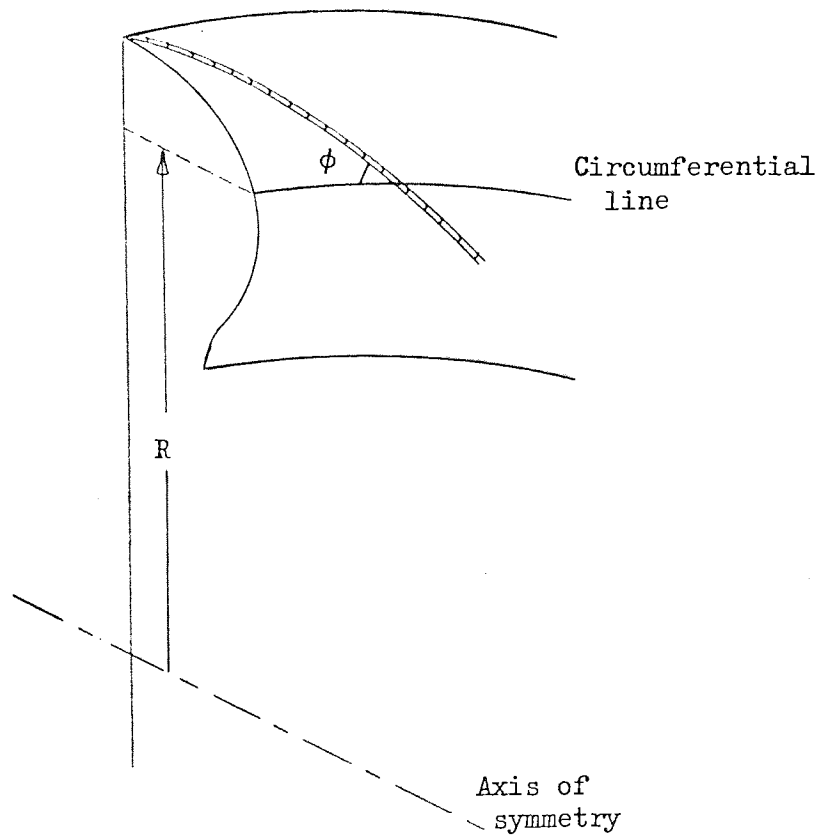


Figure 3.4 Variation of cord bias angle.

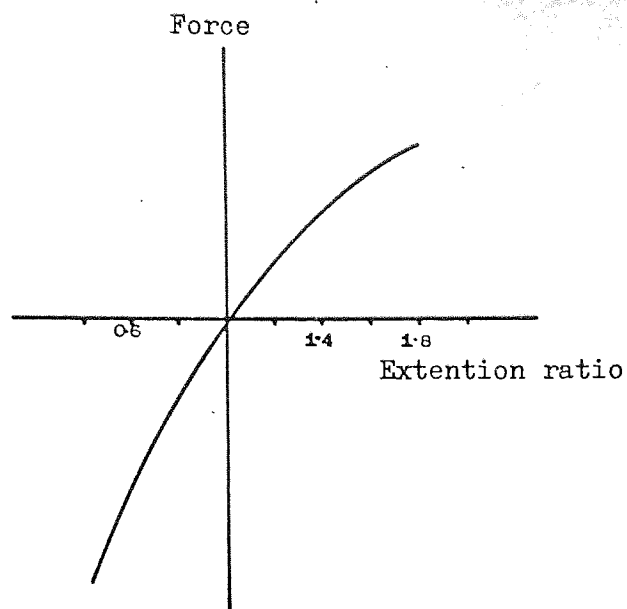


Figure 3.5 Stress-strain curve for rubber (large strain).

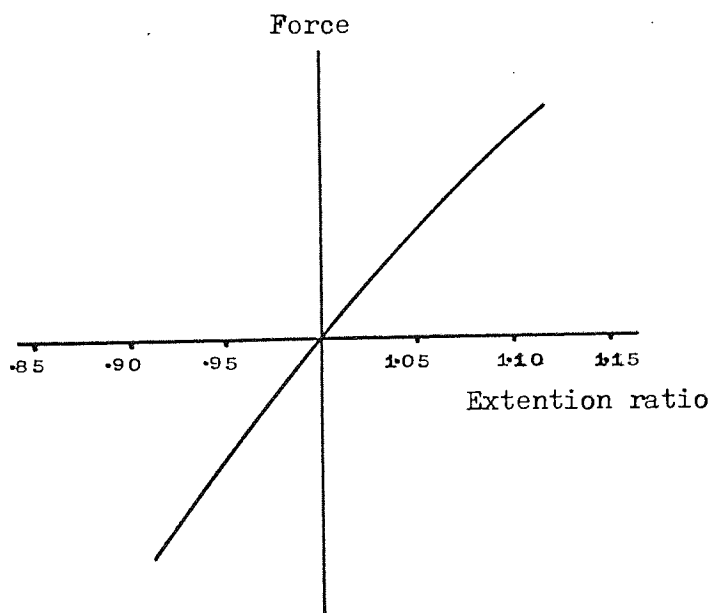


Figure 3.6 Stress-strain curve for rubber (small strain).

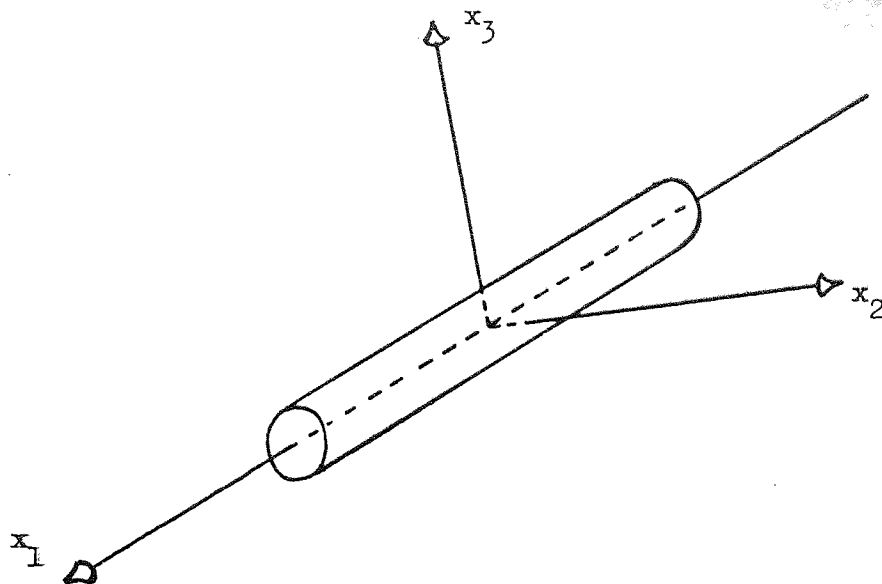


Figure 3.7 Axes of elastic symmetry for orthotropic cord.

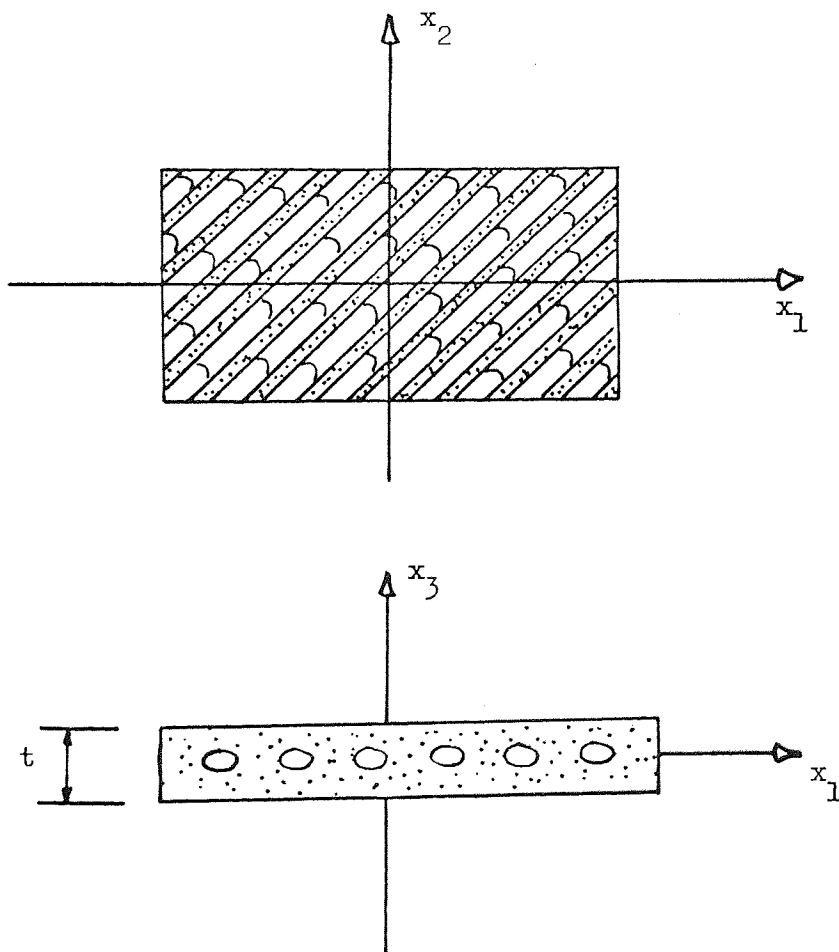


Figure 3.8 Co-ordinate axes of laminate.

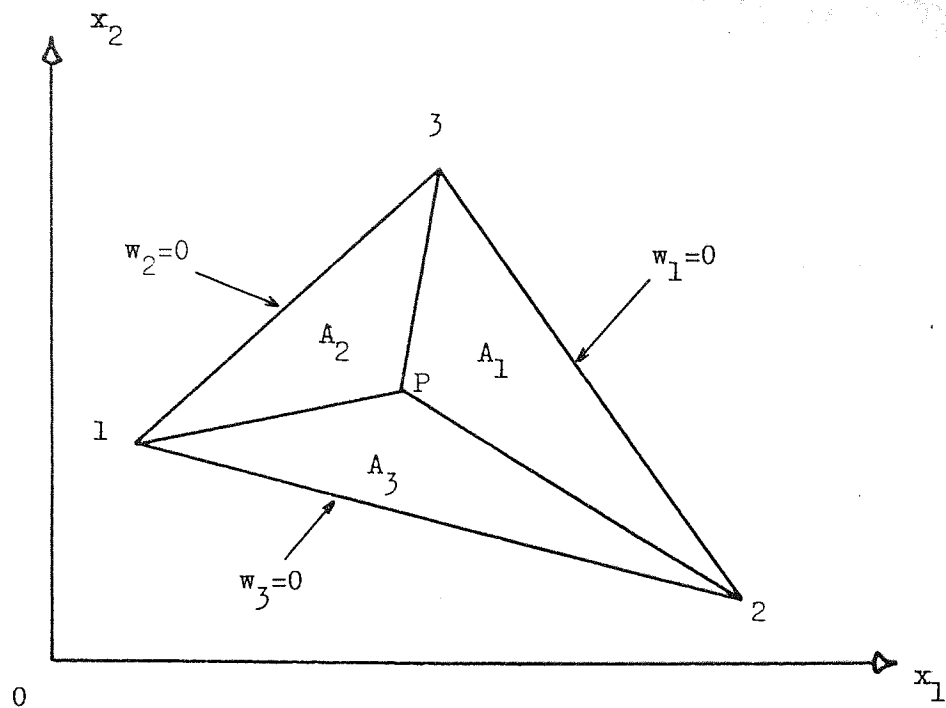


Figure 3.9 Areal co-ordinates.

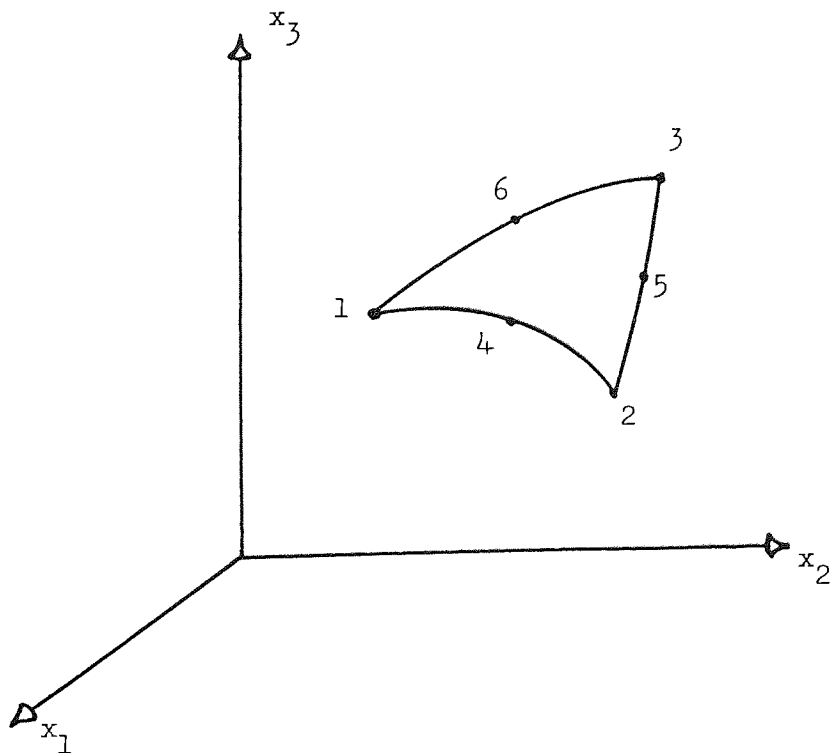


Figure 3.10 Curvilinear triangle.

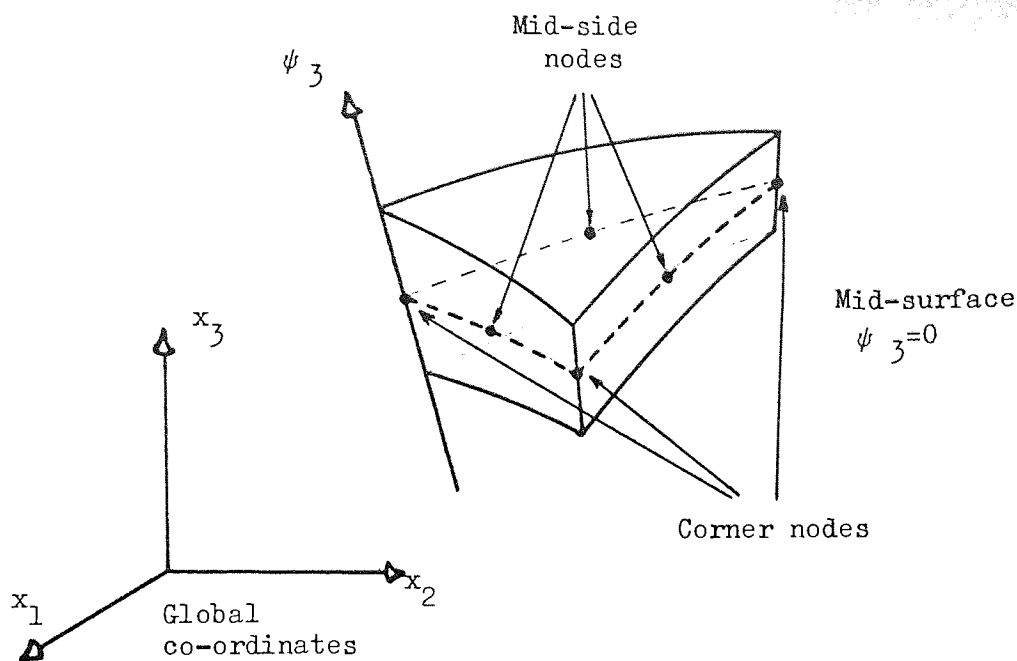


Figure 3.11 Thick shell element.

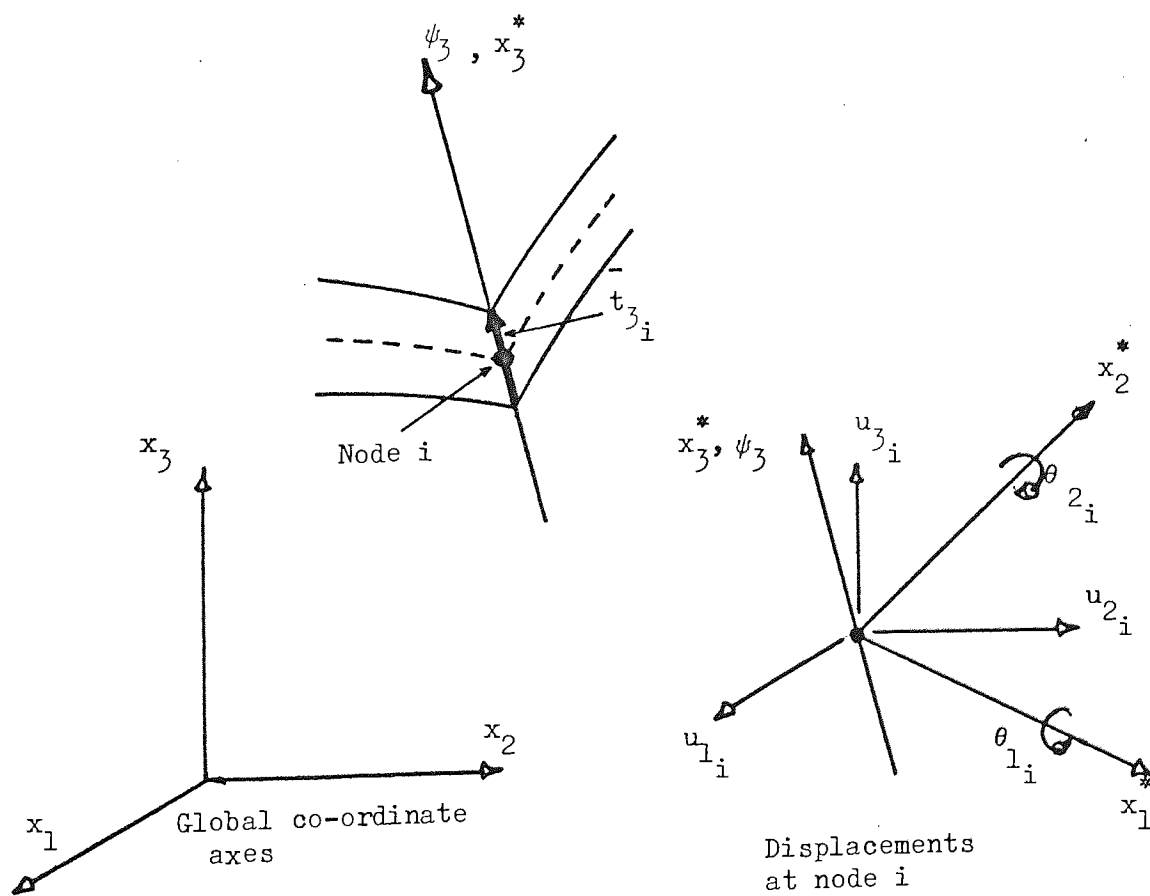


Figure 3.12 Local and global co-ordinate axes for element.

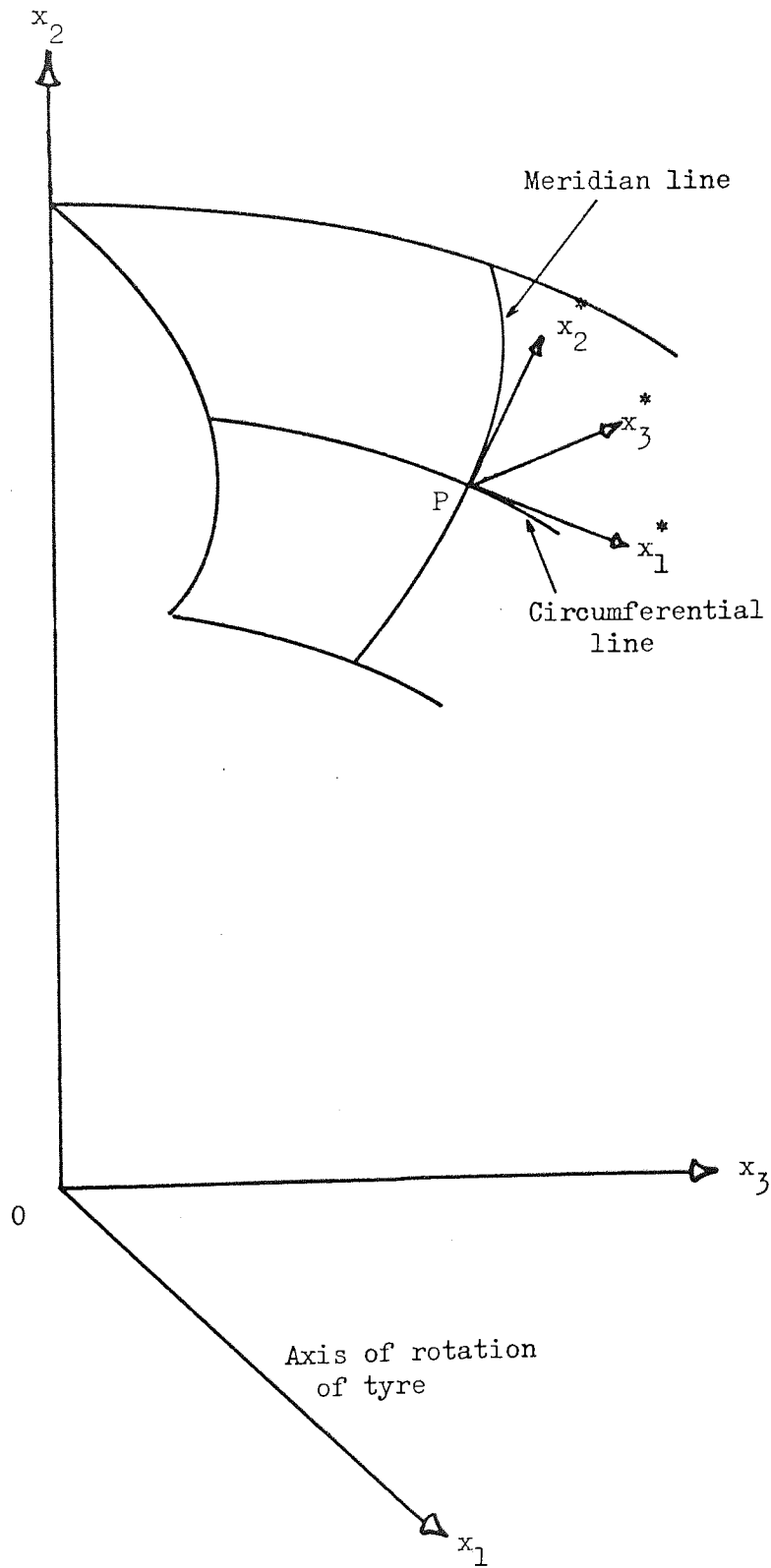


Figure 3.13 Local and global Cartesian axes for tyre.

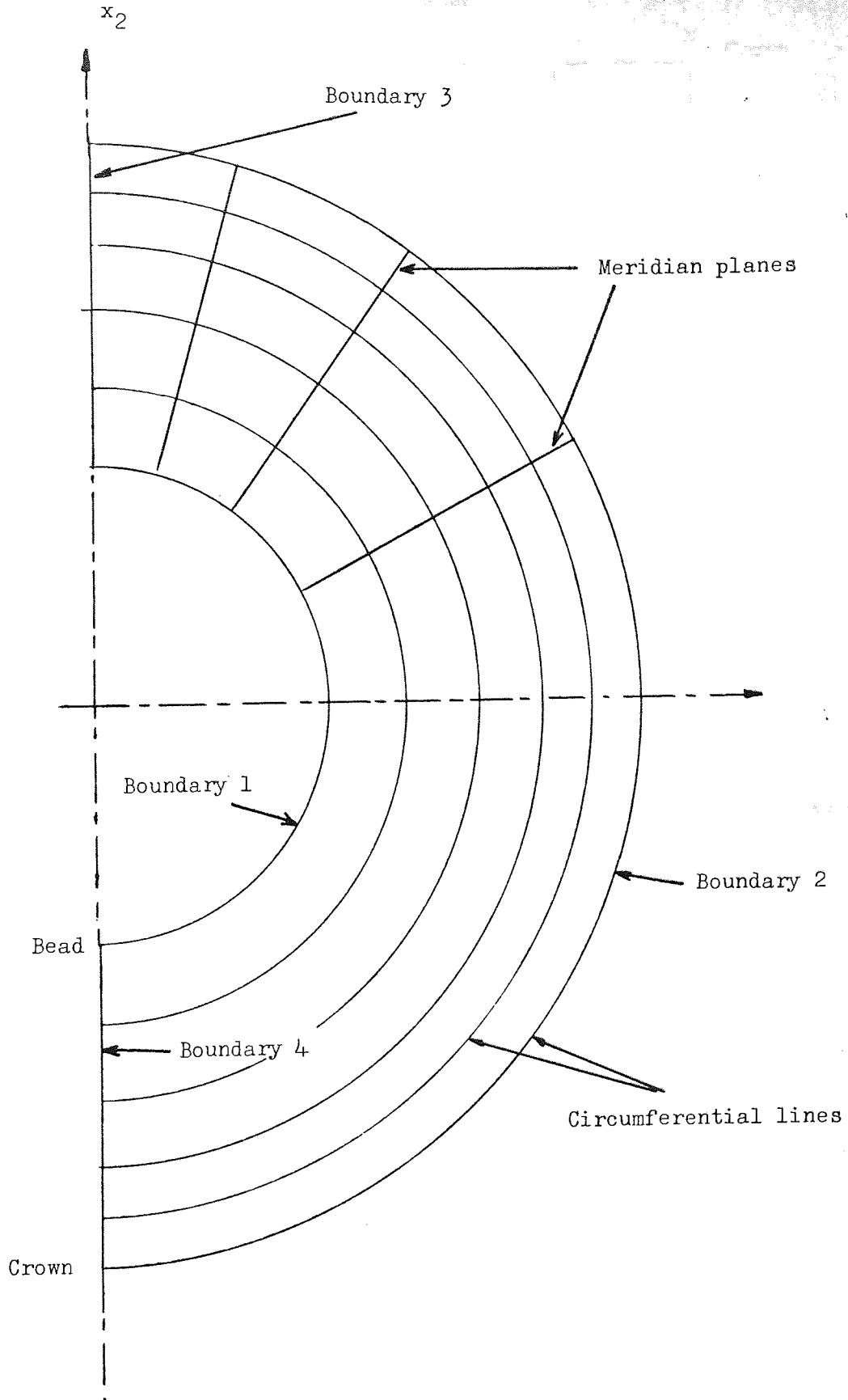


Figure 4.1 Elements on mid-surface of tyre.

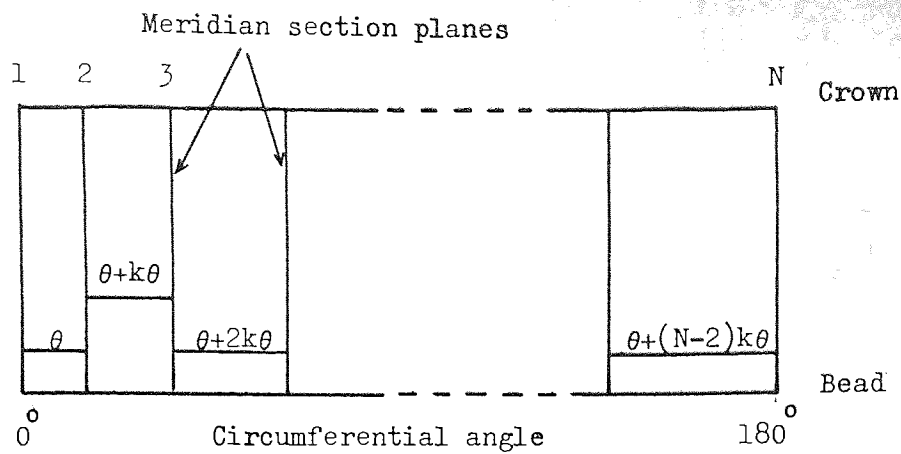


Figure 4.2 Rectangular development of mid-surface.

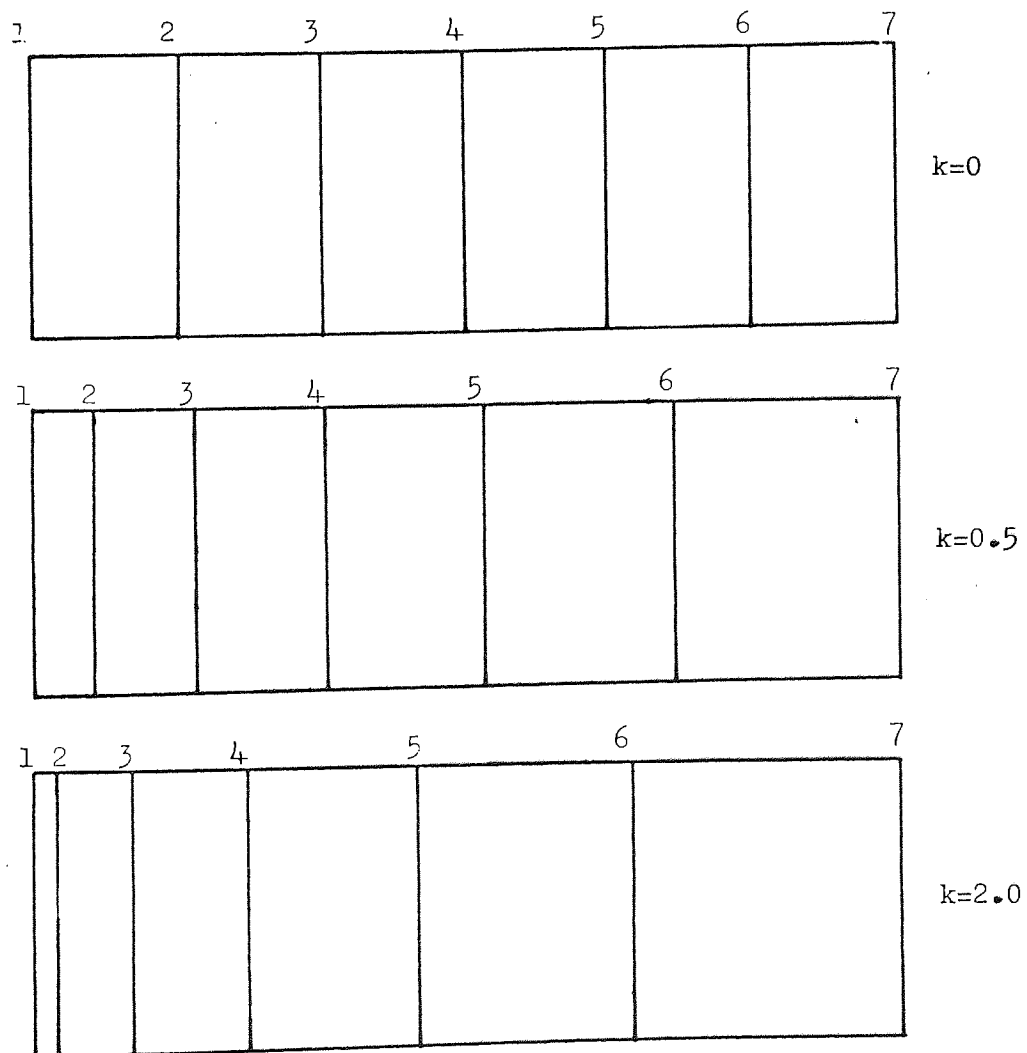


Figure 4.3 Variation of meridian plane with k (N=7).

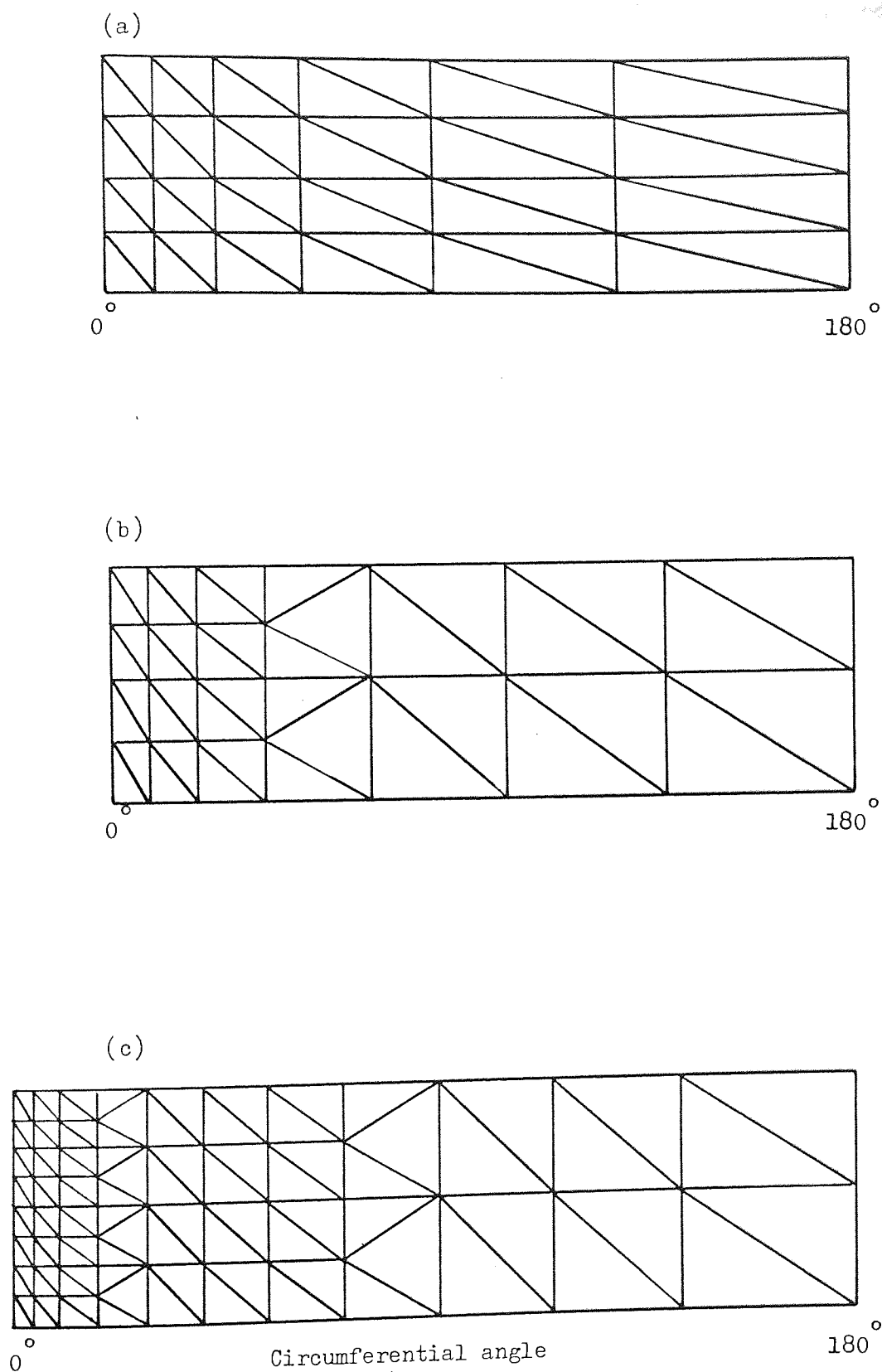
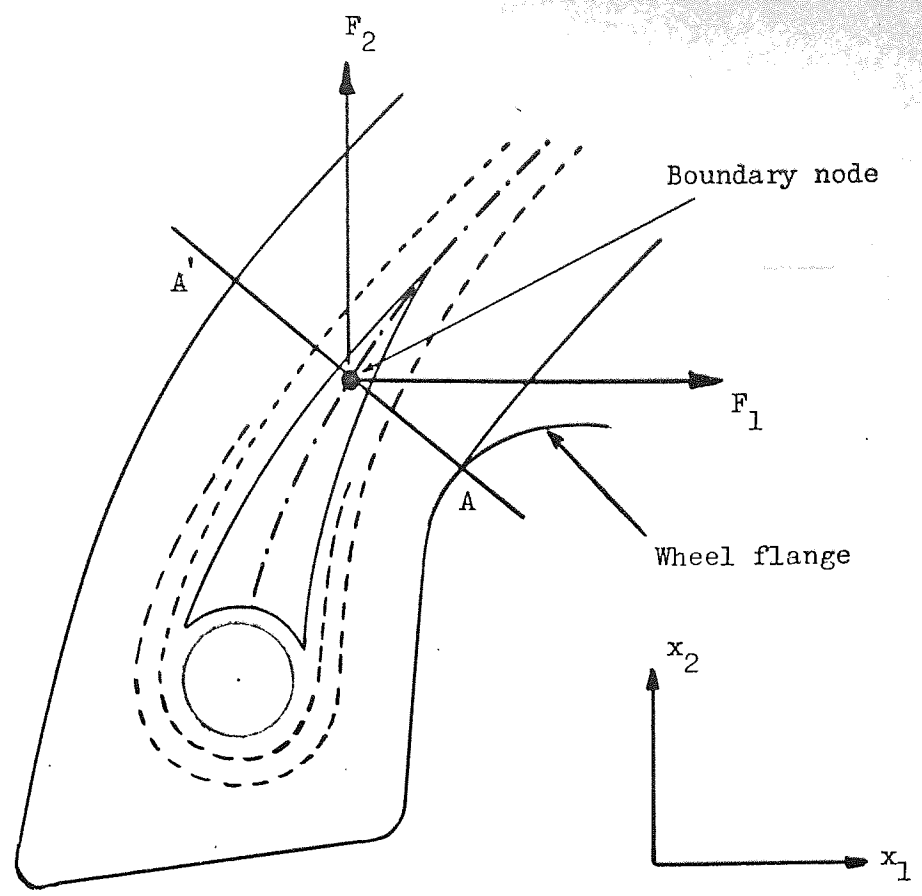
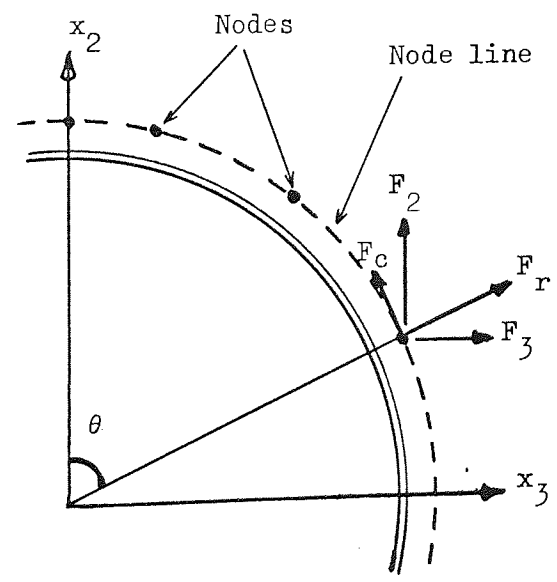


Figure 4.4 Element mesh patterns.



(a)



(b)

Figure 4.5 Bead region

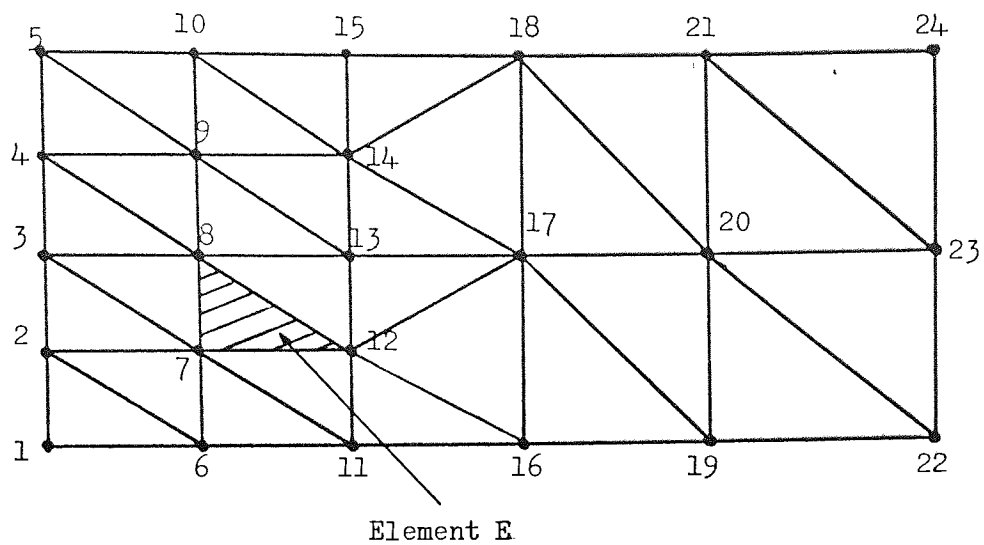
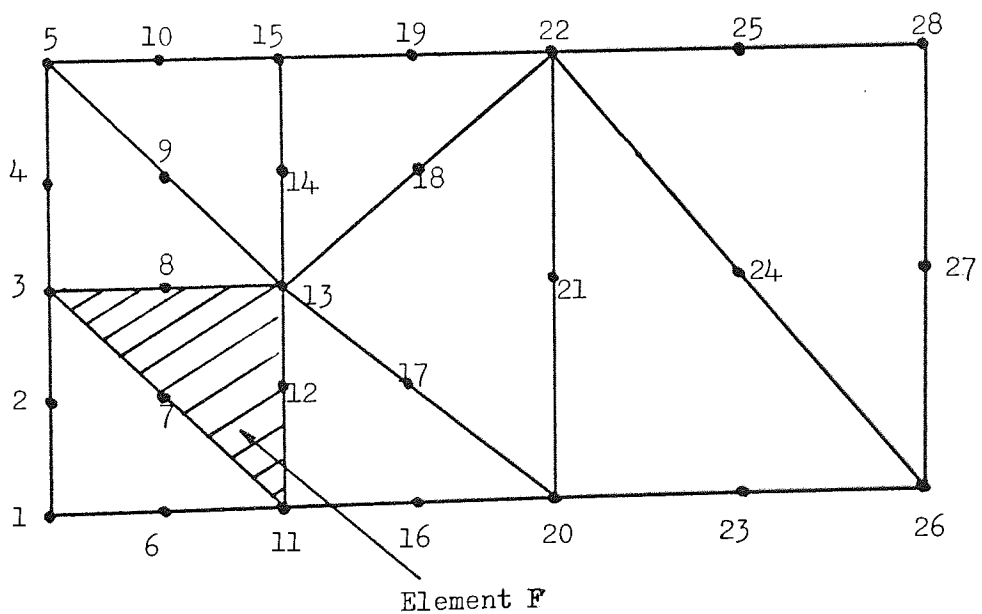
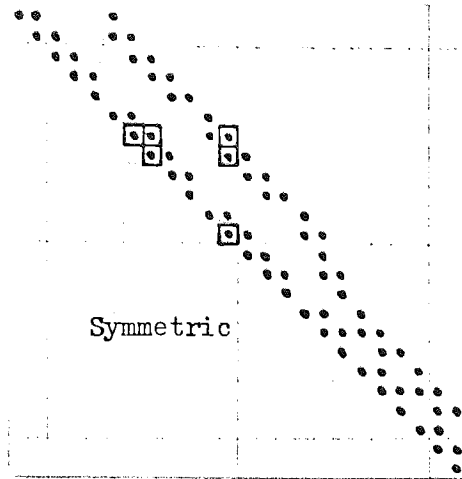
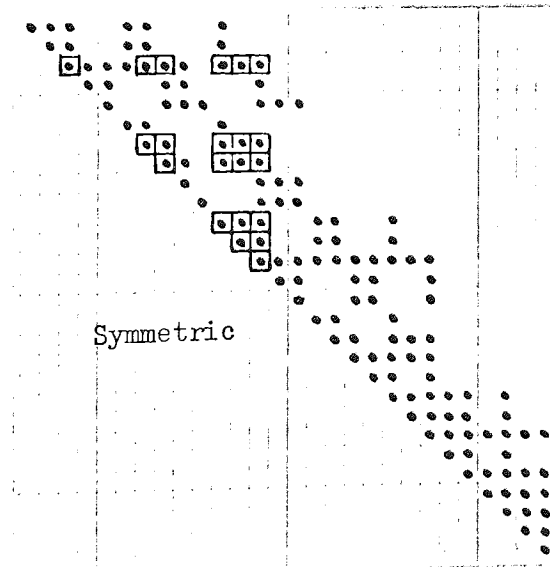
(a) $M=3$ (b) $M=6$

Figure 4.6 Node numbering sequence for $M=3$ and $M=6$.

(a) $M=3$ (b) $M=6$

Each \bullet represents a 5×5 matrix.

Figure 4.7 Example of total stiffness matrices.

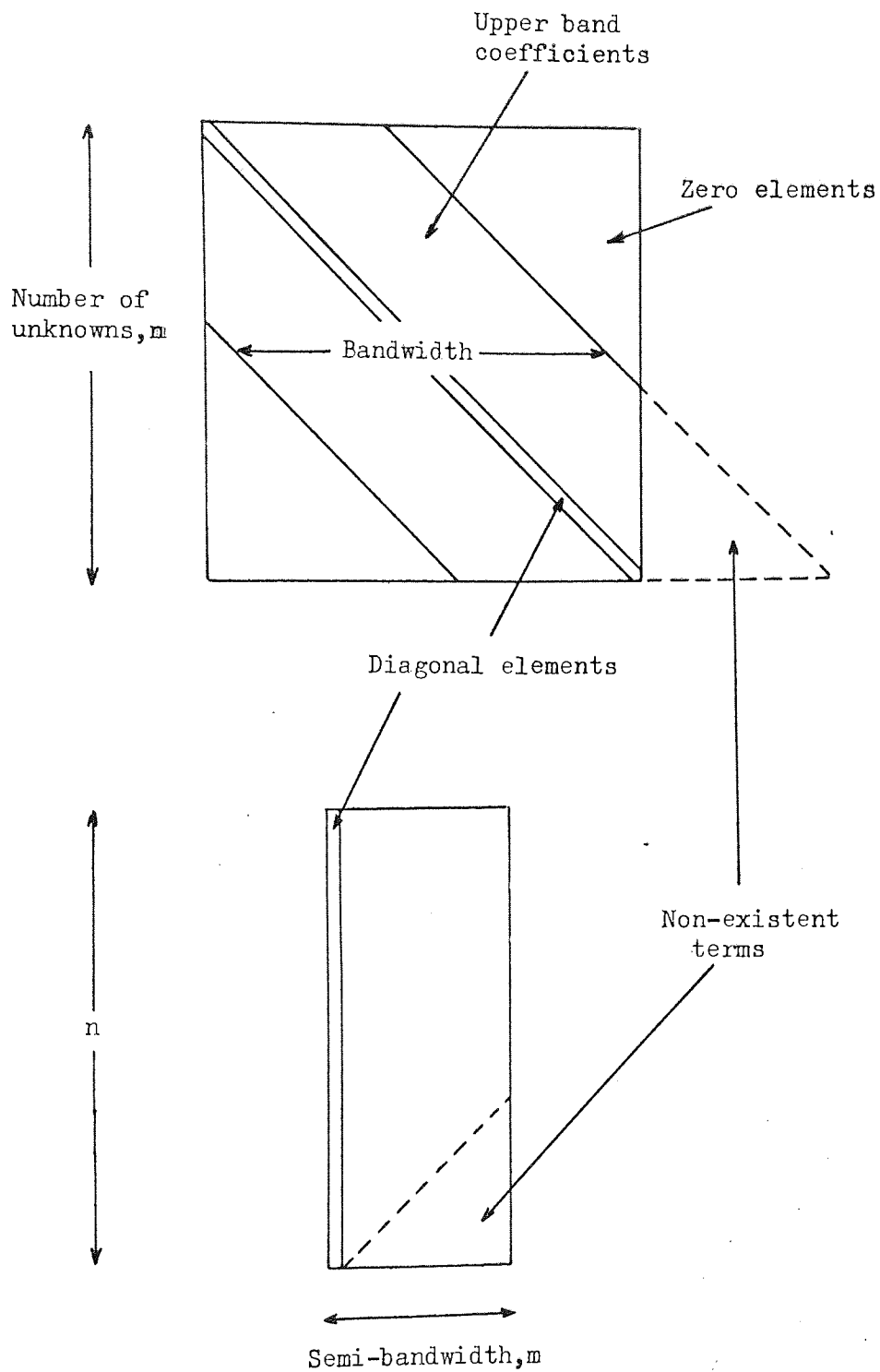


Figure 4.8 Condensed storage of $[K]$.

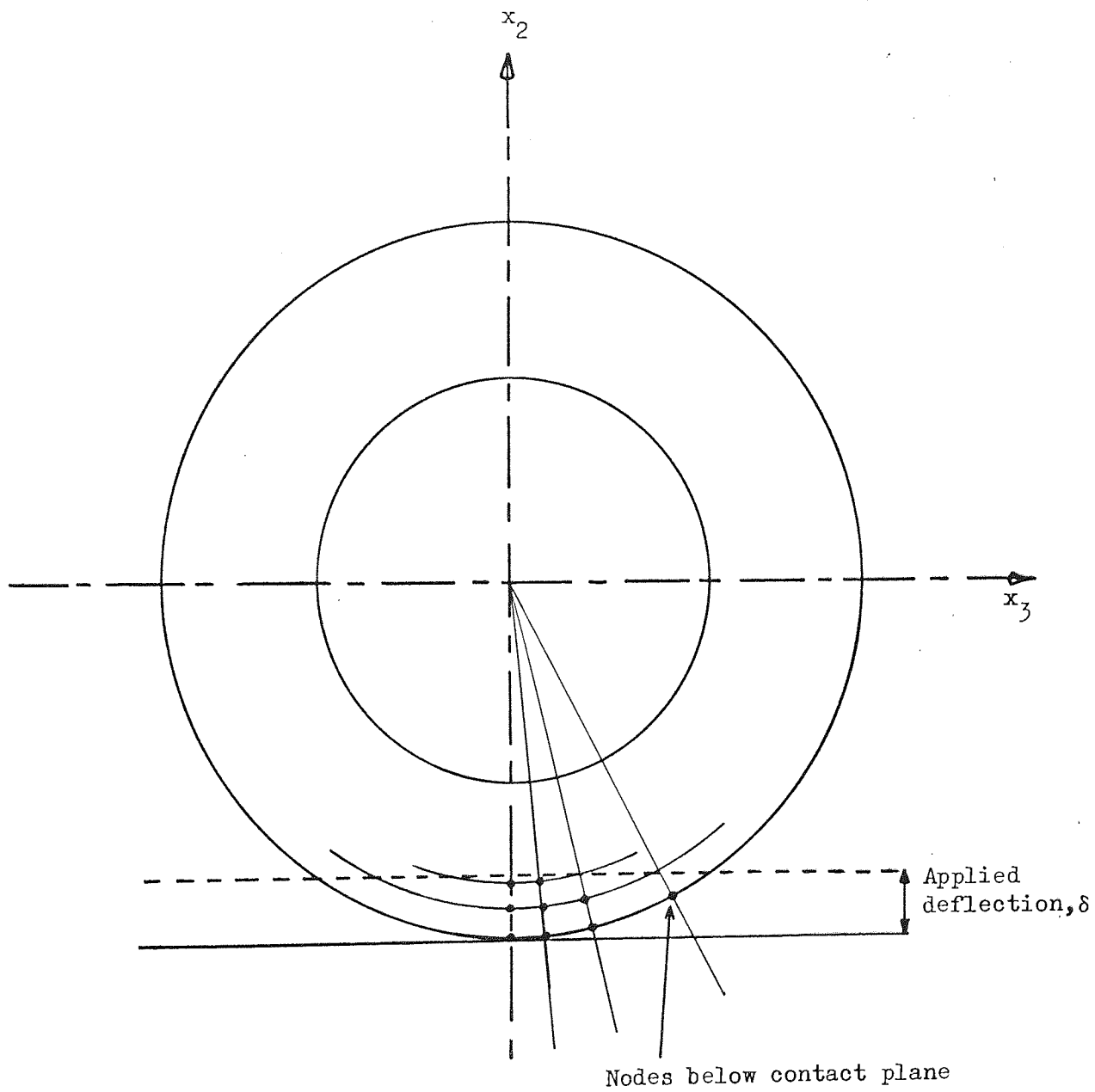


Figure 4.9 Tyre subject to flat plate load.

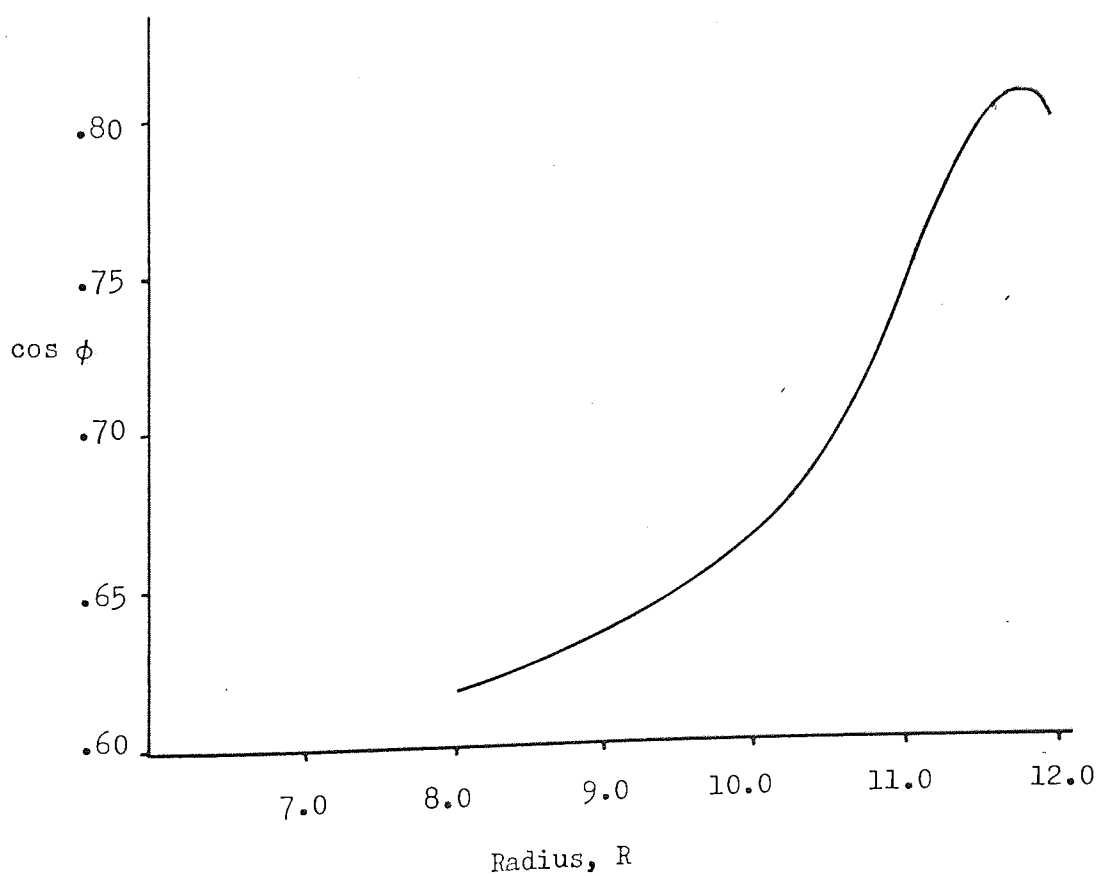
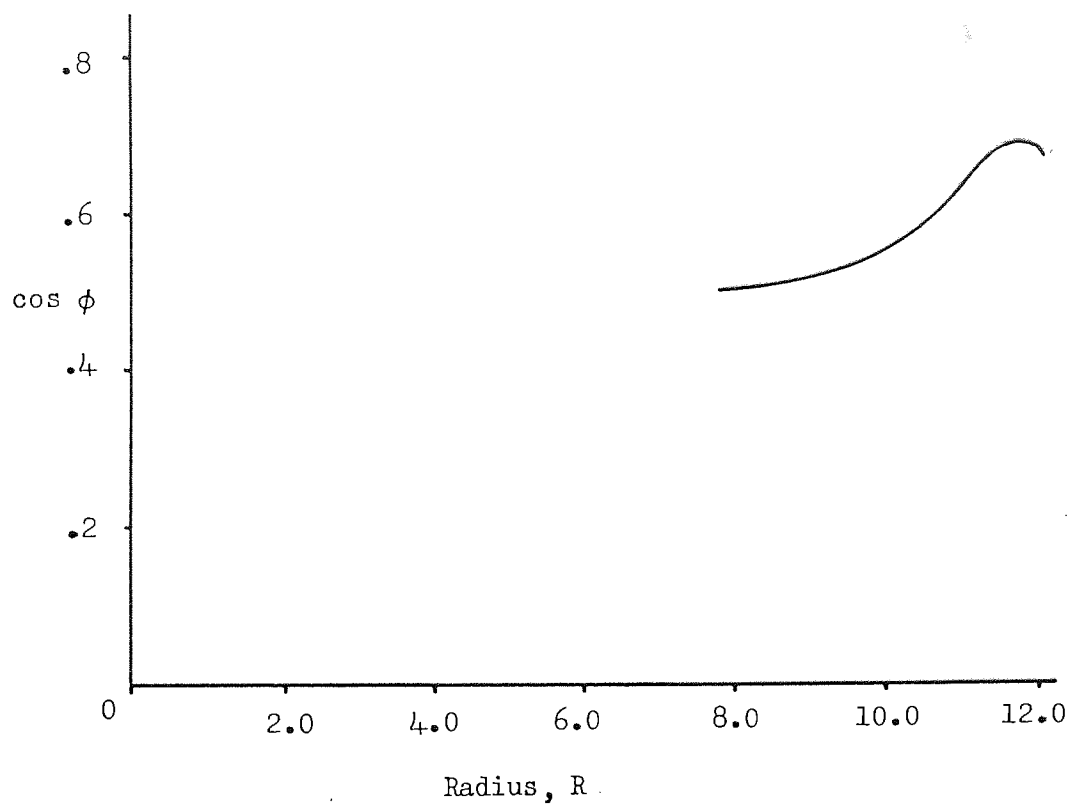


Figure 5.1 R - $\cos \phi$ curve for cross-ply tyre.

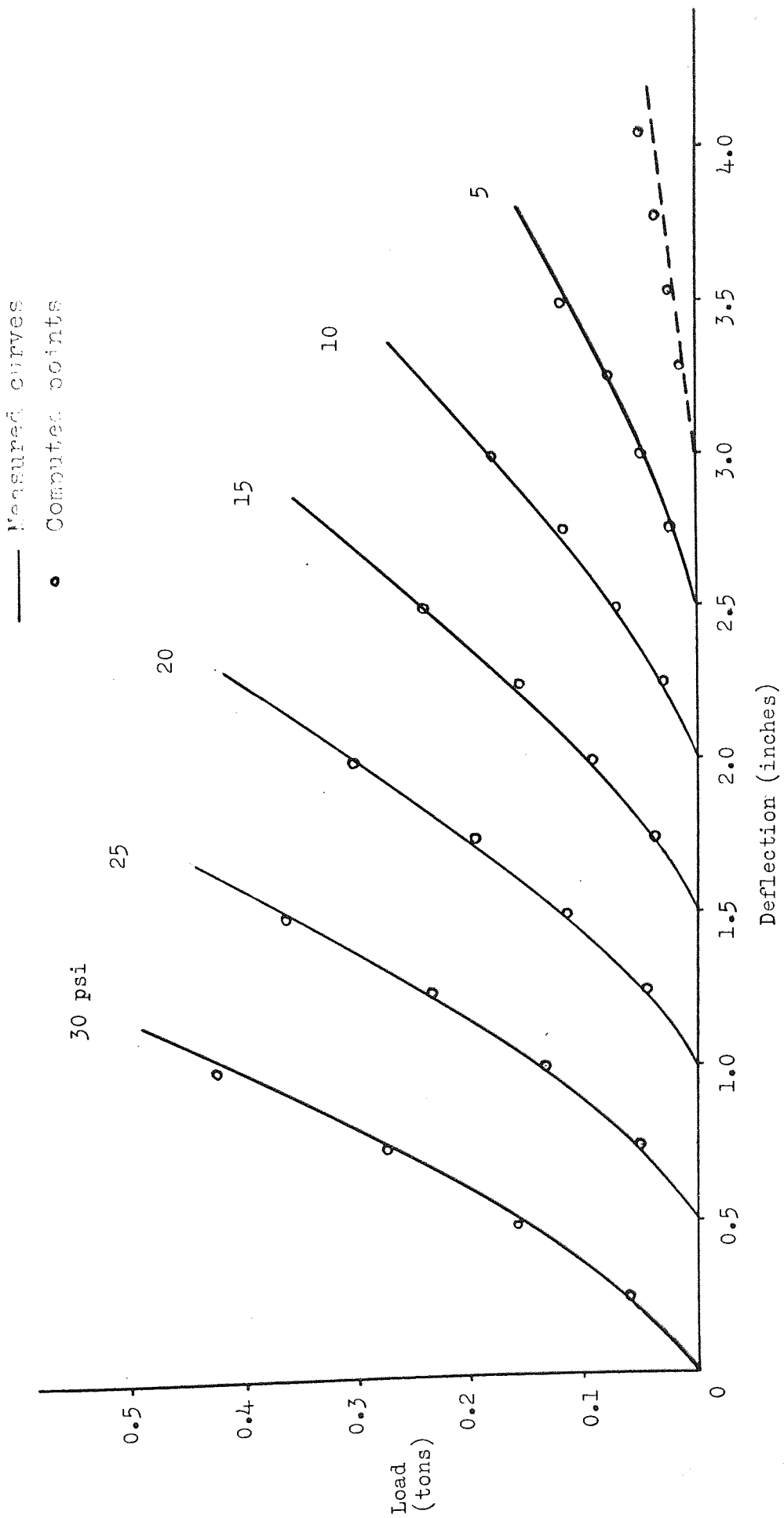


Figure 5.2 Load - deflection curve for cross-ply tyre.

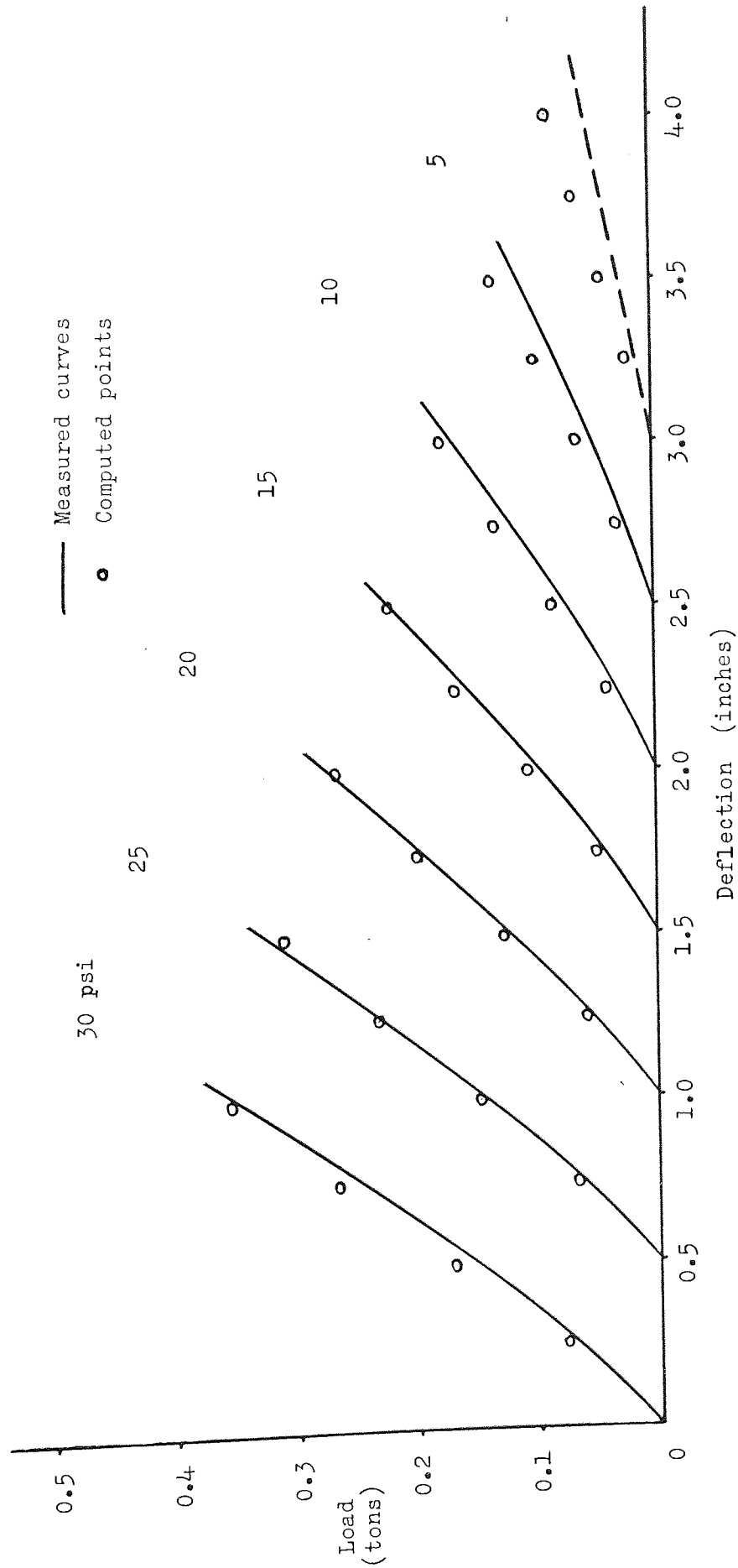


Figure 5.3 Load - deflection curves for radial ply tyre.

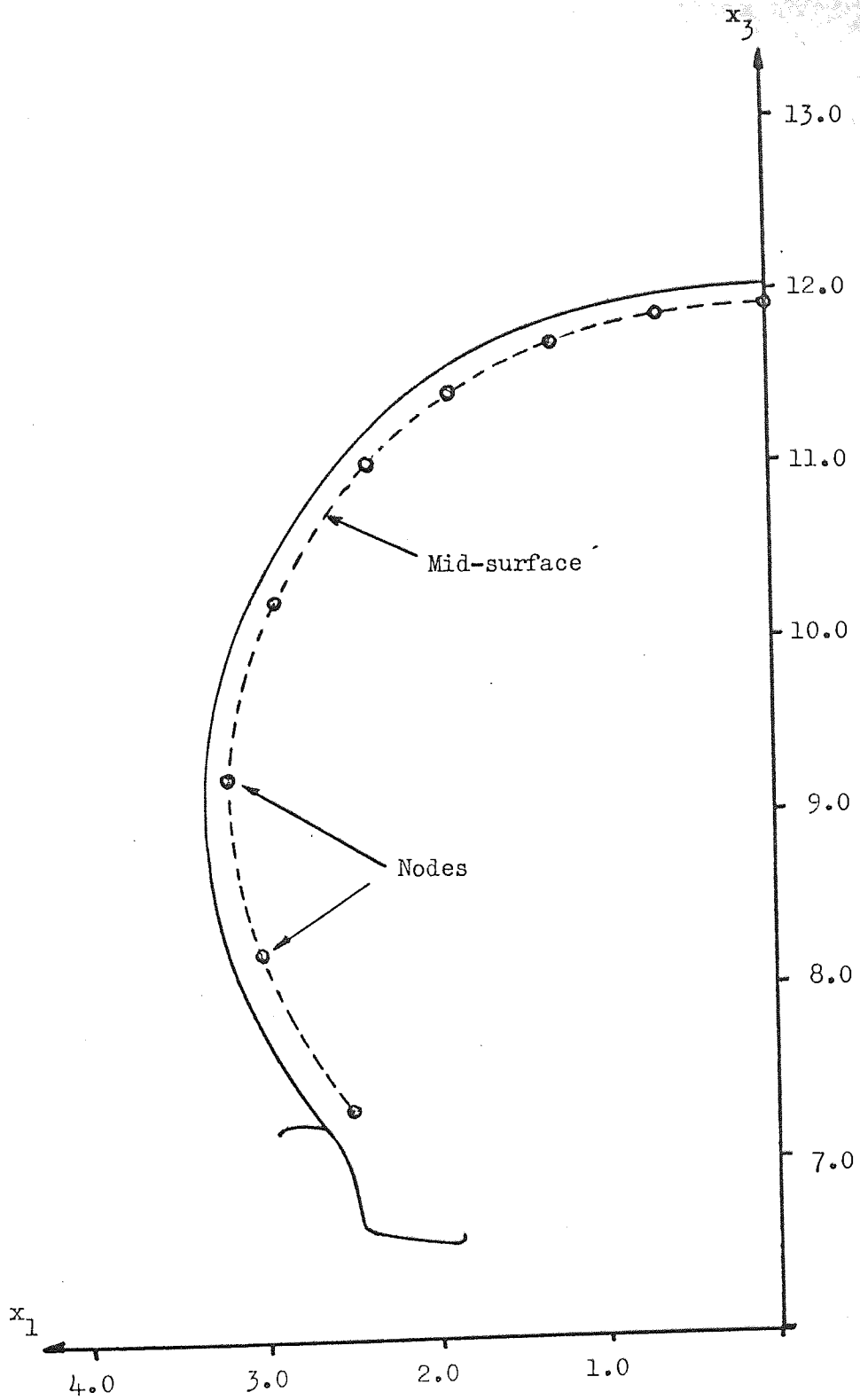


Figure 5.4 Sectional profile of cross-ply tyre.

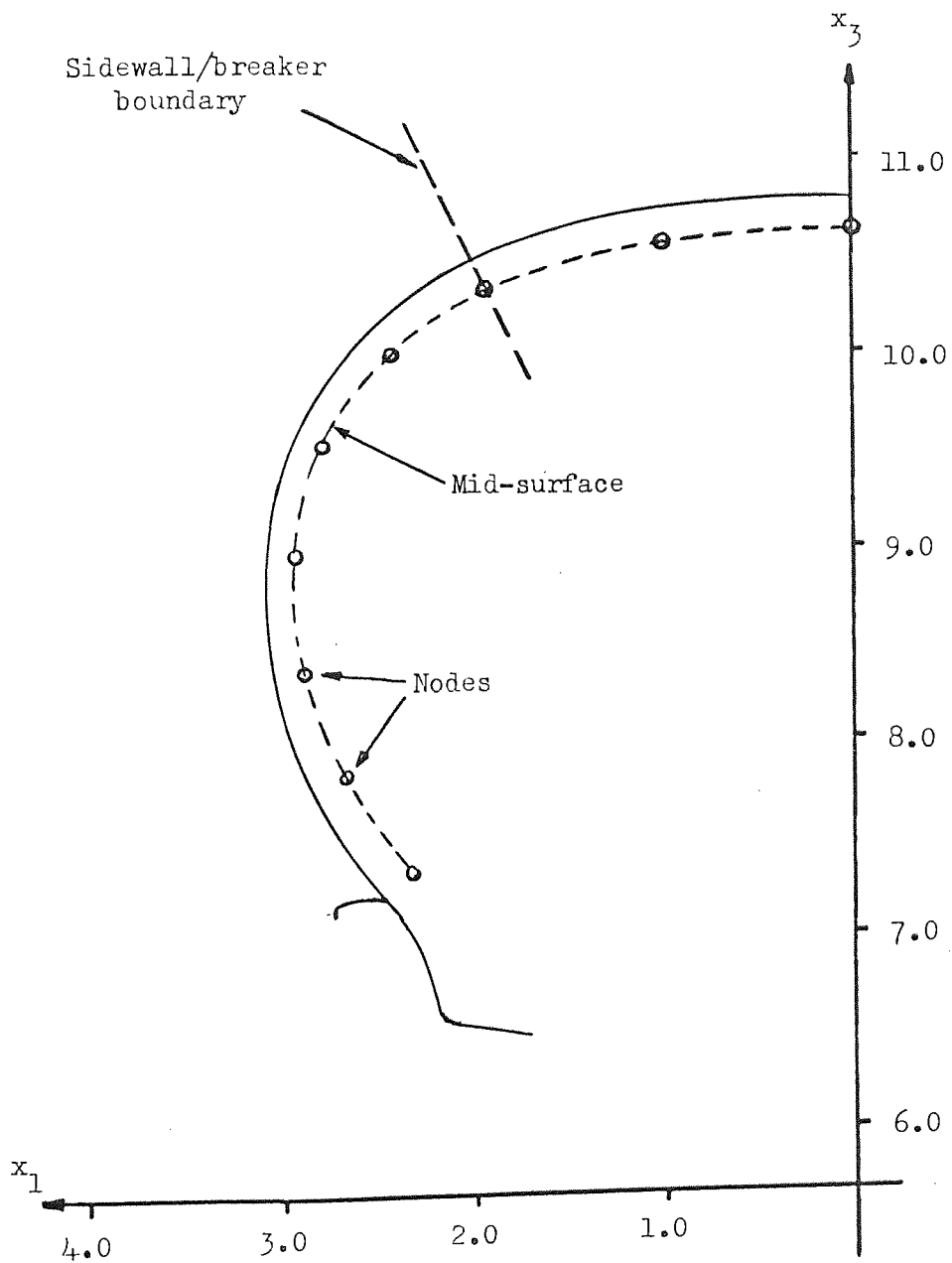
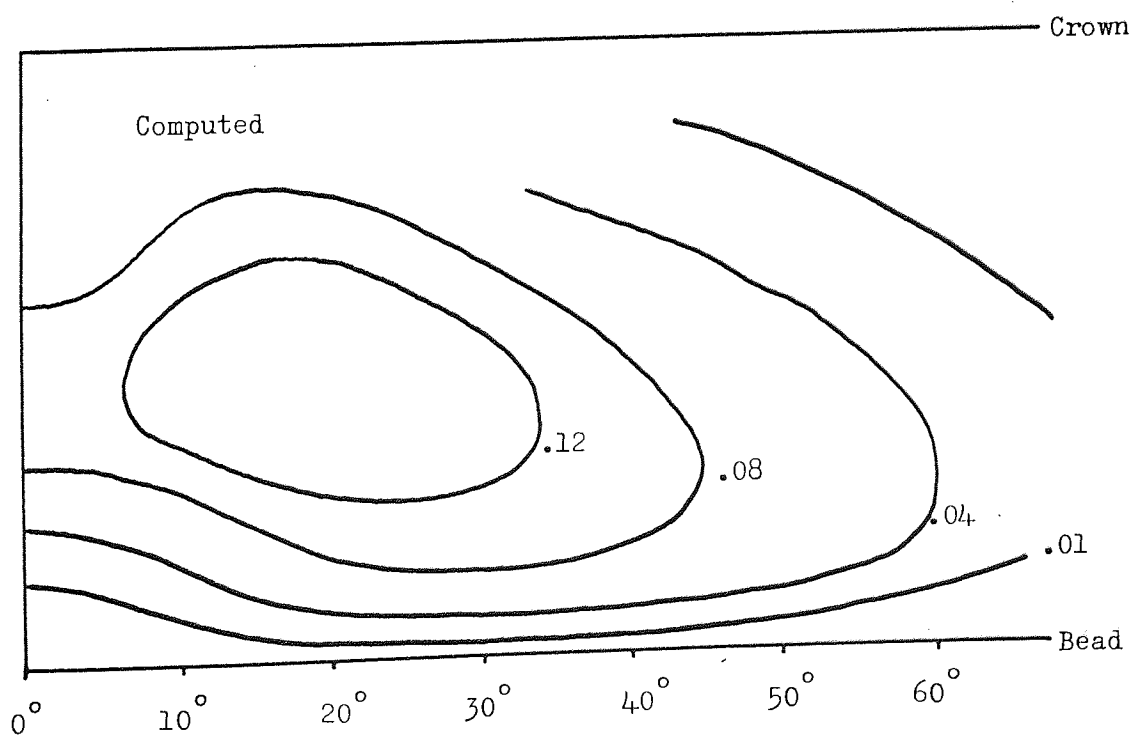
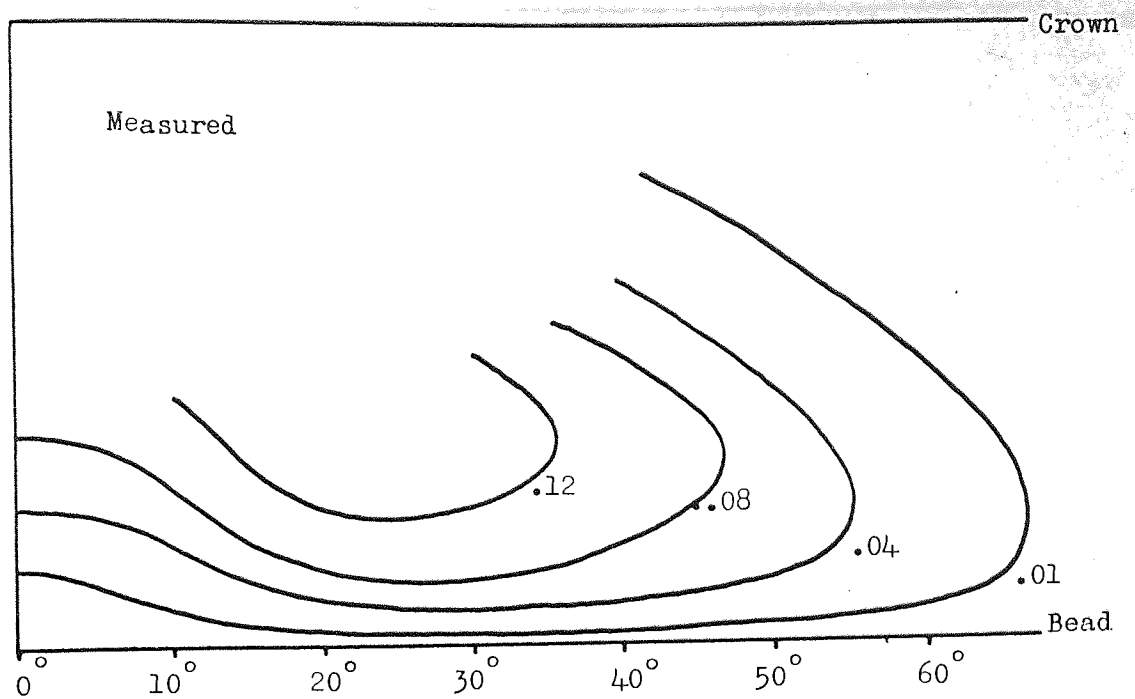


Figure 5.5 Sectional profile of radial ply tyre.



Circumferential angle from centre of contact

Figure 5.6 Displacement (inches) in the x_1 direction for the cross-ply tyre at 0.5 inches deflection.

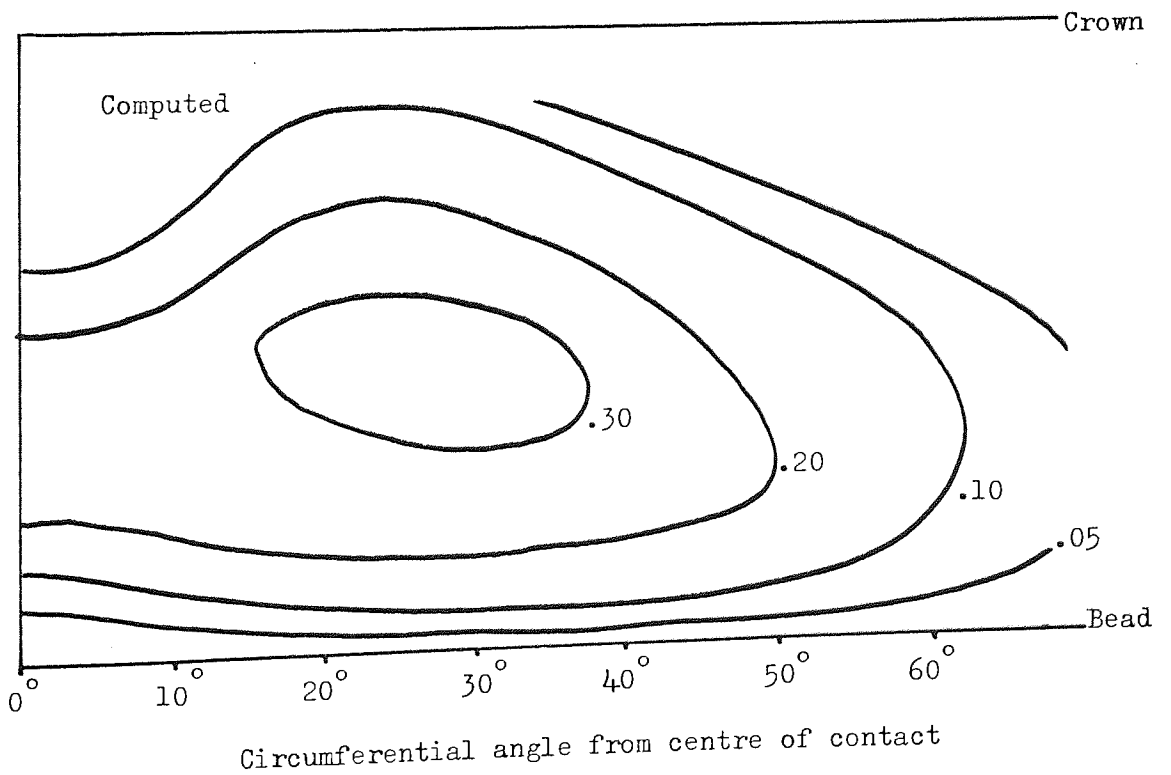
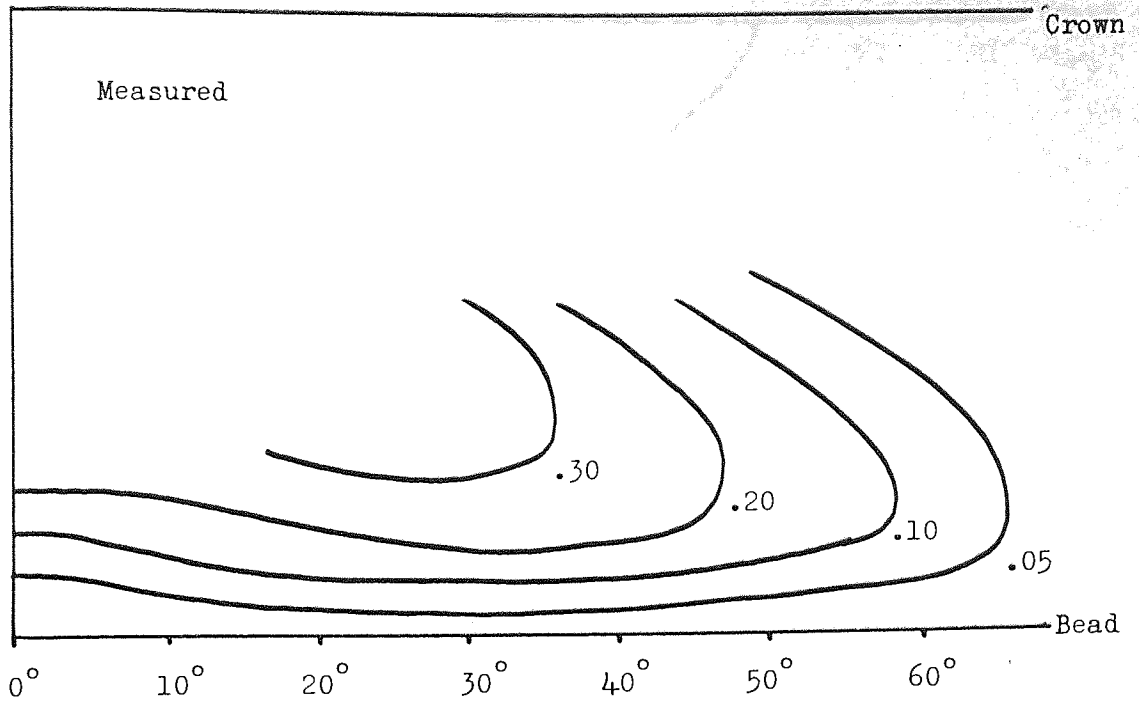


Figure 5.7 Displacement (inches) in the x_1 direction for the cross-ply tyre at 1.0 inches deflection.

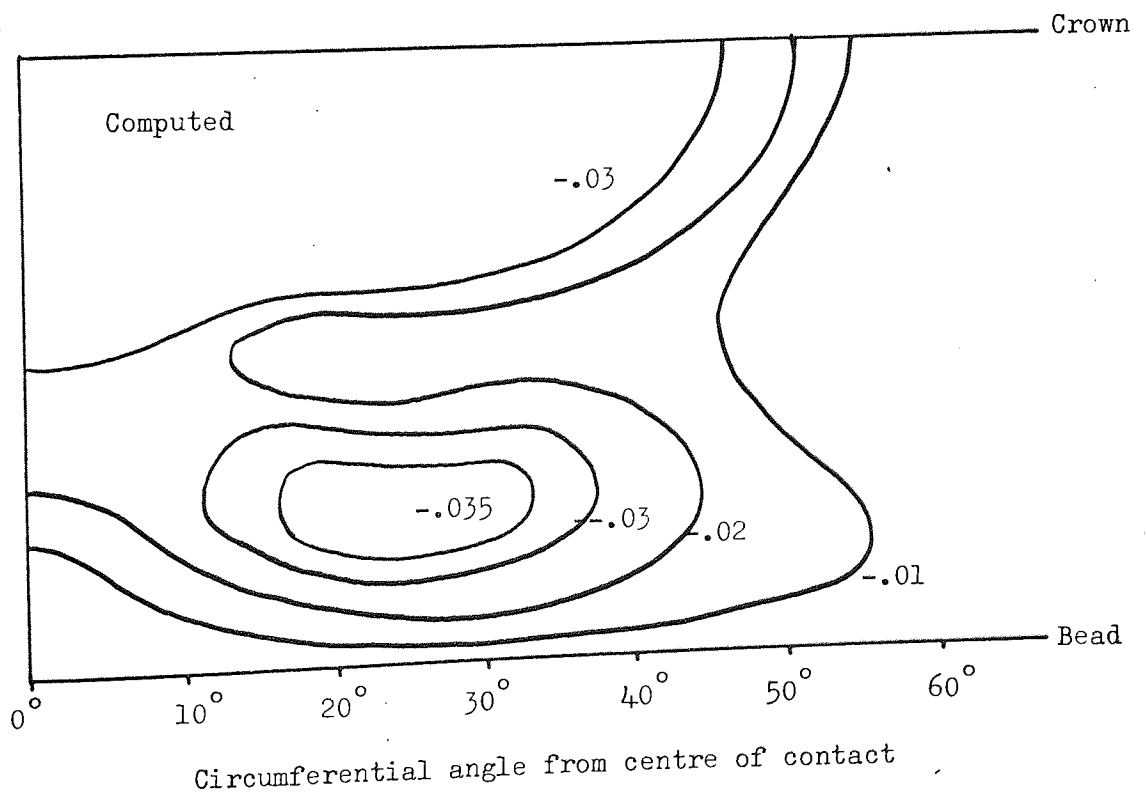
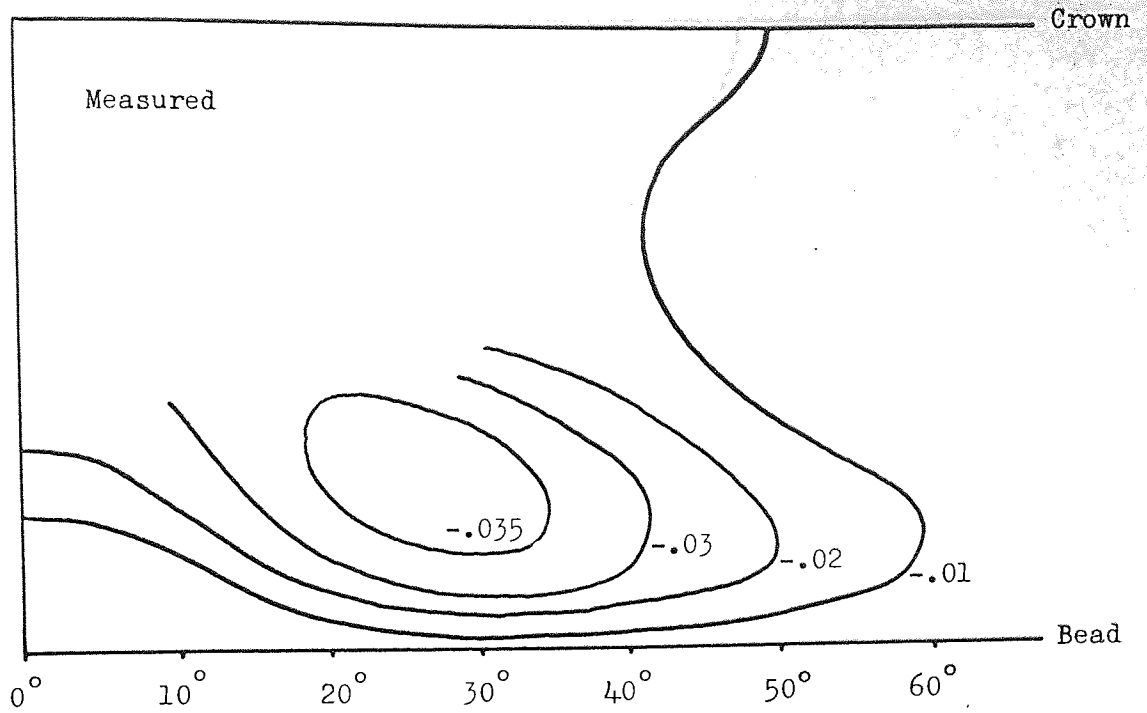


Figure 5.8 Displacement (inches) in the x_2 direction for the cross-ply tyre at 0.5 inches deflection.

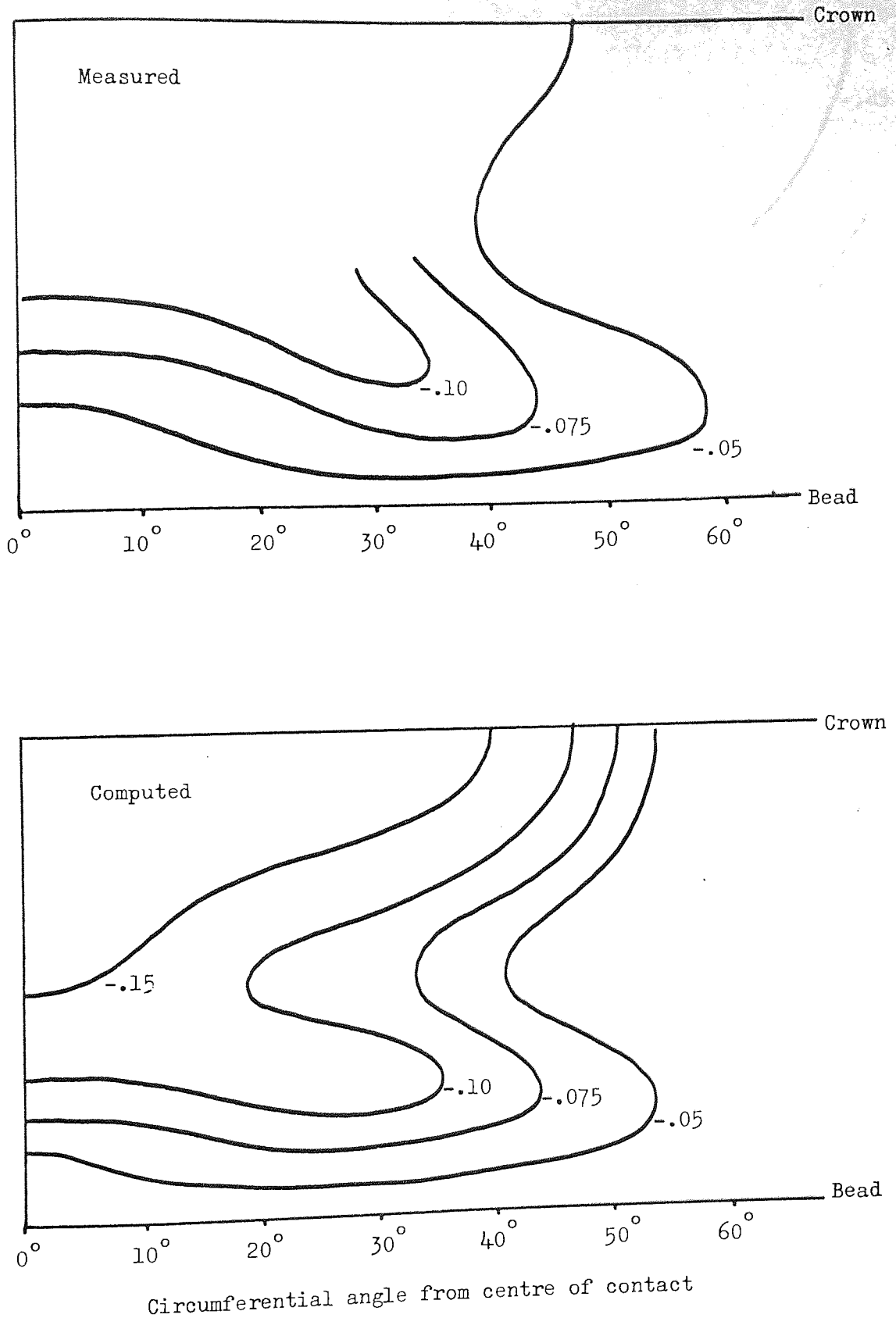
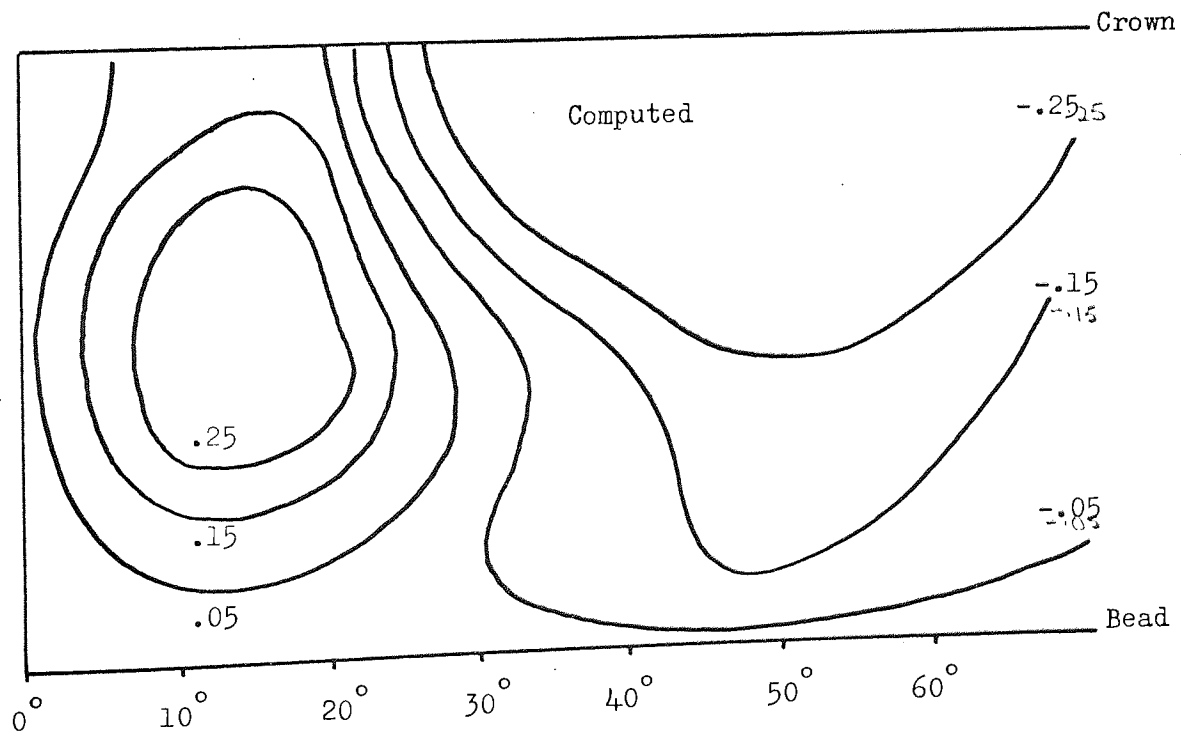
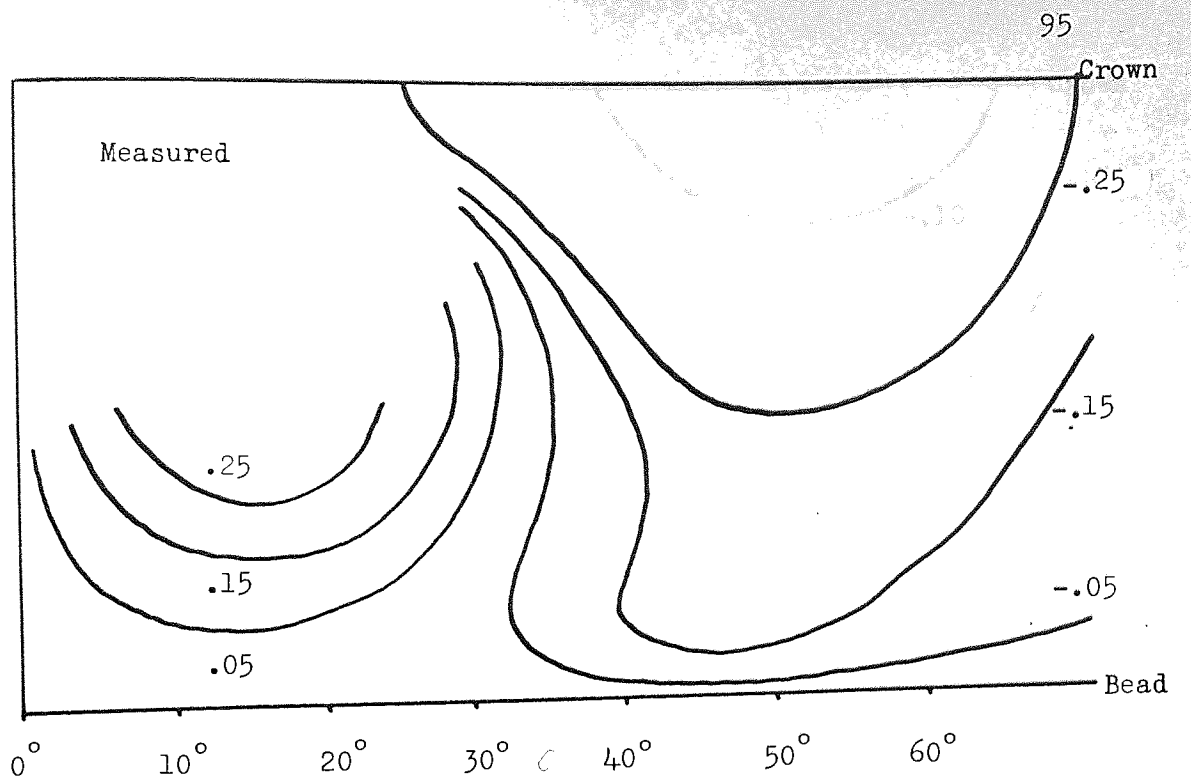
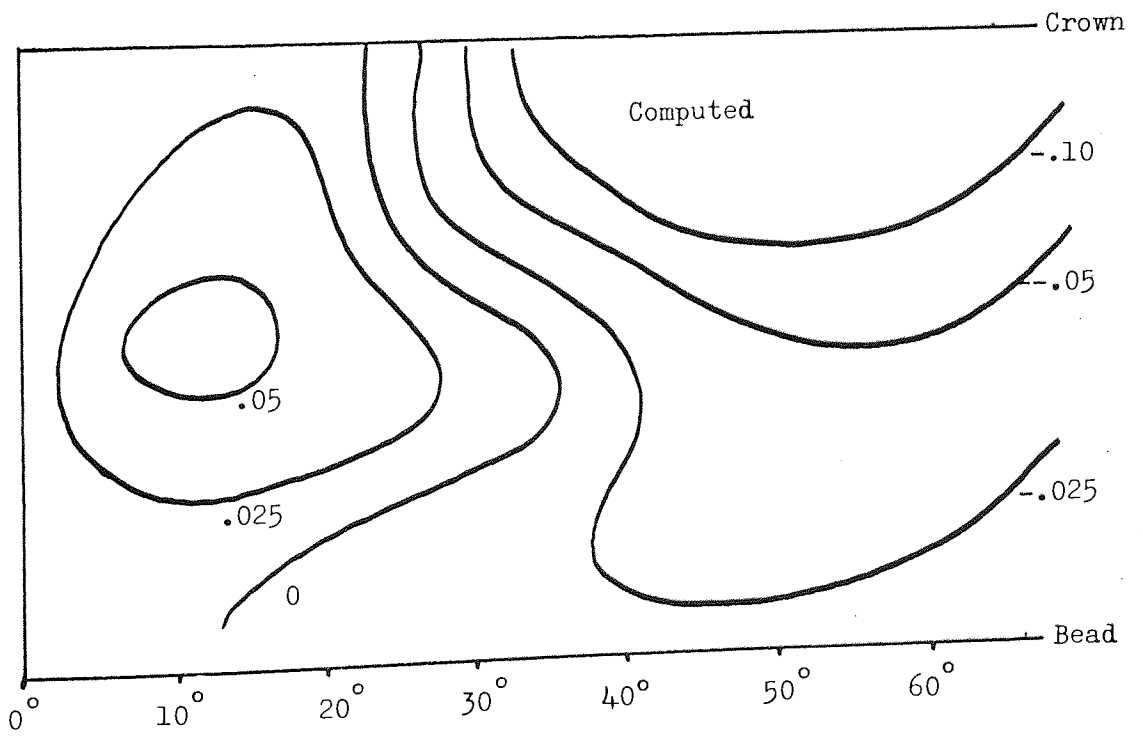
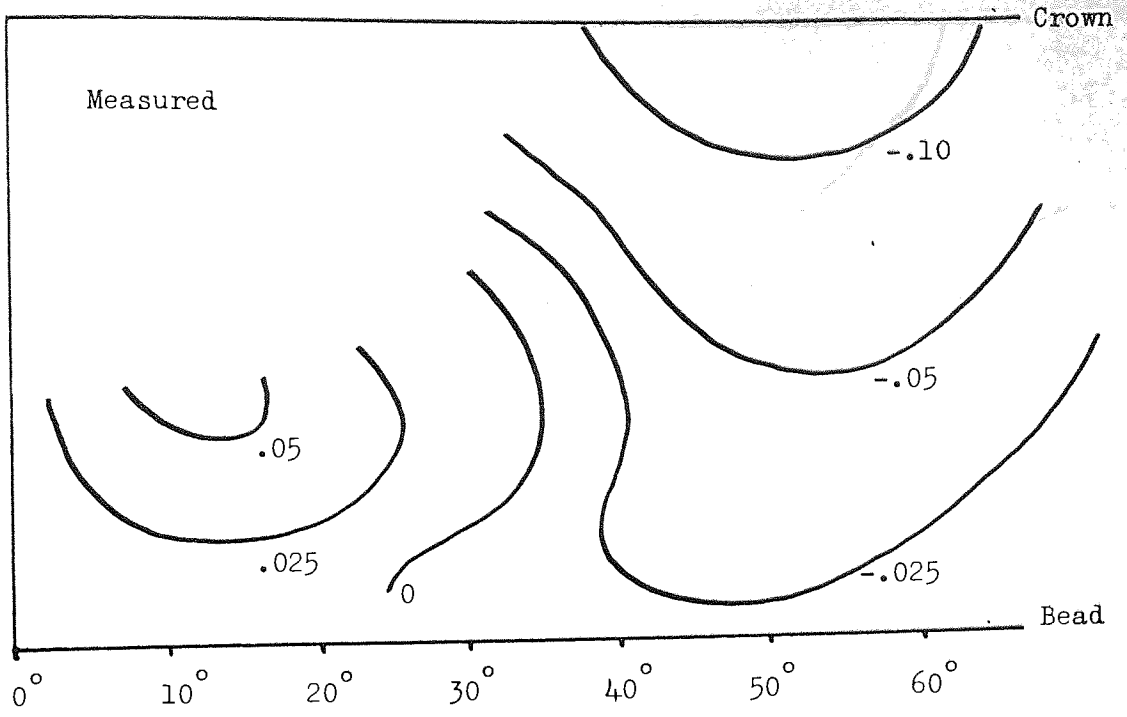


Figure 5.9 Displacement (inches) in the x_2 direction for the cross-ply tyre at 1.0 inches deflection.



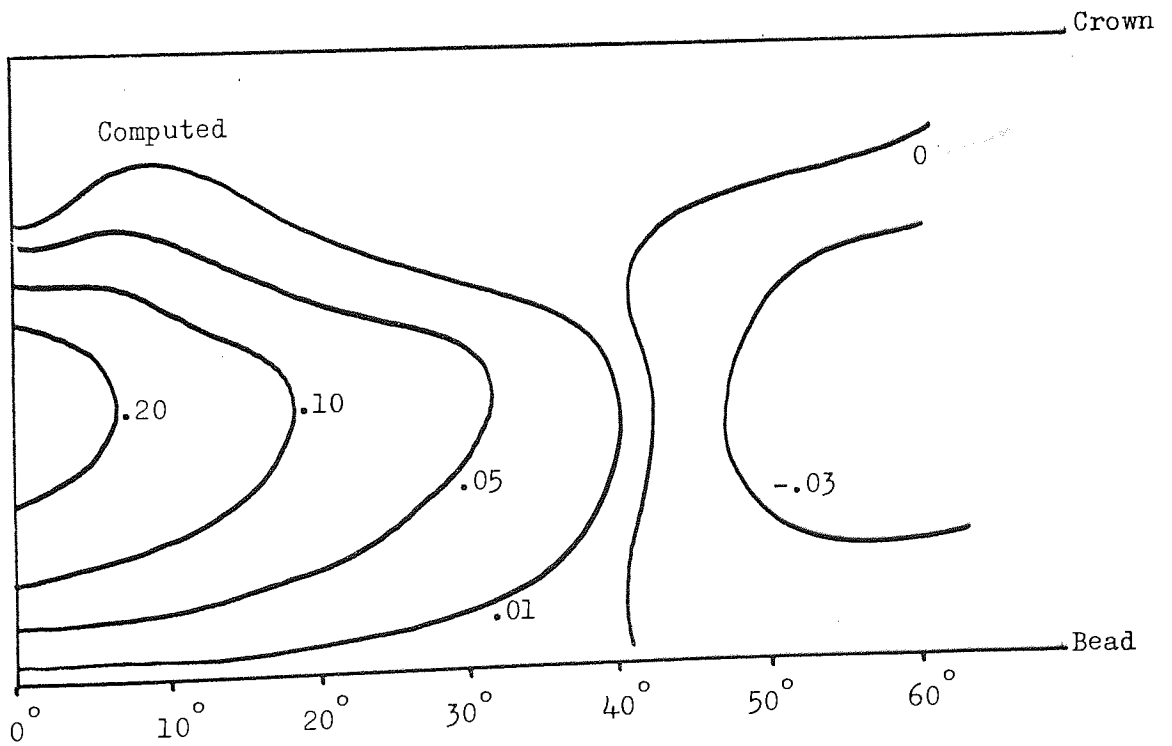
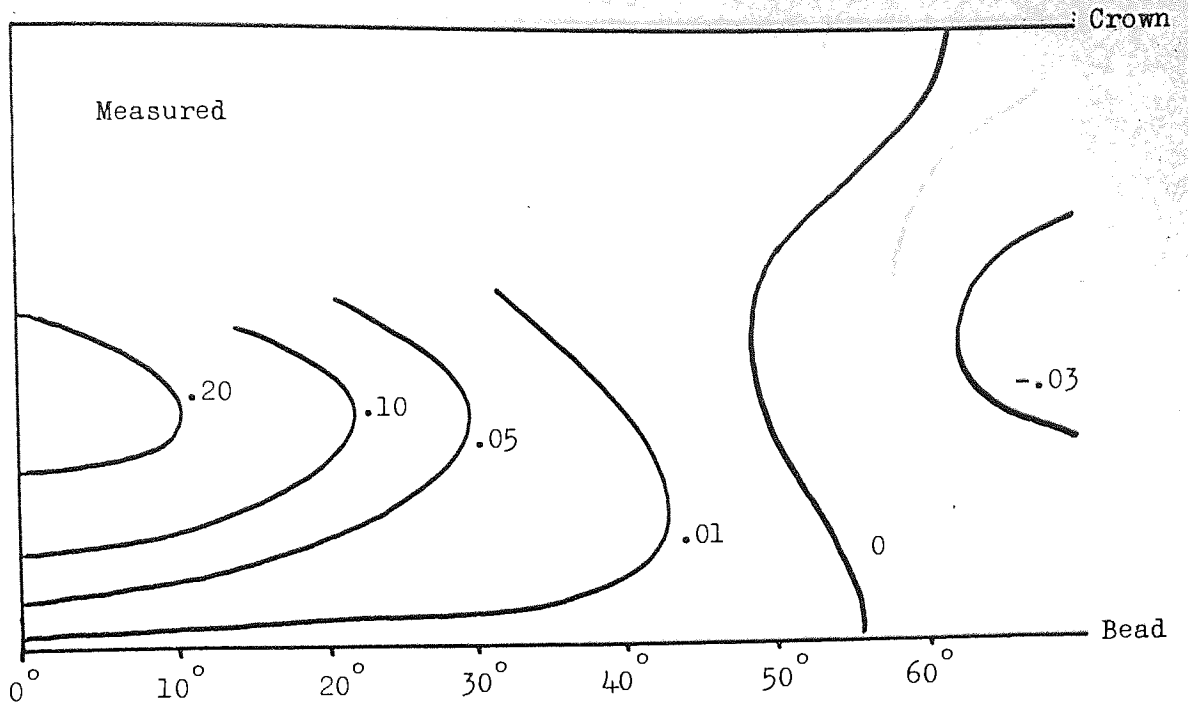
Circumferential angle from centre of contact

Figure 5.10 Displacement (inches) in the x_3 direction for the cross-ply tyre at 0.5 inches deflection.



Circumferential angle from centre of contact

Figure 5.11 Displacement (inches) in the x_z direction for the cross-ply tyre at 1.0 inches deflection.



Circumferential angle from centre of contact

Figure 5.12 Displacement (inches) in the x_1 direction for the radial ply tyre at 0.5 inches deflection.

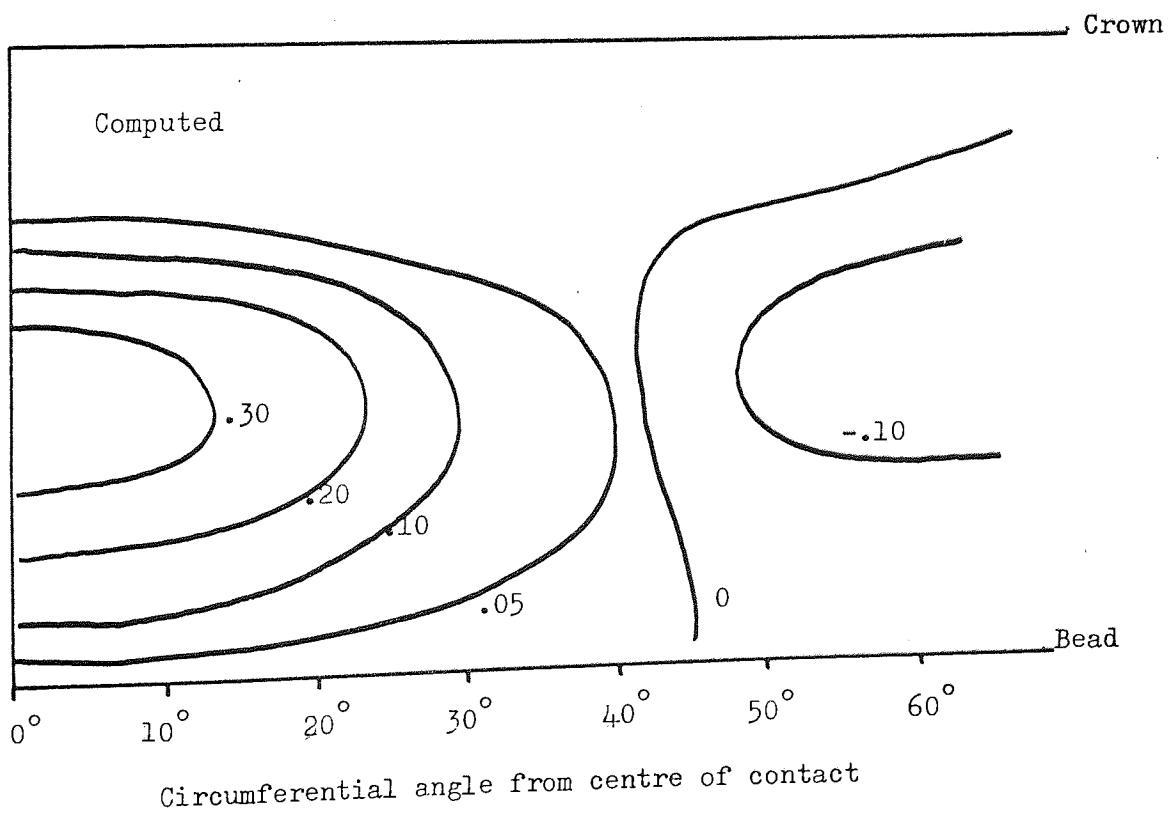
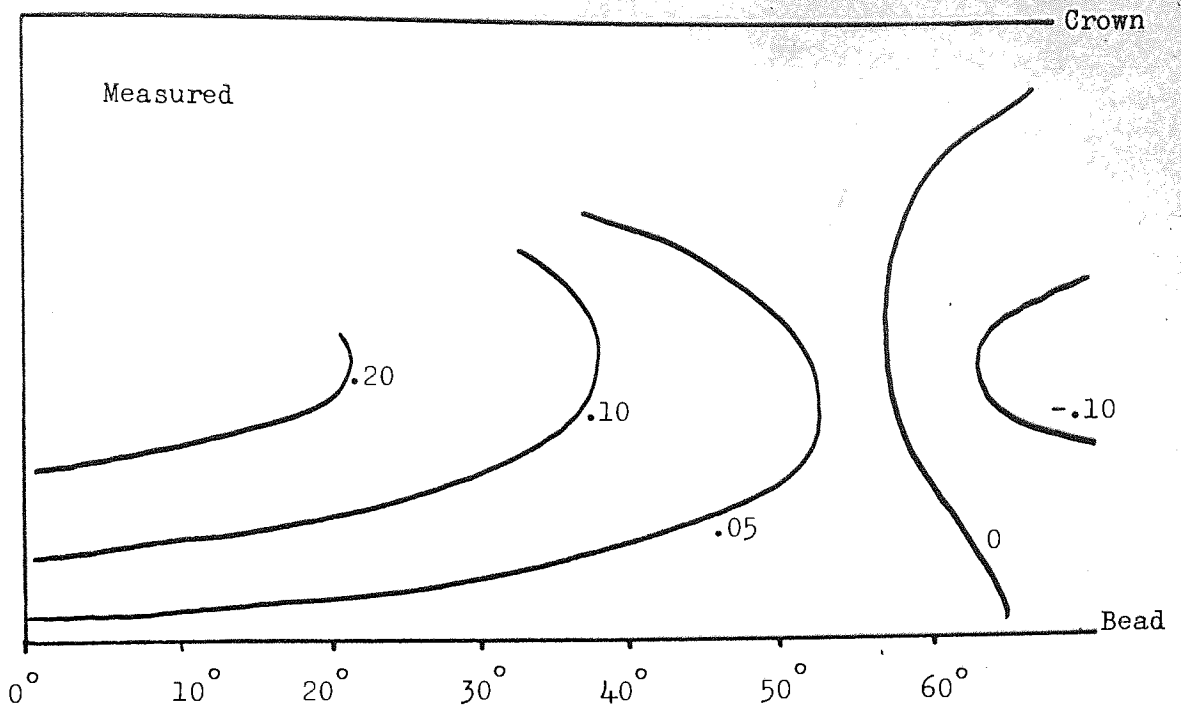
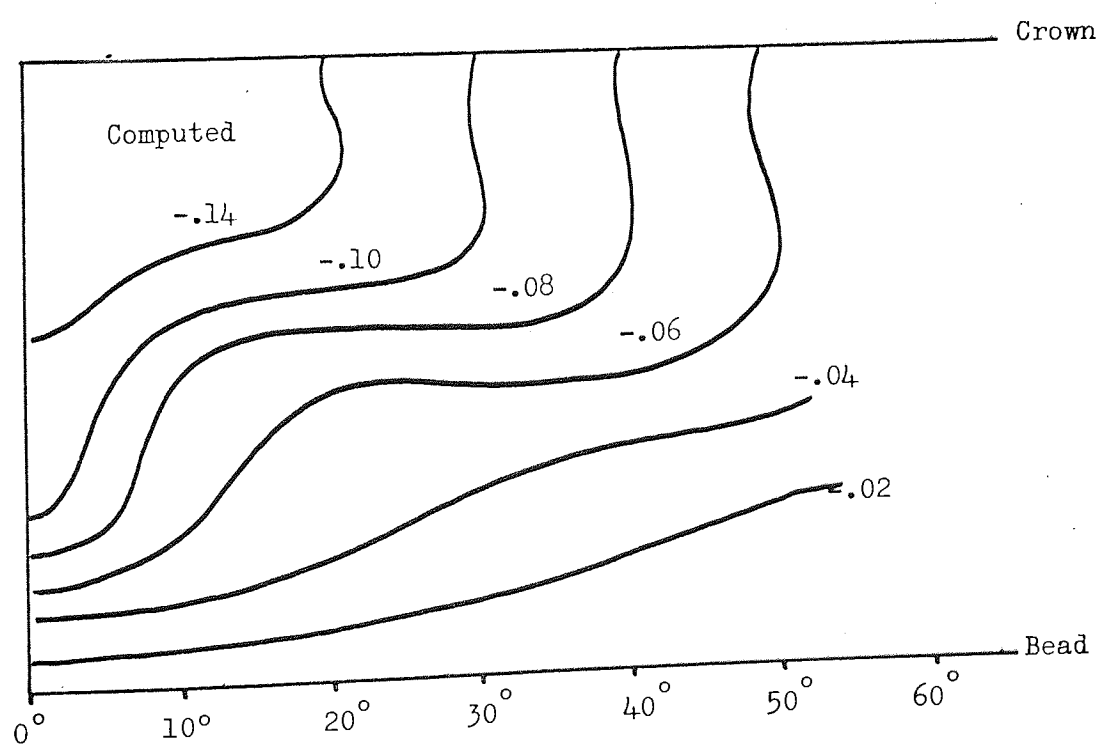
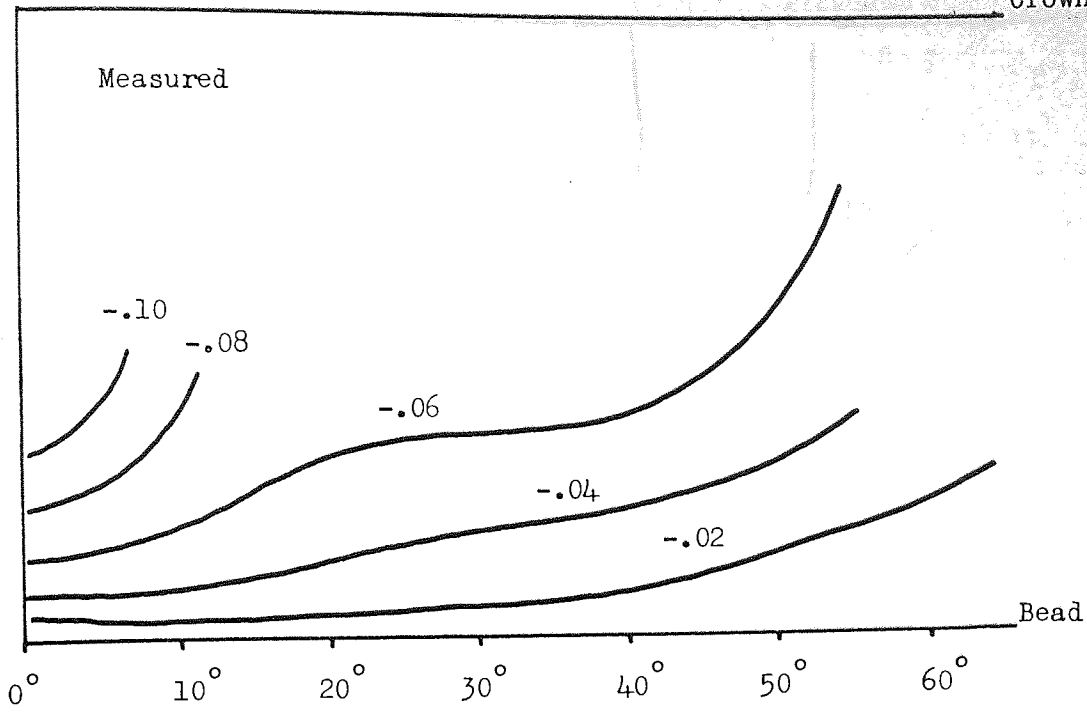
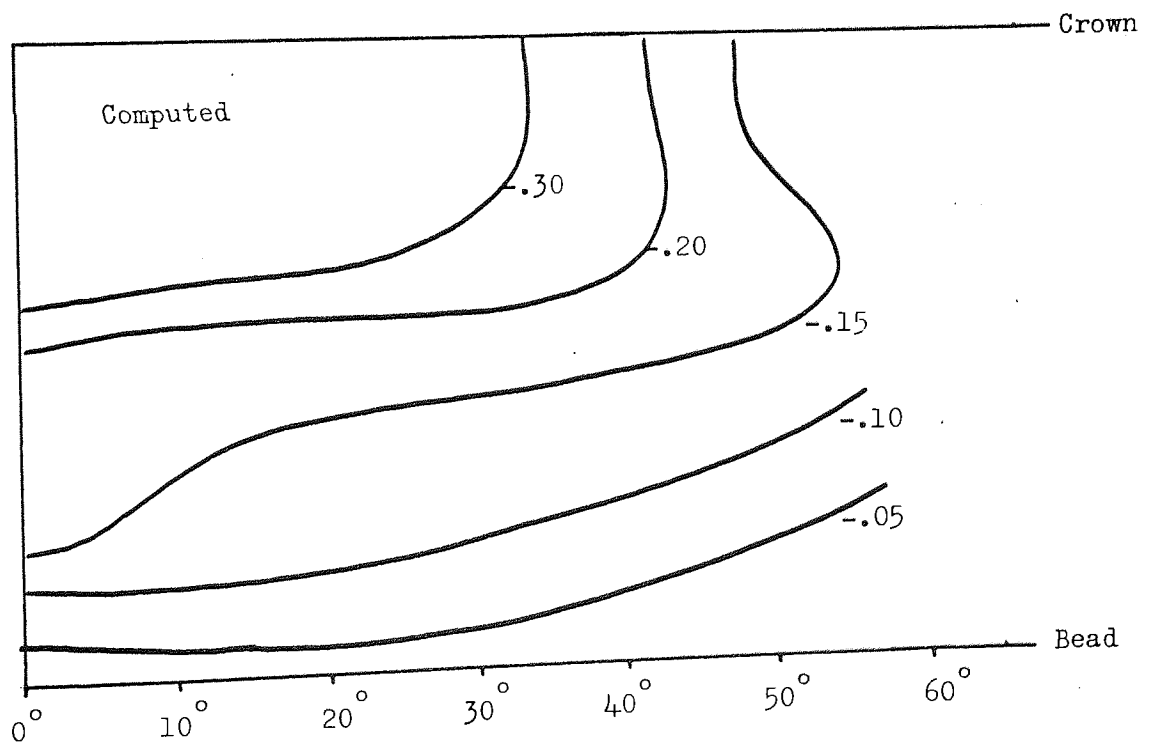
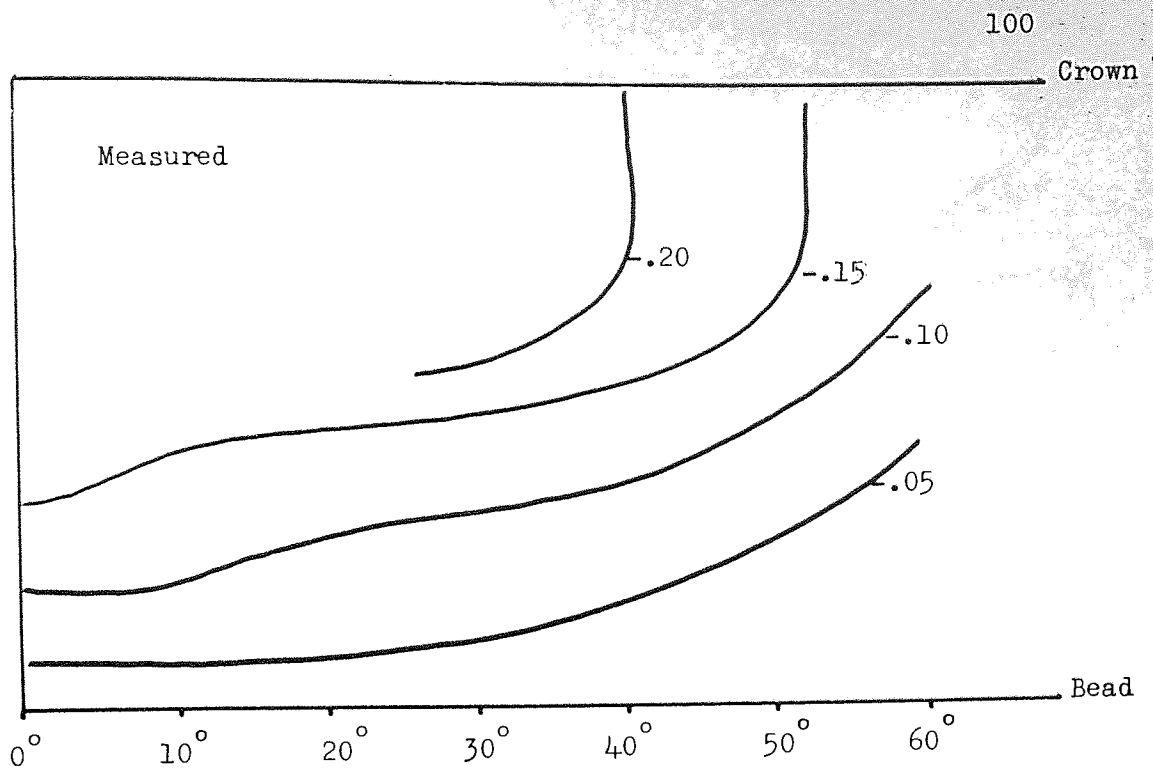


Figure 5.13 Displacement (inches) in the x_1 direction for the radial ply tyre at 1.0 inches deflection.



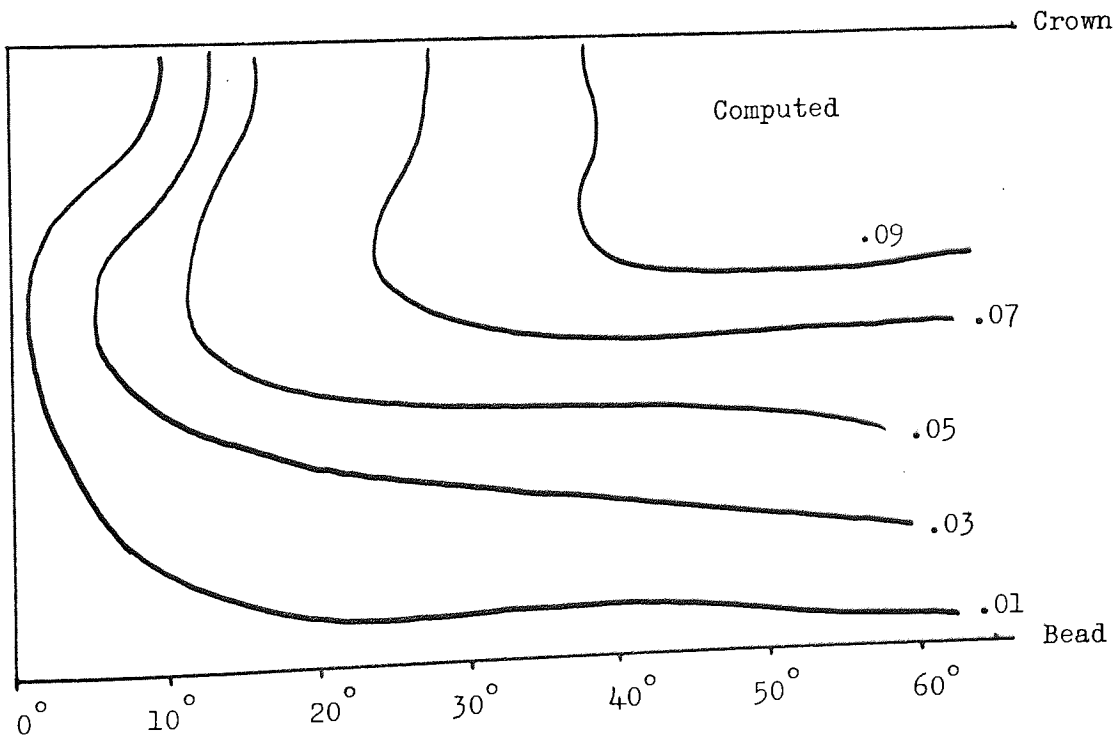
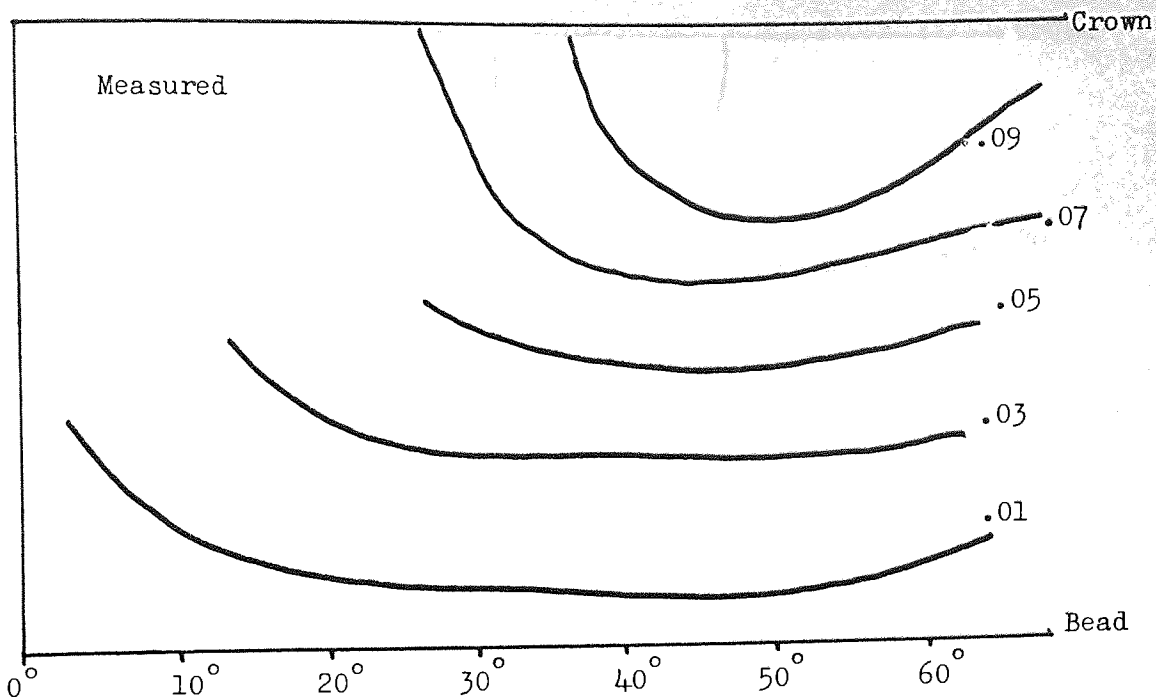
Circumferential angle from centre of contact

Figure 5.14 Displacement (inches) in the x_2 direction for the radial ply tyre at 0.5 inches² deflection.



Circumferential angle from centre of contact

Figure 5.15 Displacement (inches) in the x_2 direction for the radial ply tyre at 1.0 inches² deflection.



Circumferential angle from centre of contact

Figure 5.16

Displacement (inches) in the x_3 direction for the radial ply tyre at 0.5 inches deflection.

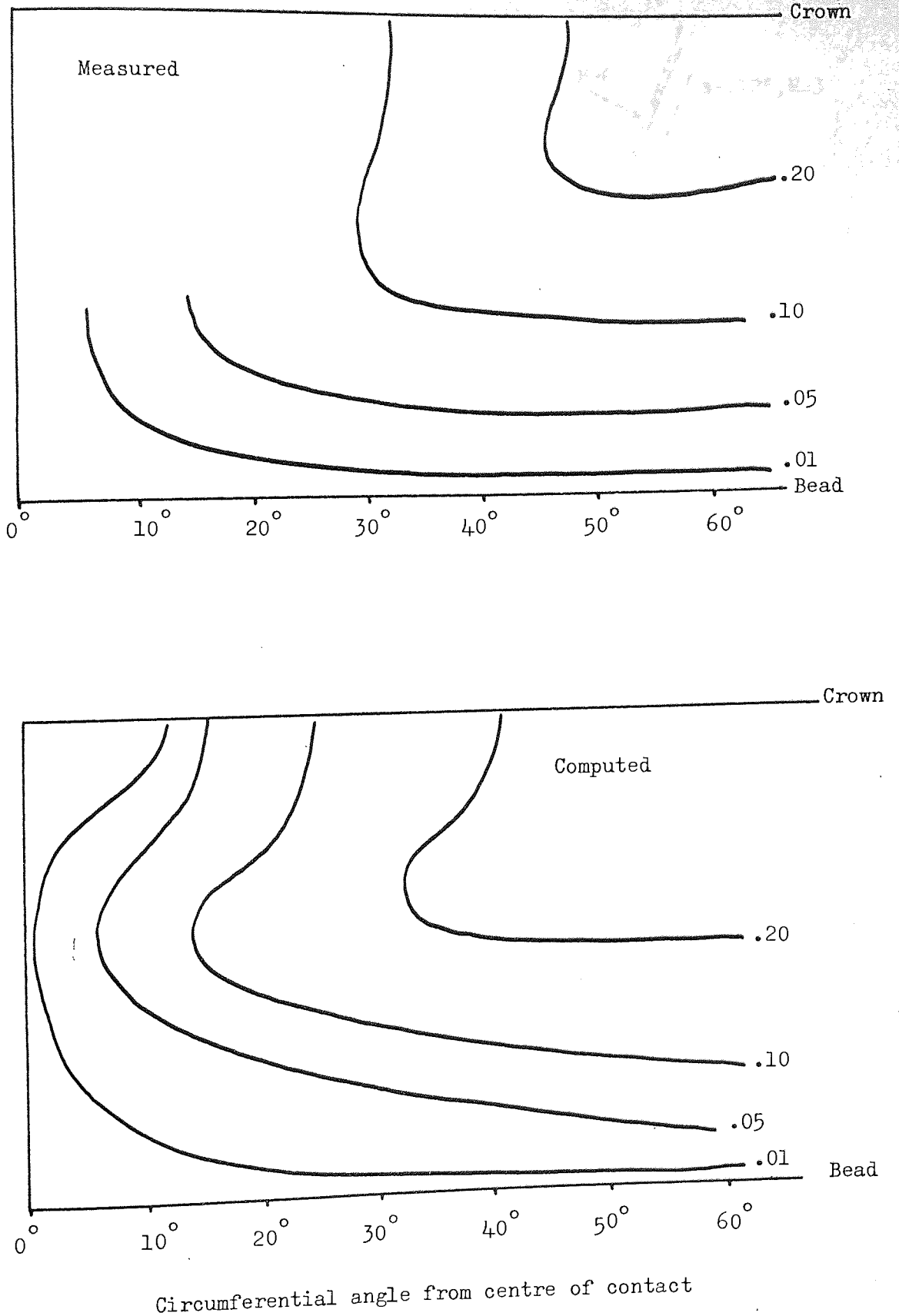


Figure 5.17 Displacement (inches) in the x_3 direction for the radial ply tyre at 1.0 inches³ deflection.

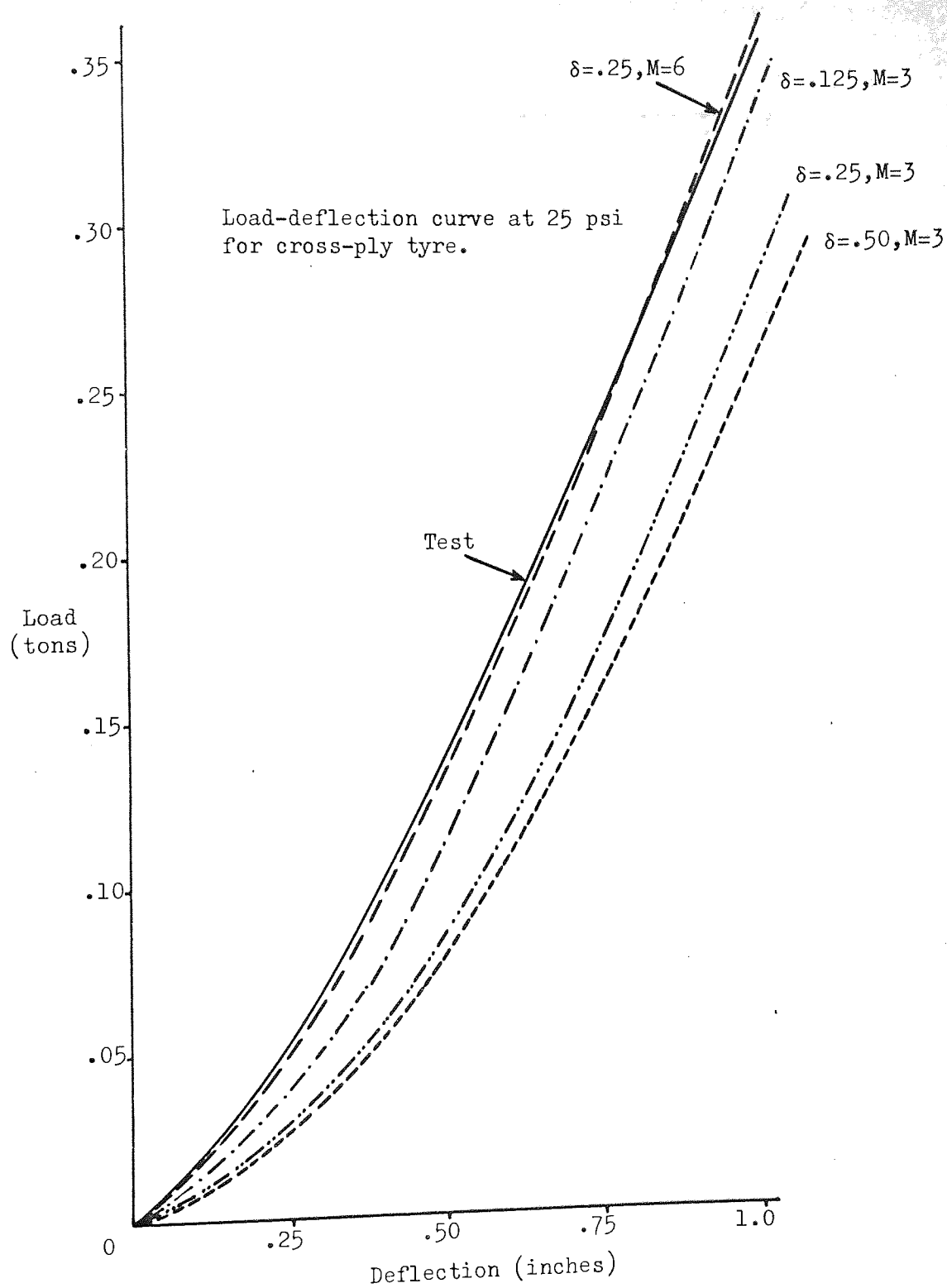


Figure 5.18 Comparison of results for $M=3$ and $M=6$.

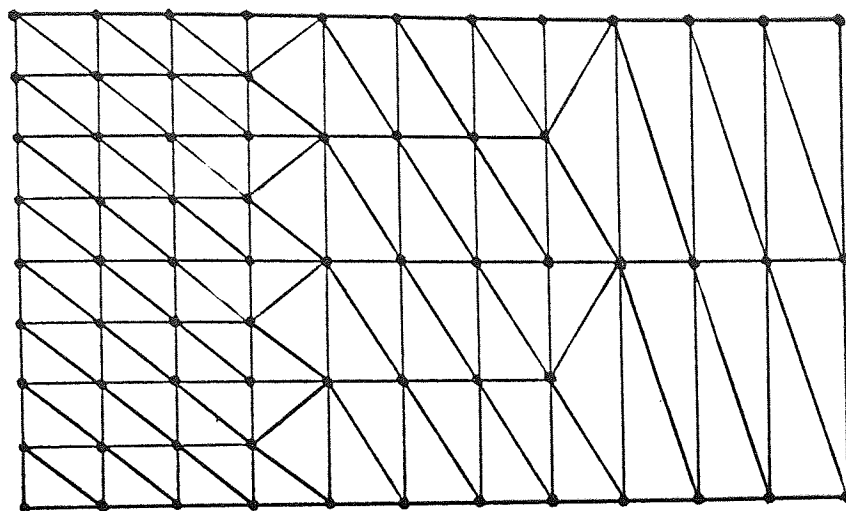
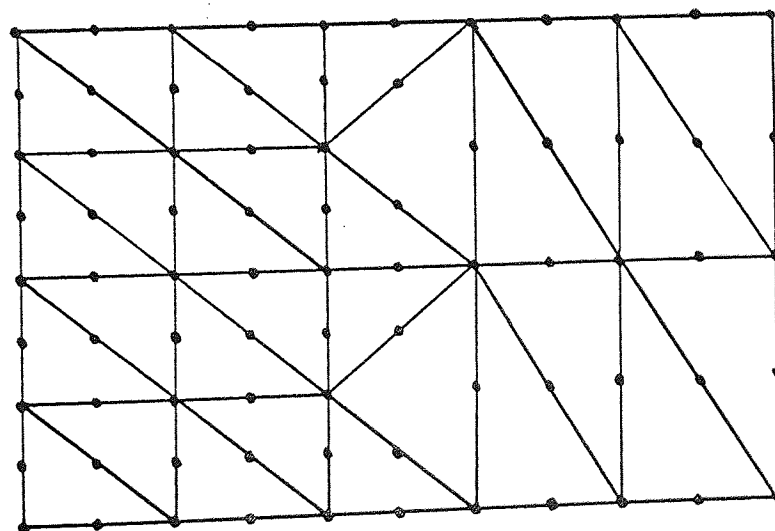
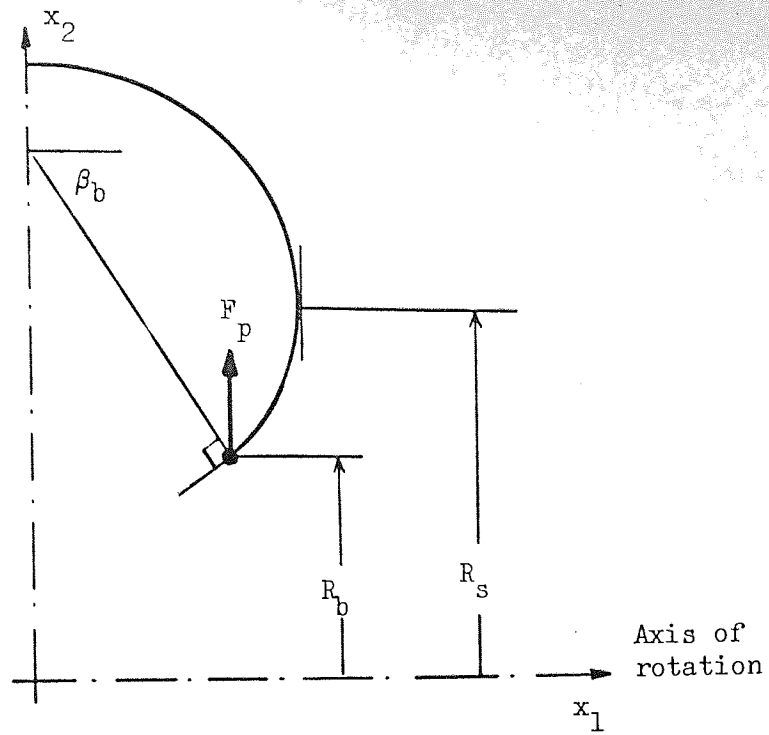
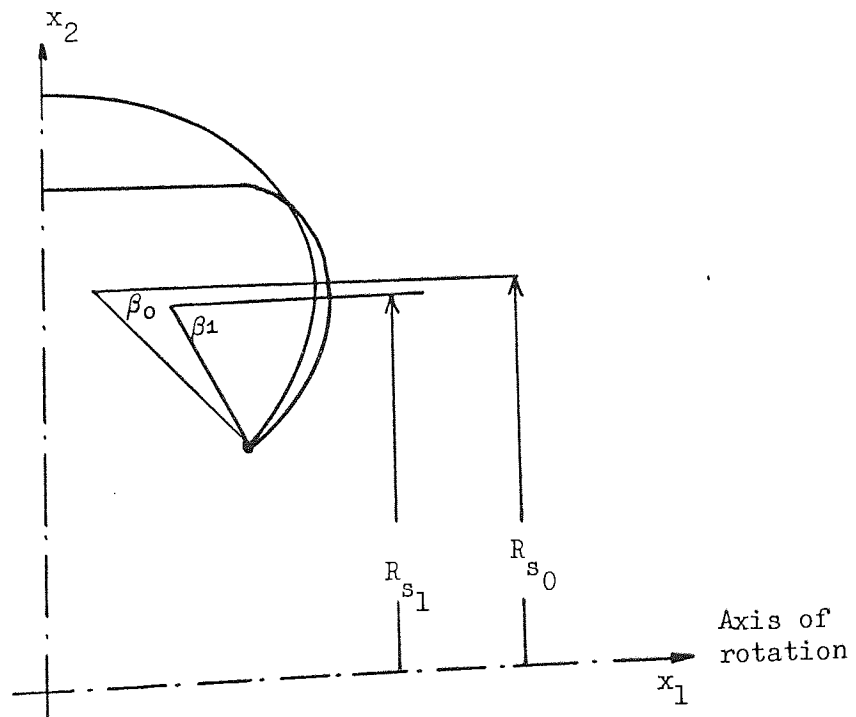
(a) $M=3$ (b) $M=6$

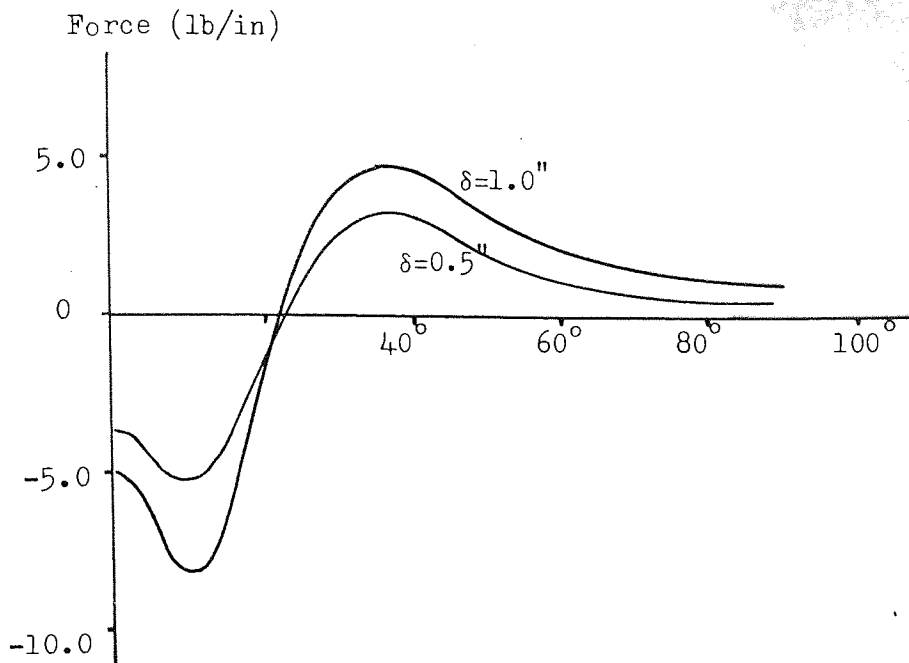
Figure 5.19 Mesh patterns for $M=3$ and $M=6$.



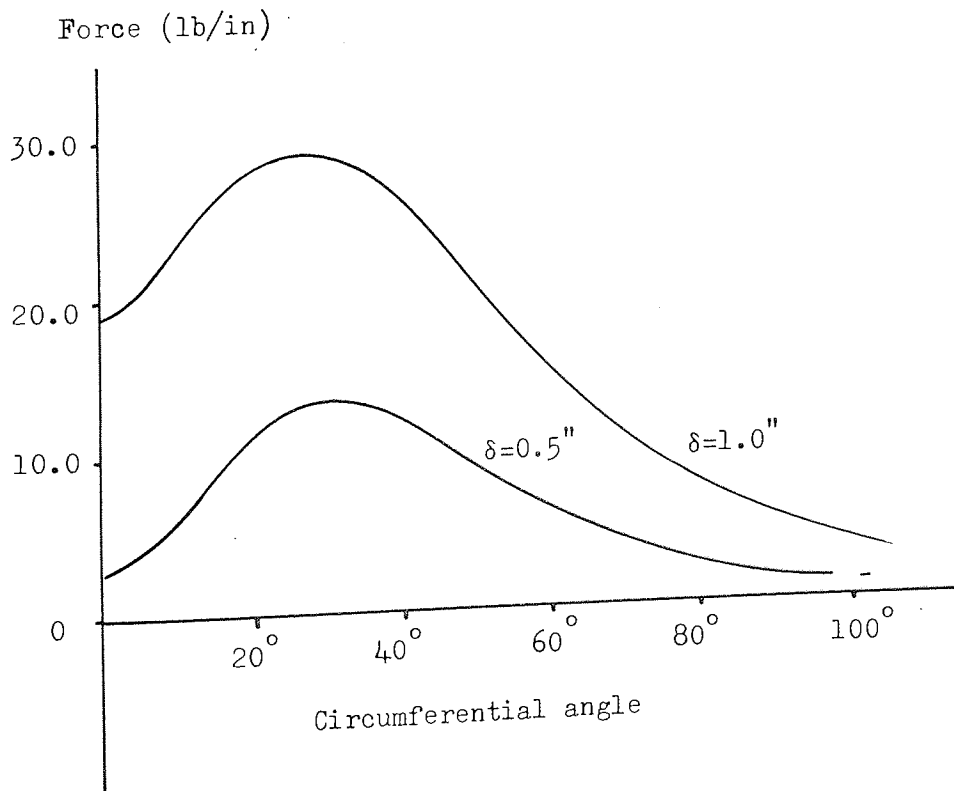
(a) Radial force on bead due to air pressure.



(b) Variation of R_s and β with deflection.



(a) Structural effect.



(b) Air pressure effect.

Figure 5.21 Reactive radial force at bead region due to deflection (Cross-ply tyre).

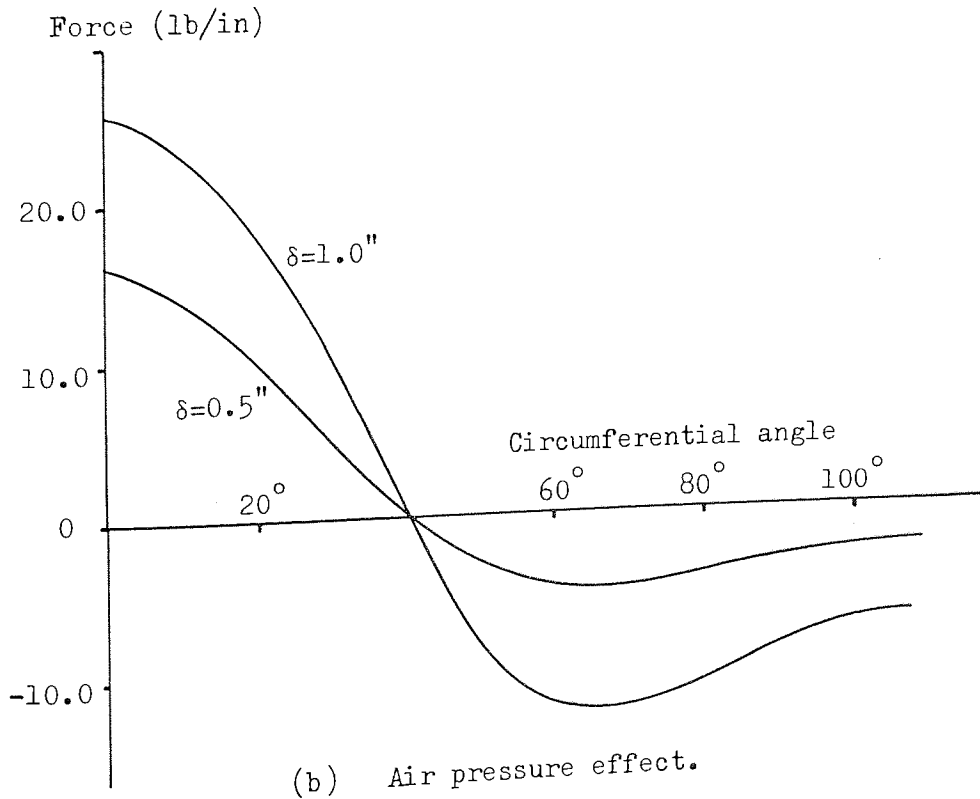
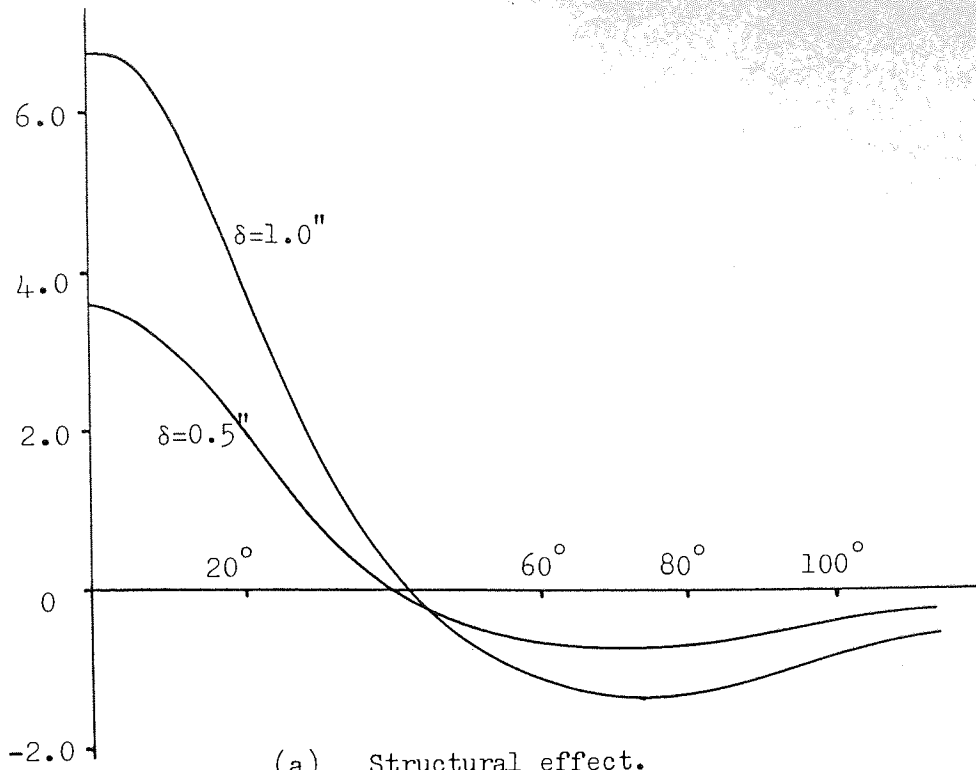
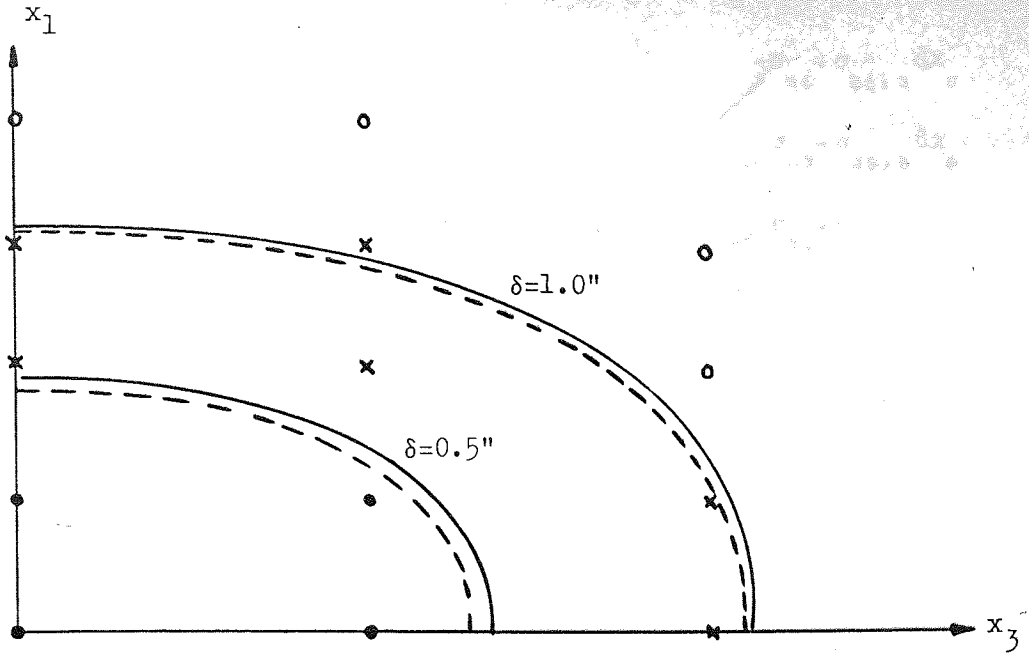
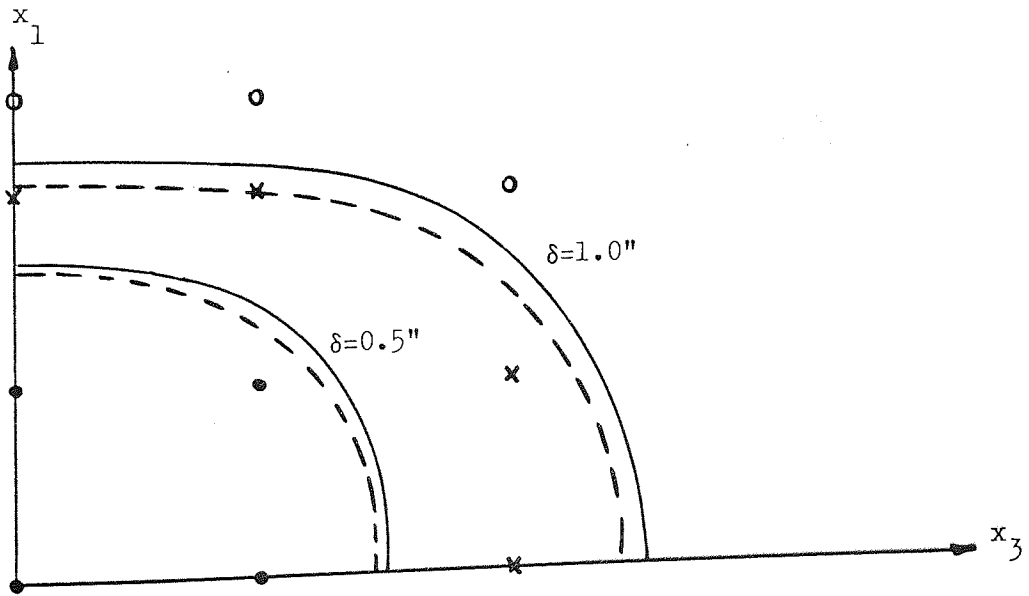


Figure 5.22

Reactive radial force at bead region due to deflection (Radial ply tyre).



(a) Cross-ply tyre.



(b) Radial ply tyre

- KEY
- Measured boundary
 - - - - Estimated boundary
 - Points in contact at $\delta=0.5''$
 - × Points in contact at $\delta=1.0''$
 - Free points

Figure 5.23 Contact areas.

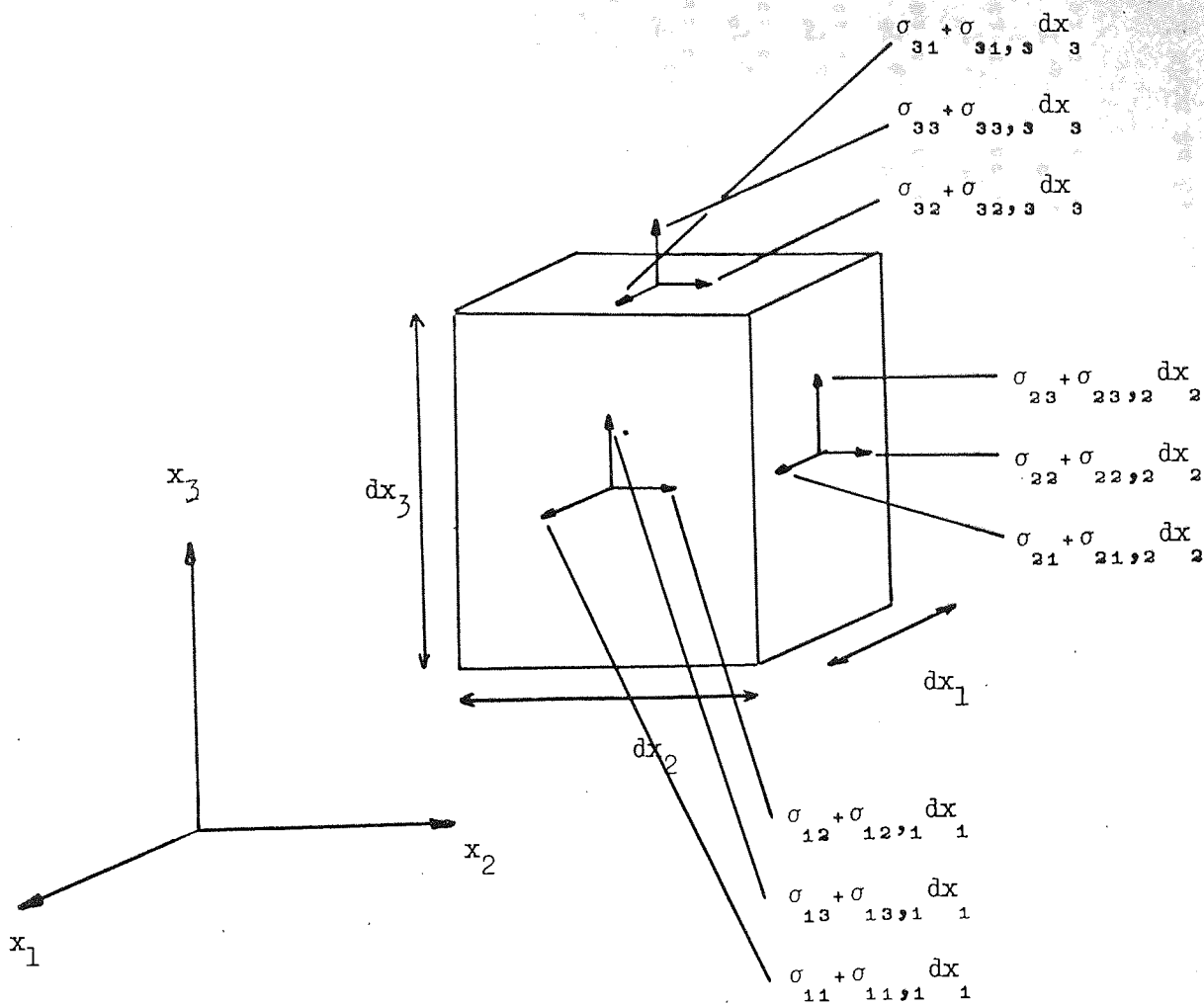


Figure 7.1 Cartesian components of stress acting on three faces of the elemental cube.

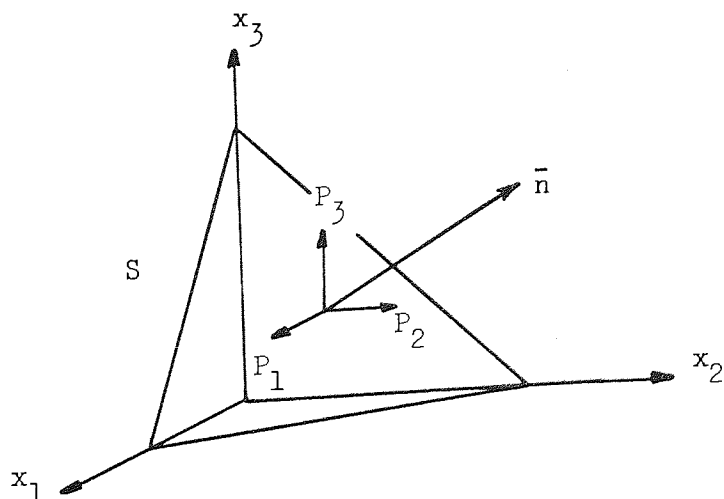


Figure 7.2 Forces acting on elementary tetrahedron.

Node 1			Node 2			Node 3		
u_1	u_2	u_3	u_1	u_2	u_3	u_1	u_2	u_3
θ_1	θ_2		θ_1	θ_2		θ_1	θ_2	
$4\omega_1-1$	$-(4\omega_1-1)$ $\psi_3 \cdot T_{21}^1$	$(4\omega_1-1)$ $\psi_3 \cdot T_{11}^1$	$4\omega_2-1$	$-(4\omega_2-1)$ $\psi_3 \cdot T_{21}^2$	$(4\omega_2-1)$ $\psi_3 \cdot T_{11}^2$	$-(4\omega_3-1)$ $\psi_3 \cdot T_{21}^3$	$(4\omega_3-1)$ $\psi_3 \cdot T_{11}^3$	$-(4\omega_3-1)$ $\psi_3 \cdot T_{11}^3$
	$-(2\omega_1-1)$ $\omega_1 \cdot T_{21}^1$	$(2\omega_1-1)$ $\omega_1 \cdot T_{11}^1$	$4\omega_2-1$	$-(2\omega_2-1)$ $\omega_2 \cdot T_{21}^2$	$(2\omega_2-1)$ $\omega_2 \cdot T_{11}^2$	$-(2\omega_3-1)$ $\omega_3 \cdot T_{21}^3$	$(2\omega_3-1)$ $\omega_3 \cdot T_{11}^3$	$-(2\omega_3-1)$ $\omega_3 \cdot T_{11}^3$
$4\omega_1-1$	$-(4\omega_1-1)$ $\psi_3 \cdot T_{22}^1$	$(4\omega_1-1)$ $\psi_3 \cdot T_{12}^1$		$-(4\omega_2-1)$ $\psi_3 \cdot T_{22}^2$	$(4\omega_2-1)$ $\psi_3 \cdot T_{12}^2$	$-(4\omega_3-1)$ $\psi_3 \cdot T_{22}^3$	$(4\omega_3-1)$ $\psi_3 \cdot T_{12}^3$	$-(4\omega_3-1)$ $\psi_3 \cdot T_{12}^3$
	$-(2\omega_1-1)$ $\omega_1 \cdot T_{22}^1$	$(2\omega_1-1)$ $\omega_1 \cdot T_{12}^1$	$4\omega_2-1$	$-(2\omega_2-1)$ $\omega_2 \cdot T_{22}^2$	$(2\omega_2-1)$ $\omega_2 \cdot T_{12}^2$	$-(2\omega_3-1)$ $\omega_3 \cdot T_{22}^3$	$(2\omega_3-1)$ $\omega_3 \cdot T_{12}^3$	$-(2\omega_3-1)$ $\omega_3 \cdot T_{12}^3$
$4\omega_1-1$	$-(4\omega_1-1)$ $\psi_3 \cdot T_{33}^1$	$(4\omega_1-1)$ $\psi_3 \cdot T_{13}^1$		$-(4\omega_2-1)$ $\psi_3 \cdot T_{33}^2$	$(4\omega_2-1)$ $\psi_3 \cdot T_{13}^2$	$-(4\omega_3-1)$ $\psi_3 \cdot T_{33}^3$	$(4\omega_3-1)$ $\psi_3 \cdot T_{13}^3$	$-(4\omega_3-1)$ $\psi_3 \cdot T_{13}^3$
	$-(2\omega_1-1)$ $\omega_1 \cdot T_{33}^1$	$(2\omega_1-1)$ $\omega_1 \cdot T_{13}^1$		$-(2\omega_2-1)$ $\omega_2 \cdot T_{33}^2$	$(2\omega_2-1)$ $\omega_2 \cdot T_{13}^2$	$-(2\omega_3-1)$ $\omega_3 \cdot T_{33}^3$	$(2\omega_3-1)$ $\omega_3 \cdot T_{13}^3$	$-(2\omega_3-1)$ $\omega_3 \cdot T_{13}^3$

Table 3.2 Matrix form of $[y]$ for $M=6$
(continued overleaf)

Node 4			Node 5			Node 6			
u_1	u_2	u_3	θ_1	θ_2	u_1	u_2	u_3	θ_1	θ_2
$4\omega_2$			$-4\omega_2$ $\cdot \psi_3 \cdot T_{21}^4$	$4\omega_2$ $\cdot \psi_3 \cdot T_{11}^4$	$-4\omega_2$			$4\omega_2$ $\cdot \psi_3 \cdot T_{21}^5$	$-4\omega_2$ $\cdot \psi_3 \cdot T_{11}^5$
	$4\omega_1$		$-4\omega_1$ $\cdot \psi_3 \cdot T_{21}^4$	$4\omega_1$ $\cdot \psi_3 \cdot T_{11}^4$	$4(\omega_3 - \omega_1)$			$-4(\omega_3 - \omega_1)$ $\cdot \psi_3 \cdot T_{21}^5$	$4(\omega_3 - \omega_1)$ $\cdot \psi_3 \cdot T_{11}^5$
		$4\omega_3$	$-4\omega_3$ $\cdot T_{21}^4$	$4\omega_3$ $\cdot T_{11}^4$				$-4\omega_3$ $\cdot T_{21}^5$	$4\omega_3$ $\cdot T_{11}^5$
			$-4\omega_2$ $\cdot \psi_3 \cdot T_{22}^4$	$4\omega_2$ $\cdot \psi_3 \cdot T_{12}^4$	$-4\omega_2$			$4\omega_2$ $\cdot \psi_3 \cdot T_{22}^5$	$-4\omega_2$ $\cdot \psi_3 \cdot T_{12}^5$
			$-4\omega_1$ $\cdot \psi_3 \cdot T_{22}^4$	$4\omega_1$ $\cdot \psi_3 \cdot T_{12}^4$	$4(\omega_3 - \omega_2)$			$-4(\omega_3 - \omega_2)$ $\cdot \psi_3 \cdot T_{22}^5$	$4(\omega_3 - \omega_2)$ $\cdot \psi_3 \cdot T_{12}^5$
			$-4\omega_3$ $\cdot T_{22}^4$	$4\omega_3$ $\cdot T_{12}^4$				$-4\omega_3$ $\cdot T_{22}^5$	$4\omega_3$ $\cdot T_{12}^5$
			$-4\omega_2$ $\cdot \psi_3 \cdot T_{23}^4$	$4\omega_2$ $\cdot \psi_3 \cdot T_{13}^4$				$-4\omega_2$ $\cdot \psi_3 \cdot T_{23}^5$	$4\omega_2$ $\cdot \psi_3 \cdot T_{13}^5$
			$-4\omega_1$ $\cdot \psi_3 \cdot T_{23}^4$	$4\omega_1$ $\cdot \psi_3 \cdot T_{13}^4$	$4(\omega_3 - \omega_1)$			$-4(\omega_3 - \omega_1)$ $\cdot \psi_3 \cdot T_{23}^5$	$4(\omega_3 - \omega_1)$ $\cdot \psi_3 \cdot T_{13}^5$
			$-4\omega_3$ $\cdot T_{23}^4$	$4\omega_3$ $\cdot T_{13}^4$				$-4\omega_3$ $\cdot T_{23}^5$	$4\omega_3$ $\cdot T_{13}^5$

Table 3.2 continued

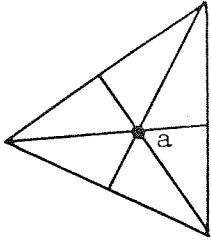
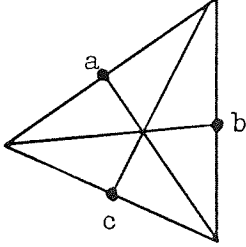
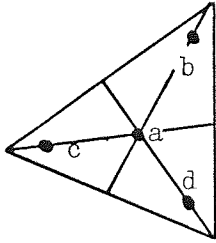
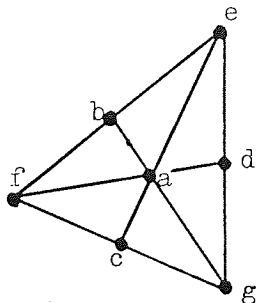
Figure	Points	Triangular co-ordinates	Weights
	a	.3333, .3333, .3333	.50
	a b c	.50 , .50 , .0 .0 , .50 , .50 .50 , .0 , .50	.1667 .1667 .1667
	a b c d	.3333, .3333, .3333 .7333, .1333, .1333 .1333, .7333, .1333 .1333, .1333, .7333	.2813 } .2604
	a b c d e f g	.3333, .3333, .3333 .50 , .50 , .0 .0 , .50 , .50 .50 , .0 , .50 1.0 , .0 , .0 .0 , 1.0 , .0 .0 , .0 , 1.0	.2250 } .0667 } .0250

Table 4.1 Numerical integration points for triangles.

$$\int_{-1}^1 g(x) dx = \sum_{j=1}^n G_j g(x_j)$$

n	$\pm x_j$	G_j
2	0.5773503	1.0
3	0.0 0.7745967	0.8755833 0.5622084
4	0.3399810 0.8611363	0.6510684 0.3489316
5	0.0 0.5384693 0.9061798	0.5652007 0.4860118 0.2313879

Table 4.2 Gaussian quadrature formulae.

Boundary number	Degree of freedom				
	u_1	u_2	u_3	θ_1	θ_2
1	0	0	0	0	0
2	0			0	
3,4			0		0

0 represents a fixed degree of freedom with a value of zero.

Table 4.3 Initial boundary conditions.

APPENDIXMathematical basis of the finite element method7.1 Stress at a point

The state of internal force at any point in a body is defined in terms of nine components of the stress tensor

$$\sigma_{ij} \quad i, j = 1, 2, 3 \quad (7.1)$$

where the first subscript denotes the plane that is normal to the i^{th} axis, and the second subscript refers to the co-ordinate direction of the stress.

An elemental cube situated in the body will be subject to the forces as shown in Figure 7.1. This shows the Cartesian components of stress acting on the three visible faces of the cube. The corresponding stresses on the opposite faces do not include the incremental stresses.

By taking moments about the Cartesian axes, it can be shown that the stress tensor is symmetric,

$$\sigma_{ij} = \sigma_{ji} \quad i, j = 1, 2, 3 \quad (7.2)$$

7.2 Equations of equilibrium

If the elemental cube is also subjected to body forces of the form

$$B_i \quad i = 1, 2, 3 \quad (7.3)$$

in the direction of the Cartesian axes, then from Figure 7.1, the equations of motion for the cube are:

$$\sigma_{ij,j} + B_i - \rho u_i = 0 \quad (7.4)$$

where ρ is the density of the body. The repeated subscript denotes

tensorial summation, and the comma denotes differentiation.

For static equilibrium, equation (7.4) reduces to

$$\sigma_{ij,j} + B_i = 0 \quad (7.5)$$

7.3 Strain-displacement relationship

The state of strain at any point is defined by the strain tensor

$$\epsilon_{ij} \quad i, j = 1, 2, 3 \quad (7.6)$$

For small deflection theory the relationship between strain and displacement is given by:

$$\epsilon_{ij} = \frac{1}{2} (u_{i,j} + u_{j,i}) \quad i, j = 1, 2, 3 \quad (7.7)$$

where the u_i are the components of displacement. From equation (7.7)

it is evident that the strain tensor is symmetric, so

$$\epsilon_{ij} = \epsilon_{ji} \quad i, j = 1, 2, 3 \quad (7.8)$$

7.4 Stress-strain relationship

In the case of a linearly elastic system, Hooke's Law represents the relationship between stress and strain. The tensorial form is:

$$\sigma_{ij} = d_{ijkl} \epsilon_{kl} \quad i, j, k, l = 1, 2, 3 \quad (7.9)$$

The equations (7.5), (7.7) and (7.9), together with the symmetry properties, give a set of fifteen equations in the fifteen unknowns, namely six stresses, six strains, and three displacements. These have to be solved subject to the relevant boundary conditions.

7.5 Boundary conditions

The surface of the body can be considered divided into two parts from the viewpoint of boundary conditions.

Corresponding to these displacements will be small variations in strain, $\delta\epsilon_{ij}$, given by

$$\delta\epsilon_{ij} = \frac{1}{2} (\delta u_{i,j} + \delta u_{j,i}) \quad (7.15)$$

Then the work done, W , by the internal stresses will be:

$$W = \int_V \sigma_{ij} \delta\epsilon_{ij} dV \quad (7.16)$$

where the stresses are assumed constant during small displacements, so that second order terms are ignored. Hence,

$$\begin{aligned} W &= \int_V \frac{1}{2} \sigma_{ij} (\delta u_{i,j} + \delta u_{j,i}) dV \\ &= \int_V \frac{1}{2} \left\{ (\sigma_{ij} \delta u_i)_{,j} + (\sigma_{ij} \delta u_j)_{,i} \right\} dV \\ &\quad - \int_V \frac{1}{2} \left\{ \delta u_i \sigma_{ij,j} + \delta u_j \sigma_{ij,i} \right\} dV \end{aligned} \quad (7.17)$$

Further, Gauss's Divergence Theorem states that

$$\int_V X_{i,i} dV = \int_S X_i \cos(\bar{n}, x_i) dS \quad (7.18)$$

so that by letting

$$\sigma_{ij} \delta u_i = X_j \quad (7.19)$$

equation 7.17 becomes

$$W = \int_V X_{j,j} dV - \int_V \delta u_i \sigma_{ij,j} dV \quad (7.20)$$

since i and j are dummy subscripts in equation 7.17. Hence using equation 7.18 in equation 7.20 gives

$$W = \int_S \sigma_{ij} \delta u_j \cos(\bar{n}, x_j) dS - \int_V \delta u_i \sigma_{ij,j} dV \quad (7.21)$$

Application of the boundary condition equation (7.11) into equation 7.21 gives

$$W = \int_S P_j \delta u_j dS - \int_V \delta u_i \sigma_{ij,j} dV \quad (7.22)$$

and using boundary conditions (7.14) together with equation (7.12) reduces equation (7.22) to

$$W = \int_{S_f} P_j^* \delta u_j dS - \int_V \delta u_i \sigma_{ij,j} dV \quad (7.23)$$

The equation of equilibrium (7.5) finally reduces equation (7.23) to

$$W = \int_{S_f} P_j^* \delta u_j dS + \int_V \delta u_i B_i dV \quad (7.24)$$

The first term is the work done by the applied, specified, surface loads, and the second is the work done by the body forces.

7.7 Strain energy density

From equation (7.16), the work done by the internal stresses per unit volume is

$$\delta W = \sigma_{ij} \delta \epsilon_{ij} \quad (7.25)$$

Then the strain energy density is given by

$$U = \int_0^\epsilon \sigma_{ij} \delta \epsilon_{ij} \quad (7.26)$$

This can be re-written in matrix form as

$$U = \int_0^\epsilon [\sigma] \{d\epsilon\} \quad (7.27)$$

where $[\sigma]$ denotes a 1 x 9 row vector

$\{d\epsilon\}$ denotes a 9 x 1 column vector.

From equation (7.9) we have

$$\{\sigma\} = [D] \{\epsilon\} \quad (7.28)$$

where $[D]$ is a 9×9 matrix of material constants. Taking the transpose of equation (7.28) gives

$$[\sigma] = [\epsilon] [D] \quad (7.29)$$

since $[D]$ is a symmetric matrix. Thus equation (7.27) becomes

$$U = \int_0^{\epsilon} [\epsilon] [D] \{d\epsilon\} \quad (7.30)$$

$$\text{If } \alpha = [\epsilon] [D] \{d\epsilon\}, \text{ a } 1 \times 1 \text{ matrix,} \quad (7.31)$$

$$\text{then } \alpha^T = \alpha = [d\epsilon] [D] \{\epsilon\}$$

$$\therefore \alpha = \frac{1}{2} ([\epsilon] [D] \{d\epsilon\} + [d\epsilon] [D] \{\epsilon\})$$

$$\therefore \alpha = \frac{1}{2} d([\epsilon] [D] \{\epsilon\}) \quad (7.32)$$

Thus equation 7.30 becomes

$$U = \frac{1}{2} [\epsilon] [D] \{\epsilon\} \quad (7.33)$$

From physical considerations, this can be shown to be positive definite.

7.8 The Principle of Minimum Total Potential Energy

Since the stress components can be expressed in terms of strain (equation 7.9) and the strains expressed as functions of displacements (equation 7.7) then the increment in strain energy density, given by

$$\delta U = \sigma_{ij} \delta \epsilon_{ij} = \delta W \quad (7.34)$$

is also a function of displacements, i.e.

$$\delta U = \delta U(u_i) \quad (7.35)$$

Hence the principle of virtual work becomes

$$\int_V \delta U(u_i) dV - \int_{S_F} P_i^* \delta u_i dS - \int_V \delta u_i B_i dV = 0 \quad (7.36)$$

Then, if the surface and body forces can be assumed constant during the infinitesimal displacements δu_i ,

$$P_i^* \delta u_i = \delta(P_i^* u_i) \quad (7.37)$$

and

$$B_i \delta u_i = \delta(B_i u_i) \quad (7.38)$$

Equation (7.36) then becomes

$$\int_V \delta U(u_i) dV - \int_{S_f} \delta(P_i^* u_i) dS - \int_V \delta(B_i u_i) dV = 0$$

$$\therefore \delta\pi = 0 \quad (7.39)$$

$$\text{where } \pi = \int_V (U - B_i u_i) dV - \int_{S_f} P_i^* u_i dS \quad (7.40)$$

The function π is the total potential energy of the body.

Equation (7.40) shows that for all admissible displacements satisfying the prescribed geometric boundary conditions, the true displacements are these which ensure that the total potential energy is stationary. By taking small variations and applying Taylor's theorem, it can be deduced that the stationary value is a minimum.

7.9 The Rayleigh-Ritz method

This is a method for determining, by successive approximation, functions which give a stationary value to a functional. Thus for the functional $\pi(u)$, where u is the required function solution, a solution is assumed of the form

$$u_n = \sum_{j=1}^n \alpha_j u_j \quad (7.41)$$

where the α_j are unknowns, and the u_j are the selected functions which are admissible, i.e. they satisfy the geometric boundary conditions and

continuity requirements. Then the constants α_j are determined by ensuring $\delta\pi = 0$,

$$\therefore \frac{\partial\pi}{\partial\alpha_j} = 0 \quad \text{for } j = 1 \text{ to } n \quad (7.42)$$

which produces a set of n simultaneous equations for the n α_j .

7.10 The finite element method as a Rayleigh-Ritz process

In the finite element method, the displacements with each element are defined as functions of the nodal displacements. The displacement functions (or shape functions) will be of the form:

$$\{u_i\} = [S] \{\delta\}^e \quad (7.43)$$

where $\{u_i\}$ is a column vector representing the displacement of any point in the element

$[S]$ is the matrix of shape functions of the displacements, being functions of the co-ordinate system.

$\{\delta\}^e$ is the column vector of nodal displacements for the element.

In general, if the nodes are characterised by m, n, \dots etc., then $[S]$ and $\{\delta\}^e$ can be expressed in a partitioned form as

$$[S] = [S_m, S_n, \dots] \quad (7.44)$$

$$\text{and } \{\delta\}^e = \begin{pmatrix} \delta_m \\ \delta_n \\ \vdots \\ \vdots \\ \vdots \\ \vdots \end{pmatrix} \quad (7.45)$$

where δ_m are the displacements at node m , etc.

The functions S_m , etc. have to be chosen to satisfy the prescribed displacements. Thus, for example,

$$S_m(x_{1m}, x_{2m}, x_{3m}) = I \quad (7.46)$$

$$S_m(x_{1n}, x_{2n}, x_{3n}) = \phi \quad (7.47)$$

where I is the identity matrix

ϕ is the null matrix

With the displacements defined at all nodes, the strains can be evaluated from equation (7.7). This will result in a relationship of the form

$$\{\epsilon\} = [C] \{\delta\}^e \quad (7.48)$$

$$\text{or } [\epsilon] = \{\epsilon\}^T = [\delta]^e [C]^T \quad (7.49)$$

When the continuum is divided into a set of discrete elements, V_n , the total potential energy, given by equation (7.40) is

$$\Pi = \sum_n \left(\int_{V_n} (U(u_i) - B_i u_i) dV - \int_{S_{fn}} (P_i^* u_i ds) \right) \quad (7.50)$$

Using the expressions for the strain energy density, equation (7.33), equation (7.50) becomes, in matrix form:

$$\Pi = \sum_n \left(\int_{V_n} \left(\frac{1}{2} [\epsilon] [D] \{\epsilon\} - [B] \{u\} \right) dV - \int_{S_{fn}} [P^*] \{u\} ds \right) \quad (7.51)$$

By using equations (7.43), (7.48), and (7.49), equation (7.51)

becomes

$$\Pi = \sum_n \left(\int_{V_n} \left(\frac{1}{2} [\delta]^e [C]^t [D] [C] \{\delta\}^e - [B] [S] \{\delta\}^e \right) dV - \int_{S_{f_n}} [P^*] [S] \{\delta\}^e dS \right) \quad (7.52)$$

or

$$\Pi = \sum_n \left(\frac{1}{2} [\delta]^e [K]^e \{\delta\}^e - [F]^e \{\delta\}^e \right) \quad (7.53)$$

where $[K]^e = \int_{V_n} [C]^t [D] [C] dV$ (7.54)

is the stiffness matrix of the element, which can be seen to be symmetric,

and $[F]^e = \int_{V_n} [B] [S] dV + \int_S [P^*] [S] dS$ (7.55)

is the matrix of nodal forces for the element.

The principle of minimum total potential energy requires that equation (7.53) should be a minimum. Thus for each element,

$$\frac{1}{2} [\delta]^e [K]^e \{\delta\}^e - [F]^e \{\delta\}^e = \text{minimum} \quad (7.56)$$

Taking variations gives

$$\frac{1}{2} [d\delta]^e [K]^e \{\delta\}^e + \frac{1}{2} [\delta]^e [K]^e \{d\delta\}^e - [F]^e \{d\delta\}^e = 0 \quad (7.57)$$

Since $[K]^e$ is symmetric, this reduces to:

$$([\delta]^e [K]^e - [F]^e) \{d\delta\}^e = 0 \quad (7.58)$$

which, for an arbitrary column vector $\{\delta\}^e$, gives

$$[\delta]^e [K]^e - [F]^e = 0 \quad (7.59)$$

or $\{F\}^e = [K]^e \{\delta\}^e \quad (7.60)$

which is a set of simultaneous equations relating the nodal forces to the nodal displacements for an individual element. This forms the basis of the finite element method.

BIBLIOGRAPHY

1. HOFFERBERTH W.
Zur Static des Luftreifens.
Kautschuk und Gummi. VOL.9. 1956
2. RIVLIN R.S.
The deformation of a membrane formed by inextensible cords.
Archives for Rational Mechanics and Analysis Vol.2. 1958-9.
3. BUKHIN B.L.
Calculations of the equilibrium configuration of a pneumatic
tyre, taking into account the elongation of the cords.
Soviet Rubber Technology No.10. 1963.
4. LAUTERBACH H.G. and AMES W.F.
Cord stresses in inflated tyres.
Textile Research Journal, Nov. 1959.
5. AMES W.F.
Stresses in cylindrically symmetric membranes reinforced with
extensible cords.
Journal of Franklin Institute. Vol. 272 1961.
6. WALTER J.D.
Centrifugal effects in inflated, rotating bias ply tyres.
Textile Research Journal Vol.40.
7. ZOROWSKI C.F. , DUNN S.E.
Measurement and prediction of cord strain and loadings in
inflated pneumatic tyres. Chemstrand Research Centre, North
Carolina, 1967.
8. FRANK F.
Theory and calculation of static forces and cross-sectional forms
of bias layered and radial layered tyres.
Rubber Conference of the K.D.G. Berlin, 1968.

9. GOUGH V.E.
Thick shells of double curvature.
Dunlop Internal Report.
10. USYUKIN V.I.
Non-linear deformations of toroidal membrane shells.
Mekhanika Tverdogo Tela Akademiya Nauk, 1969.
11. DUNN S.E.
A mathematical model of the pneumatic tyre
Raleigh U.S.A. 1970.
12. BREWER H.K.
Stresses and deformations in multi-ply aircraft tyres subject
to inflation pressure loading.
Wright-Patterson Air Force Base, Technical Report.
AFFDL-TR-70-62, 1970.
13. GREEN A.E. , ZERNA W.
Theoretical Elasticity.
Clarendon Press, 1968.
14. GODFREY D.E.R.
Theoretical elasticity and plasticity for engineers.
Thames and Hudson. London. 1959.
15. REISSNER E. , STAVSKY Y.
Bending and Stretching of certain types of heterogeneous
anisotropic elastic plates.
Journal of Applied Mechanics, Vol.28. 1961
16. CLARK S.K.
The plane elastic characteristics of cord-rubber laminates.
Textile Research Journal. April 1963.
17. CLARK S.K.
Internal characteristics of orthotropic laminates.
Textile Research Journal. Novr. 1963.

18. GOUGH V.E.
Stiffness of cord-rubber constructions
Deutsche Kautschuk-Gesellschaft. June 1965.
19. WAINWRIGHT H.V.
Elasticity and strength of various types of cord and rubber constructions
Dunlop Internal Report. June 1952.
20. LAWTON H.J.
Calculation of modulus of cord and rubber constructions, taking account of interaction between cord and rubber.
Dunlop Internal Report. Jan.1953.
21. FRANK F. , HOFFERBERTH W.
Mechanics of the pneumatic tyre. Rubber Chemistry and Technology, Vol.40, 1967.
22. ASHTON J.E. , HALPIN J.C. , PETIT P.H.
Primer on composite materials: Analysis.
Technomic Publishing Co. 1969.
23. CALCOTE L.R.
The analysis of laminated composite structures.
Van Nostrand. 1969.
24. ROBECCHI E. , AMICI L.
Meccanica del Pneumatico.
Pirelli, 1970.
25. HASHIN Z. , ROSEN B.W.
The elastic moduli of fiber reinforced materials
Journal of Applied Mechanics. June 1964.
26. HE RMANS J.J.
The elastic properties of fiber reinforced materials when the fibers are aligned.
Akademic Van Wetenshappen, Vol 70, 1967.

27. BARSON C.W. , OSBORNE D.J.
Stress analysis by dynamic relaxation.
Dunlop Internal Report , 1969.
28. GOUGH V.E.
The interpretation of cosine bias angle versus radius charts.
Dunlop Internal Report, May. 1955.
29. GOUGH V.E.
Cord paths in tyres
Dunlop Internal Report. Octo. 1960.
30. CLARK S.K.
A review of cord-rubber elastic characteristics.
Rubber Chemistry and Technology, Vol.37, 1965.
31. TURNER M.J. , CLOUGH R.W. , MARTIN H.C. , TOPP L.J.
Stiffness and deflection analysis of complex structures
Journal of Aeronautical Sciences, Vol.23. No.9. 1956.
32. ZIENKIWICZ O.C.
The finite element method in structural and continuum mechanics.
McGraw-Hill 1971.
33. Curved isoparametric elements and numerical integration.
Course on recent developments in finite element methods.
University of Wales, Swansea, 1970.
34. HAMMER P.C. , MARLOW O.J. , STROUD A.H.
Numerical integration over simplexes and cones.
Math. Tables. Aids. Comp. Vol.10, 1956.
35. LANCZOS
Applied Analysis.
Pitman & Sons, London, 1957.

36. IRONS B.M.
Discussion. Finite element techniques in structural mechanics.
Ed. Tottenham H, Brebbia C. Southampton Univ. Press, 1970.
37. AHMAD S. , IRONS B.M. , ZIENKIEWICZ O.C.
Analysis of thick and thin shell structures by curved
finite elements.
Int. J. Num. Meth. Eng. Vol.2, 1970.
38. ZIENKIEWICZ O.C. , TAYLOR R.L. , TOO J.M.
Reduced integration techniques in general analysis of
plates and shells.
Int. J. Num. Meth. Eng. Vol.3, 1971.
39. PAWSEY S.F. , CLOUGH R.W.
Improved numerical integration of thick shell finite elements.
Int. J. Num. Meth. Eng. Vol.3, 1971.
40. GOUGH V.E.
Wear. Vol.2, 1958/9
41. CLARK S.K.
An analysis of contact pressure distribution for pneumatic tyres.
Dept. of Engineering Mechanics, Univ. of Michigan.
42. VARGA R.S.
Matrix iterative analysis.
Prentice-Hall Inc. 1962.
43. HESTENES M. , STIEFEL E.
Method of conjugate gradients for solving linear equations.
Report 1659, Nat. Bureau of Standards, 1952.
44. FRIED I.
A gradient computational procedure for the solution of large
problems arising from the finite element discretisation method.
Int. J. Num. Meth. Eng. Vol.2, 1970.

45. FOX R.L. , STANTON E.L.
Developments in structural analysis by direct energy methods.
A.I.A.A. J. Vol.6, No.6, 1968.
46. KUNZ K.S.
Numerical Analysis.
M^CGraw Hill. 1957.
47. Collected algorithms from CACM.
Algorithm 126 : Gauss's method.
Algorithm 195 : Bandsolve.
48. BARSON C.W.
The analysis of the equilibrium shape of a tyre using
a structural method.
Dunlop Internal Report.
49. CURTISS W.W.
Mathematics underlying the design of tyres.
Tyre Mathematics Symposium, Ohio, 1971.
50. PUGIN V.A.
Stresses in the bead rings of tyres.
Soviet Rubber Tech. Vol.21, 1962.
51. ODEN J.T.
Numerical formulation of non-linear elasticity problems.
Proc. of the ASCE. June, 1967.
52. BREBBIA C. , CONNOR J.
Geometrically non-linear finite element analysis.
Proc. of the ASCE, April, 1969.
53. MARTIN H.C.
On the derivation of the stiffness matrices for the analysis
of large deflection and stability problems.
Proc. Conference on Matrix methods in Structural Mechanics
Ohio, 1965.

54. COOPER D.H. , GOUGH V.E.
The radial stiffness of the pneumatic tyre.
Dunlop Internal Report.
55. GOUGH V.E.
Mechanics of the pneumatic tyre, Chapter 3.
Ed. Clark S.K., U.S. Dept. of Commerce.
56. GOUGH V.E.
Bead coil tensions.
Dunlop Internal Report, Oct. 1963.
- 57, IRONS B.M.
A frontal solution program for finite element analysis.
Int. J. Num. Meth. Eng. Vol.2, 1970.